

POLITECNICO DI MILANO

Scuola di Ingegneria Industriale e dell'Informazione

Corso di Laurea Magistrale in Ingegneria Biomedica



RAPID PROTOTYPING TECHNIQUES TO DEVELOP CALCIFIED AORTIC VALVE MODEL FOR CLINICIANS TRAINING IN CARDIOVASCULAR THERAPIES

Relatore: Prof. Riccardo VISMARA

Correlatore: Dott. Michal Lukasz JAWOREK

Tesi di Laurea di:

Ilaria RICCIO, matricola 899441

Ece TUTSAK, matricola 885004

Anno Accademico 2018-2019

Acknowledgements

We would like to acknowledge our supervisor Professor Vismara for giving us the possibility to work on this project and for helping us to improve our work with his advice.

Our gratitude goes infinitely also to Michal, Francesca and Eleonora for the great support, availability, and technical advices they gave us during the entire work, in laboratory and also from home during this particular period.

We would like to share our thank to each other for the mutual support and encouragement during these months of collaboration.

A special acknowledgment goes to my parents, my brother Davide and my grandfather for the opportunity they gave me to follow my dreams and for supporting me during this experience with a lot of patience. Moreover, I would particularly like to thank some special people that have been close to me along the way of this journey. Thank you, Andrea, for making me smile when I was anxious. A big hug goes to Matteo, Marta and Elena, who has accompanied me through all these years, and via video calls when we couldn't physically see each other. A kindly thought goes to all my friends, for the lovely time we have spent together and all their support.

Ilaria

I would like to take this opportunity to thank my family. I could not have achieved the completion of this thesis project without their support during COVID-19 pandemic in the world.

Finally, I would like to thank my friends Aydan, Bora, Eren and Begüm who have experienced with me this pandemic process in Italy.

“Science is the only true guide for everything in the world, civilization, life and success”

(MUSTAFA KEMAL ATATÜRK)

Ece

Table of Contents

ABSTRACT	8
SOMMARIO	16
INTRODUCTION	25
1. ANATOMICAL AND PATHOLOGICAL BACKGROUND	29
1.1. Anatomy of the Heart	29
1.2. The Cardiac Cycle	31
1.3. Anatomy of the Aortic Root and the Aortic Valve	33
1.4. Aortic Valve Pathologies	38
1.4.1. Aortic Valve Stenosis	39
1.4.2. Bicuspid Aortic Valve	47
1.5. Transcatheter Therapies for Aortic Stenosis	48
2. STATE OF ART	54
2.1. Non-Functional Models	55
2.1.1. Maragiannis et al., Aortic Stenosis Model, 2014 [71]	55
2.1.2. Weber et al., Fibrin Aortic Valve Model, 2015[72]	57
2.1.3. Ripley et al., Aortic Root Models, 2016 [76]	58
2.1.4. Schmauss et al., Calcified Porcelain and Flexible Ascending Aorta Model, 2012 [77]	59
2.2 Functional Models	61
2.2.1 Maleki et al., Stenotic Aortic Root model, 2014 [74]	61
2.2.2 Sacco Model, Politecnico di Milano, 2015 [18]	63
2.2.3. Izzo et al., Calcified Mitral Valve Model, 2016 [78]	64
2.2.4. Schiena Model, Politecnico di Milano, 2018 [4]	66
2.2.5. Rotman et al., Replicator model, 2018 [75]	69
2.3 Aim of the study and objectives	70
3. MATERIALS AND METHODS	72
3.1. Technologies and Tools	72
3.1.1. Software	77
3.1.2. 3D Printer	81
3.2. Materials for Mold Production	84
3.2.1. PLA	84
3.2.2. XTC-3D®	85
3.2.3. E-30 Epoxy Resin	86
3.3. Material for Flexible Structures	87

3.3.1. Silicone.....	87
3.4. Spinning Device.....	90
3.5. Workflow of the Manufacturing Process	96
3.6. Molds Design.....	97
3.6.1. Tricuspid Aortic Valve Mold	98
3.6.2. Bicuspid Aortic Valve Mold.....	100
3.6.3. Aortic Root Molds.....	101
3.6.4. Custom Inner Mold	104
3.7. Calcification Pattern.....	106
3.8. Assessment of the Leaflets Thickness with Preliminary Pattern.....	111
3.9. Assessment of the Cusp Surface Covered by Preliminary Pattern	112
3.10. Manufacturing Protocols	113
3.10.1. Leaflets Manufacturing Protocol	113
3.10.2. Custom Inner Mold Manufacturing Protocol	114
3.10.3. AR Manufacturing Protocol	115
4. RESULTS.....	116
4.1. Verification of the Manufacturing Technique of the Aortic Valve	116
4.2. Aortic Root.....	119
5. CONCLUSION, LIMITATIONS AND FURTHER DEVELOPMENTS	122
ABBREVIATIONS.....	125
APPENDIX A.....	127
APPENDIX B.....	134
BIBLIOGRAPHY.....	150
Index of Figures	157
Index of Tables.....	160

ABSTRACT

INTRODUCTION

Aortic Stenosis is the most frequent disease among the left-sided Valvular Heart Diseases, affecting 13% of elderly patients (≥ 75 years) [1]. Even though the gold standard treatment of aortic stenosis is surgical valve replacement through sternotomy, there are non-negligible percentages of patients (31.8% from Euro Heart Survey) who cannot undergo this type of operation because of elder age and presence of comorbidities. These patients are categorized as high-surgical-risk and their number is rising, because of the projected aging of the population and the associated increase in comorbidities. Transcatheter therapies are a worthwhile less invasive option to enable cardiac intervention to this patient category. Their main benefits comparing to surgical therapies are the reduction of traumas, post-treatment recovery times and costs. Despite their advantages, intra procedural errors can cause life-threatening outcomes, mainly because of the limited vision of the interventional field. Therefore, hands-on training could serve as support in the practical preparation of interventional cardiologists. Studies highlighted how a standardized interventional hands-on

training, in transcatheter procedures, can lead to an exponential rise in the initial phase of the learning curve, increasing the technical proficiency, in terms of reduction of intraprocedural times, radiation doses and contrast volumes [2].

Training simulators, as hydraulic test benches, are used to train transcatheter therapies in similar conditions of intervention. However, they still lack in the simulation of pathological conditions, as aortic stenosis.

Simulators comprise natural tissue or polymeric components. Even though biological components originating from food industry animals present anatomical similarity to human structures, they generally lack the reproduction of pathological conditions, need a specific know-how in their management and could present problems related to the conservation and storage. Fully artificial simulators instead comprise polymeric models characterized by patient-specific or paradigmatic anatomy. Patients-specific phantoms are generally aimed to pre-procedural planning on specific pathologies, hence could help in the assessment of the feasibility of the transcatheter procedures and give a hint about their possible outcomes. Paradigmatic phantoms provide a typical

physio- or pathological anatomy, useful for interventional cardiologists training.

In this context the aim of this thesis was to develop a protocol for manufacturing of paradigmatic models of calcified aortic valve for clinicians hands-on training in transcatheter procedures.

MATERIALS AND METHODS

Method of Realization

The rapid prototyping manufacturing process from the design to the obtainment of the calcified valvular model consisted in the steps shown in Figure 1.

Since the calcified valve model was intended for clinical training, a general geometry of the valve structure and calcification pattern were defined in order to design inner/outer molds and calcific deposits on SolidWorks, *CAD software* (Mold Design, Figure 1). After the molds were designed, they were converted into *mesh* models, automatically corrected by Netfabb Standard software and imported into Cura, in order to optimize the printing parameters and to convert the molds file into a format suitable for 3D manufacturing (Mold Manufacturing, Figure 1).

After obtaining the 3D printed molds, they underwent postprocessing by polishing and coating of the inner surfaces that would have matched with the silicone during

casting technique. This phase (Mold Post-Processing, Figure 1), as shown by the literature [3], intended to increase the smoothness and transparency of the silicone models. Once this step was completed, the molds were employed in manufacturing technologies (Phantom Production, Figure 1): silicone dip-spin coating of the leaflets, embedding of the calcifications into the cusps and silicone casting of the aortic root around the valve.

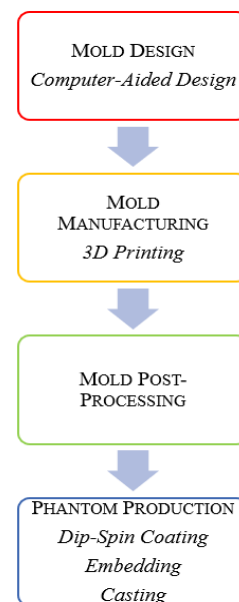


Figure 1 Manufacturing process for the obtainment of the silicon model.

Manufacturing Technologies

The manufacturing process developed in the present work of thesis consisted in the combination of three protocols:

1. Calcified Aortic Valve (CAV) Production
2. Custom Inner Mold Production
3. Aortic Root (AR) Production

The calcified leaflets of the aortic valve were produced by applying the dip-spin coating manufacturing process. In this technique an aortic valve mold was dipped into liquid silicone, in order to obtain a thin silicone film where the calcific deposits were embedded. The polymerization process was completed in an ad-hoc designed Spinning Device, that allowed a homogenous and thin distribution of the coating material and the contemporary production of 4 aortic valves, as shown in Figure 2.

Protocol 1: Calcified Leaflets Production



Figure 2 The protocol involves dip-coating, calcification embedding and polymerization in ad-hoc designed Spinning Device.

The second protocol regarded the production of a custom inner mold to be used successively for the AR production; 3D printed, and silicone molds were needed to produce it. The custom inner mold allowed to obtain the replica of any type of calcification pattern embedded in aortic leaflets and the inner shape of the ascending aorta tract (AA),

Figure 3.

Protocol 2: Custom Inner Mold Production

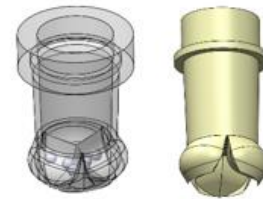
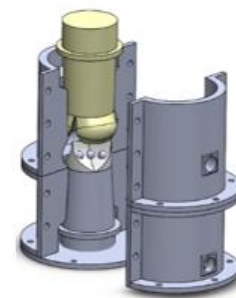


Figure 3 The protocol allows to obtain a mold that replicates any type of calcification pattern embedded in the aortic valve.

Finally, the casting technique was used to merge the calcified aortic valve in the AR. Silicone was casted in the interspace between inner molds (Inflow Tract mold, CAV and Custom Inner Mold) and outer

Protocol 3: Aortic Root Production



molds (Figure 4).

Figure 4 The protocol allows to merge CAV and AR.

Materials

The materials used for the manufacturing of the calcified valvular models are Sorta Clear 18 (Smooth-on, Macungie, PA, US)

for the flexible structures which are leaflets and aortic root. PLA (Poly-lactic-Acid, 3D Italy, Rome, Italy) was used for the calcification patterns.

Sorta Clear 18 is a silicone rubber that cures at room temperature, and it was selected according to its mechanical properties, processing characteristics, transparency, compatibility with echocardiography, and cost-effectiveness. PLA is a thermoplastic polyester, and it was selected according to its mechanical properties and its easy moldability through 3D printing technology.

The materials used for the realization of the molds were PLA, according to its cost-effectiveness and easy 3D printability, and E-30 epoxy resin (Prochima, Calcinelli di Saltara, Italia), because of its thermosetting properties.

Description of the Molds

Aortic Valve Mold

Three different geometries of aortic valve mold were developed. A preliminary geometry of aortic valve mold (AV mold, Figure 5) was created for the verification of the efficacy of the dip-coating manufacturing process. The simplified geometry was obtained following Schiena's experimental work [4].

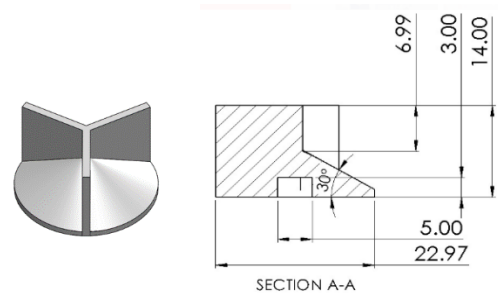


Figure 5 Preliminary CAD model of tricuspid aortic valve.

A final geometry, more realistic, was designed for tricuspid and bicuspid valve molds, as shown in Figure 6. Final geometry differed from preliminary one, also for the shape of the commissure area. The commissure shape was rectangular in preliminary valve mold, but it was designed triangular in the final mold.



Figure 6 Tricuspid and bicuspid realistic CAD models.

Calcification patterns and their shape were identified after the analysis of Thubrikar's work [5] and two common configurations were chosen: radial and arc/partial arc patterns. Calcification patterns were obtained through preliminary and parametrized designs (

Figure 7). Stenosis severity can be simulated by increasing the surface area covered by the pattern and its thickness.

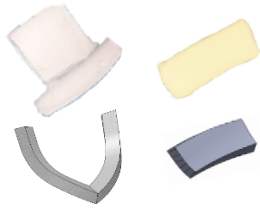


Figure 7 Calcification patterns: upper, preliminary 3D printing, lower parametrized 3D printing.

The thickness of obtained aortic valve leaflets, with and without the calcifications, was measured and this result were compared with real aortic valves. The measurements were assessed by digital caliper at two different points (Figure 8): Free Margin and Belly.

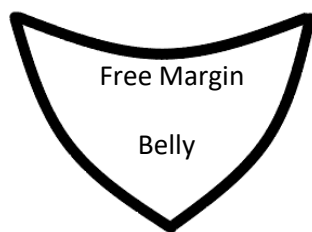


Figure 8 Schematic representation of the measured areas of the cusp.

These measured areas were selected according to literature and because they were recognized as critical points due to silicone accumulation during the spinning phase.

Aortic Root Molds

Aortic Root silicone configuration was achieved through the assembly of outer and inner molds (Figure 9): outer molds were responsible for the external geometry; the

inner molds gave the internal conformation of the structure. Inner molds were a 3D printed part, representing the valve from annulus to Sino Tubular Junction (STJ), the Inflow Tract, and a custom epoxy part (circled in red in Figure 9) that represented the ascending aorta (AA) tract. The custom inner mold made in epoxy was tailored for each calcified valve configuration and allowed to obtain AR inner molds for any type of calcification pattern.

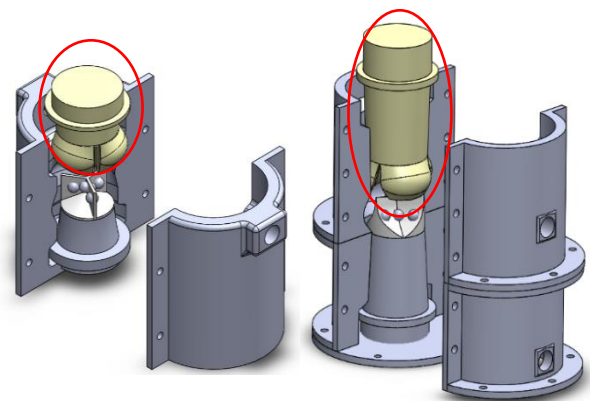


Figure 9 Assembly of outer and inner aortic root molds.

Preliminary and Final AR were designed to be compatible with the AV molds geometries. They differed for the length of the Inflow and AA tracts and also for the shape of the commissure area, that was rectangular in preliminary design and triangular in final design.

RESULTS

The objective of the thesis was the development of a manufacturing method for the realization of calcified aortic valve models aimed to clinicians training. The results obtained analyzing the produced

phantoms can allow to assess the feasibility of the method. Dip-spin coating allowed to produce thin valve leaflets, where calcific deposits were embedded. A full phantom comprising aortic root and calcified leaflets was obtained through casting technique.

Aortic Valve

Through the proposed manufacturing dip-spin process, it was possible to realize the aortic valve models without the calcification shown in Figure 10 based on Aortic Valve Molds.



Figure 10 Physiological Aortic Valve Model obtained through dip-spin coating of Sorta Clear 18.

In Table 1, the mean values of thickness of 4 manufactured phantoms were compared to natural heart mean values and a previous work where casting method was employed to produce a physiological aortic valve model. It was possible to obtain phantoms leaflets' thickness values within the range of physiologic natural valves and lower than a previous work, hence, the proposed dip-spin coating allowed to go beyond the technological limitations of the 3D printed molds of casting process.

	Natural Aortic Valve [99]	Schiema Model [2]	Phantom Model
Free Margin Thickness [mm]	0.87 ± 0.27, 20-59 years 1.42 ± 0.51, ≥ 60 years	1	0.79 ± 0.03
Belly Thickness [mm]	0.41 ± 0.09	1	0.69 ± 0.02

Table 1 Comparison between mean values and standard deviation of thickness of natural physiological aortic valve, previous work from literature and manufactured phantom model.

Calcified Aortic Valve

Another benefit brought by the manufacturing technique introduced in the present work of thesis is the capability to embed calcific deposits into the leaflets, keeping thickness values within the range of natural pathological valves [6]. 8 calcified aortic valve models were obtained, that differ with respect to the calcific deposit pattern: radial and arc/partial arc patterns, shown in Table 2. The preliminary pattern configuration, using 3D printed deposits 1 mm thick, gave results of leaflets thickness consistent with literature. Patterns in parametrized configuration were standardized to improve the matching with the valve shape and to easily increase the severity stenosis grade.




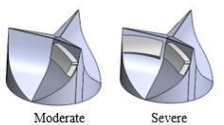
	Preliminary Pattern Configuration	Parametrized Pattern Configuration
Radial Pattern		
Thickness [mm]	2.34 ± 0.29	Hypothetical 2.58 mm (0.79 mm 1 st dip-coating + 1 mm calc + 0.79 mm 2 nd dip-coating)
Partial Arc / Arc Pattern		
Thickness [mm]	2.76 ± 0.10	Hypothetical 2.58 mm (0.79 mm 1 st dip-coating + 1 mm calc + 0.79 mm 2 nd dip-coating)

Table 2 Manufactured Calcified Aortic Valves.

Aortic Root

Aortic Root (AR) prototypes validated the feasibility of the multi-step manufacturing process. The obtained preliminary and final ARs (Figure 11) included Calcified Aortic Valves, Aortic Root (from the annulus to STJ, comprising Valsava Sinuses), Inflow Tract, Ascending Aorta tract (AA) and extension portions of the aortic root wall to connect the model to hydraulic set-ups. The resulting dimensions for preliminary design and final design were shown in Table 3, consistent with literature.

	Preliminary AR	Final AR
Annulus and STJ Diameters	23 mm (min value from liter.)	26 mm (average value from liter.)
VS Maximum Diameter AR	30 mm	35 mm
Inflow + AA tracts	16.18 mm	16.8 mm
Total Height of the Model	20 mm	70 mm
Wall Thickness	60 mm	110 mm
Commissure Geometry	5 mm	2.5 mm
	Rectangular	Triangular

Table 3 Summary of the ARs dimensions.

The triangular area at commissures level, improvement done in Final AR (Figure 11), provided a wider fusion zone between the leaflets and the aortic root wall, which can result in a more stable and durable structure. The final AR presented longer Inflow and AA tracts, to allow the implant of different sizes and designs of TAVI valves, considering the training purpose.

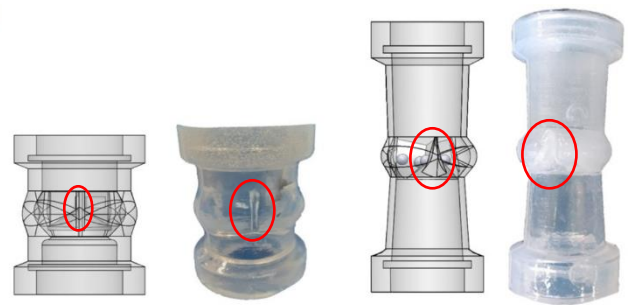


Figure 11 Commissure shape is highlighted in CAD and silicone models, for both preliminary and final ARs.

CONCLUSIONS AND FUTURE DEVELOPMENTS

In this thesis a protocol was developed for the realization of a paradigmatic polymeric model of calcified aortic valve, aimed to hands-on clinicians training in transcatheter therapies, using cost-effective and easily accessible materials and manufacturing technologies.

Dip-coating technique allowed the realization of thin leaflets, whose values are comparable to natural valves and it allowed the embedding of ad-hoc designed calcification patterns. The ad-hoc designed

Spinning Device speeded up the manufacturing process, allowing the contemporary production of 4 valves, and provided a method to obtain uniform thickness of the silicone leaflets' models. The replica of any type of calcification pattern was possible thanks to the exploitation of epoxy resin as custom inner molds. Silicone casting into molds provided flexible anatomical shapes, characterized by complex geometries and allowed the fusion between leaflets and aortic root at commissures and annulus level.

However, this work has several limitations. The stability of the PLA deposits into the silicone leaflet should be assessed through hemodynamic tests.

The reproduction of mechanical characteristics of natural valvular tissue and calcific deposits was not the objective of the thesis, but its fulfillment could broaden the application of the proposed manufacturing method also in testing of new devices or preprocedural planning.

Sorta Clear 18 showed a good visibility inside the model. Since the models are designed for TAVI training purposes, the compatibility with standard medical imaging techniques, such as echocardiography or X rays/fluoroscopy, should be assessed. Literature highlighted PLA attenuation coefficient compatible with fluoroscopy imaging, nonetheless

specific PLA filled with high density ceramics could provide improved visibility under X- rays.

In conclusion, the results obtained demonstrate the feasibility of the manufacturing process and the fulfillment of the initial design specifications. Hence, this work could be believed as a contribute in the development of interventional training of students and cardiologists. A broadening to pre-procedural planning could be evaluated, applying the present manufacturing method to patient-specific geometries.

SOMMARIO

INTRODUZIONE

La stenosi aortica è la patologia più frequente tra le malattie valvolari del cuore sinistro e affligge il 13% dei pazienti in età avanzata (≥ 75 anni) [1]. Nonostante il gold-standard per il trattamento della stenosi aortica sia la sostituzione valvolare attraverso l'operazione chirurgica e la sternotomia, esiste una percentuale non trascurabile di pazienti (31.8%, citando la Euro Heart Survey), che non può essere sottoposta a questo tipo di operazione, a causa dell'età avanzata o per la presenza di comorbidità. Tali pazienti rientrano nella categoria di alto rischio chirurgico e la loro prevalenza è in continuo aumento, a causa del progressivo allungamento dell'aspettativa di vita e di conseguenza la maggiore incidenza delle comorbidità. Le terapie transcateretere offrono un'opzione meno invasiva, che consente la possibilità di intervento a tale categoria di pazienti. I loro principali vantaggi, se paragonate con la chirurgia a cuore aperto, sono una riduzione dell'incidenza di traumi, tempistiche di ricovero post terapia e costi. Nonostante i vantaggi, errori intraprocedurali possono dar luogo a effetti potenzialmente letali, dovuti principalmente alla visione limitata del campo di intervento. Per questa ragione,

l'esercitazione pratica può essere considerata come un supporto nella preparazione dei cardiologi interventisti. Studi dimostrano come i training pratici, nell'ambito delle terapie transcateretere, possano consentire una crescita esponenziale nella fase iniziale della curva di apprendimento, andando ad incrementare dunque la competenza tecnica dei cardiologi, in termini di riduzione dei tempi intraprocedurali, dosi di radiazione e volumi di contrasto [2].

Simulatori artificiali, come banchi prova idraulici, sono utilizzati per consentire un training delle terapie trans-cateretere ricreando condizioni simili a quelle di intervento. Tuttavia, è ancora riscontrata una mancanza nella simulazione di condizioni patologiche, come ad esempio la stenosi aortica.

I simulatori possono comprendere componenti cardiache di origine animale o polimeriche. Sebbene le componenti biologiche, provenienti dall'industria alimentare, presentino una buona similarità anatomica delle strutture umane, generalmente non sono fedeli nella riproduzione delle condizioni patologiche, necessitano di specifiche competenze di gestione e possono presentare problematiche relative alla conservazione e il mantenimento. Simulatori interamente artificiali, invece, sono costituiti da modelli polimerici con anatomia paziente-specifica

o paradigmatica. I modelli paziente-specifici sono generalmente impiegati per planning pre-procedurali, volti ad investigare la fattibilità delle procedure transcatertere in particolari condizioni patologiche e ipotizzare l'esito dell'operazione. I modelli paradigmatici forniscono invece un'anatomia fisiopatologica generale, dunque utile per l'allenamento di studenti e cardiologici interventisti.

In questo contesto l'obiettivo del presente lavoro di tesi è stato lo sviluppo di un protocollo per la produzione di modelli paradigmatici di valvola aortica calcificata, che possano essere impiegati nel training pratico nelle procedure transcatertere.

MATERIALI E METODI

Metodo di Realizzazione

Il processo di prototipazione rapida, dalla progettazione all'ottenimento del modello di valvola calcificata, è schematizzato in Figura 1.

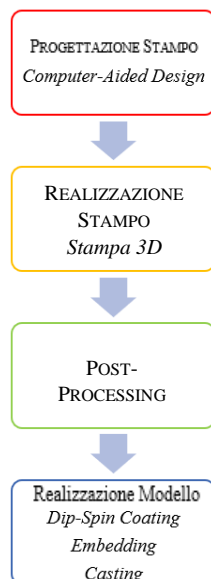


Figura 1 Processo di produzione per l'ottenimento del modello siliconico.

Dal momento che il modello è stato progettato per essere impiegato nel training clinico, è stata definita una geometria generica della struttura valvolare e dei pattern di calcificazione, in modo da poter progettare stampi interni/esterni e pattern calcifici su SolidWorks, un software CAD (Progettazione Stampo, Figura 1). Successivamente, ogni design è stato convertito in un modello *mesh*, automaticamente corretto degli errori di conversione dal software Netfabb Standard e importato in Cura, per l'ottimizzazione dei parametri di stampa e la conversione dei files in un formato adatto alla stampante 3D (Realizzazione Stampo, Figura 1). Dopo aver ottenuto i modelli stampati 3D, è stato necessario sottoporre i componenti ad un processo di levigatura e verniciatura delle superfici che sarebbero andate in contatto con il silicone durante il casting. Tale fase (Post-Processing Stampo, Figura 1) ha diminuito la rugosità superficiale e incrementato la trasparenza dei modelli siliconici, come mostrato dalla letteratura [5]. Terminato tale processo, gli stampi sono stati impiegati in 3 tecnologie di produzione (Realizzazione Modello, Figura

1): dip-spin coating dei foglietti valvolari, embedding delle calcificazioni nelle cuspidi siliconiche e casting della radice aortica attorno alla valvola.

Tecnologie di Produzione

Il processo di produzione sviluppato nel presente lavoro di tesi è la combinazione di tre protocolli specifici:

1. Produzione della valvola aortica calcificata (CAV)
2. Produzione dello stampo interno su misura
3. Produzione della radice aortica (AR)

Il modello di CAV è stato ottenuto attraverso la tecnica del “*dip-spin coating*”. Lo stampo della valvola aortica è stato immerso nel silicone allo stato liquido, in modo da ottenere un sottile film di materiale nel quale includere i depositi calcifici (*calcification embedding*). Il processo di polimerizzazione del silicone è stato completato in uno *Spinning Device* appositamente progettato, che ha consentito una omogenea distribuzione del silicone di rivestimento e la simultanea produzione di 4 valvole aortiche, come mostrato in Figure 2.

Protocollo 1: Produzione dei Foglietti Valvolari Calcificati



Figura 2 Il protocollo prevede l'uso della tecnica di “*dip-coatig*”, l'inclusione delle calcificazioni e la polimerizzazione del modello attraverso uno *Spinning Device* appositamente progettato.

Il secondo protocollo ha interessato la produzione dello stampo interno su misura, da impiegare in seguito per la produzione della AR; per la realizzazione sono stati necessari stampi sia siliconici che stampati 3D. Lo stampo su misura ha consentito di replicare qualsiasi pattern di calcificazione incluso nella valvola aortica e la forma interna del tratto di aorta ascendente (AA), Figura 3.

Protocollo 2: Produzione dello Stampo Interno su Misura

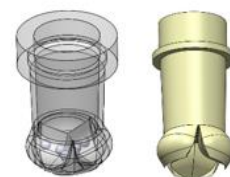


Figura 3 Il protocollo permette di ottenere lo stampo di qualsiasi pattern di calcificazione incluso nella valvola aortica.

Infine, la tecnica del *casting* ha consentito la fusione della CAV all'interno della AR. Il silicone è stato colato nell'intercapedine

tra gli stampi interni (stampo tratto d'ingresso, CAV e stampo interno su misura) e gli stampi esterni (Figura 4).

Protocollo 3: Produzione Radice Aortica

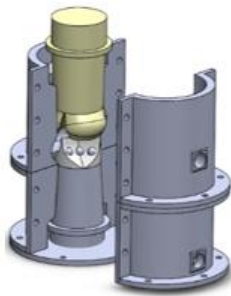


Figura 4 Il protocollo permette la fusione tra CAV e AR.

Materiali

I materiali impiegati per la produzione dei modelli di CAV sono Sorta Clear 18 (Smooth-on, Macungie, PA, US) per le strutture flessibili come foglietti valvolari e radice aortica. PLA (Poly-lactic-Acid, 3D Italy, Rome, Italy) è stato utilizzato per i pattern calcificici. Sorta Clear 18 è una gomma siliconica che polimerizza a temperatura ambiente, ed è stato selezionato in base alle sue proprietà meccaniche, alle caratteristiche di lavorabilità, trasparenza, alla sua compatibilità con l'ecografia e costo. Il PLA è un poliestere termoplastico, selezionato per la realizzazione degli stampi in merito alle sue proprietà meccaniche e la sua facile stampabilità, grazie alla tecnologia di stampa 3D. E-30 (Prochima, Calcinelli di Saltara, Italia) è una resina epossidica impiegata per l'ottenimento

degli stampi interni, per la caratteristica di termoindurezza.

Descrizione degli Stampi

Stampo Valvola Aortica

Tre differenti geometrie di stampi di valvola aortica sono state sviluppate. Inizialmente è stata creata una configurazione preliminare (*preliminary mold*) per lo stampo della valvola aortica (AV, Figura 5), in modo da verificare l'efficacia della tecnica di dip-coating. La geometria semplificata è stata ottenuta seguendo il lavoro sperimentale di Schiena [2].

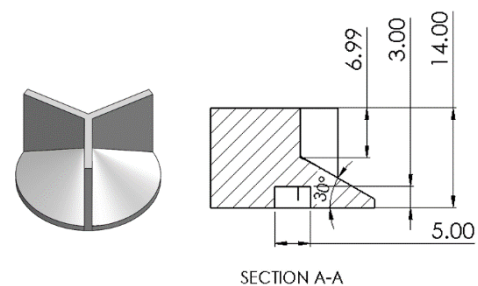


Figura 5 Disegno 3D del preliminary mold per la valvola tricuspide. A sinistra, disegno tecnico.

Successivamente è stata realizzata una geometria finale (*final mold*), più realistica, per valvole aortiche tricuspidi e bicuspidi, come mostrato in Figura 6. Gli stampi finali sono stati differenziati da quelli preliminari anche per la forma della zona delle commissure: forma rettangolare negli stampi preliminari, forma triangolare negli stampi finali.



Figura 6 modelli CAD in configurazione finale, di valvola tricuspide e bicuspide. A sinistra, disegno tecnico.

Le geometrie dei pattern di calcificazione sono state identificate dall'analisi dello studio svolto da Thubrikar [4] e sono: pattern radiale e arco/arco parziale. I pattern sono stati realizzati in configurazione preliminare e parametrizzata (Figura 7). Il grado di stenosi può essere simulato incrementando i valori di area superficiale occupata dal pattern calcifico e lo spessore del pattern stesso.

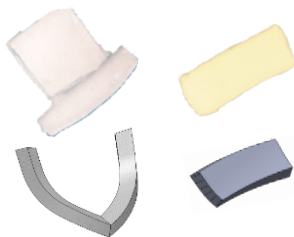


Figura 7 Pattern calcifici: superiormente, configurazione preliminare, inferiormente modelli di configurazione standardizzata.

Lo spessore dei lembi delle AVs ottenute, fisiologiche o calcificate, è stato misurato per effettuare confronti con le valvole aortiche naturali. Ogni misurazione è stata eseguita attraverso calibro digitale per analizzare due principali aree (Figura 8): margine libero (*free margin*) e zona centrale del lembo (*belly*).

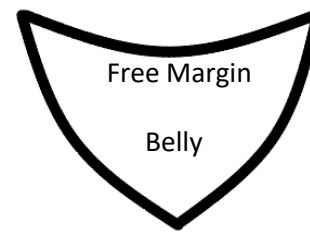


Figura 8 Rappresentazione schematica delle zone misurate nella cuspid.

Queste zone sono state selezionate per la misurazione in base alla letteratura e in quanto riconosciute come punti critici per l'accumulo di silicone durante la fase di spinning.

Stampo Radice Aortica

Per la realizzazione del modello siliconico di radice aortica sono stati previsti: stampi interni (anima), che conferiscono la conformazione interna del pezzo; stampi esterni (forma), responsabili della geometria esterna. L'anima è stata costituita da un componente stampato 3D, rappresentante il tratto a monte della valvola, la valvola sino alla giunzione sinotubulare (STJ) e un componente in resina epossidica, rappresentante il tratto a valle della valvola, ossia il tratto dell'aorta ascendente (AA). Il componente in resina epossidica ha permesso di ottenere su misura lo stampo di ogni valvola calcificata. Sono state ottenute due configurazioni di radice aortica, preliminare e finale (*preliminary and final configurations*, Figura 9) in modo da essere compatibili con gli stampi delle valvole aortiche. Sono state

differenziate per la lunghezza dei tratti a monte e a valle (AA) della valvola e per la forma della zona commissurale, rettangolare nella configurazione preliminare e triangolare in quella finale.

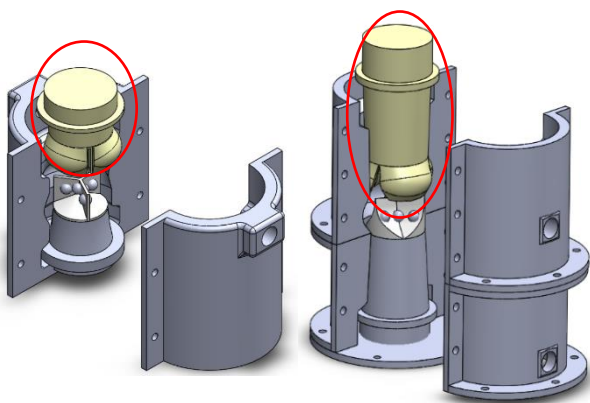


Figura 9 Stampi esterni e interni della radice aortica.

RISULTATI

L'obiettivo della tesi era lo sviluppo di un processo di manifattura per la realizzazione di modelli di CAV, con lo scopo di essere impiegati nel training clinico. I risultati ottenuti dall'analisi dei modelli prodotti consentono di convalidare il processo. La tecnica di dip-spin coating ha consentito la produzione di foglietti valvolari di basso spessore, seppur includendo depositi calcifici. La tecnica di casting ha permesso l'ottenimento di un modello completo di AR e CAV.

Valvola Aortica

I modelli siliconici di AV privi di calcificazioni, mostrati in Figura 10, sono stati realizzati attraverso il dip-spin coating degli stampi di AV.



Figura 10 Modelli di valvole aortiche ottenuti con dip-spin coating di Sorta Clear 18.

In Tabella 1 i valori medi di spessore dei 4 modelli privi di calcificazione sono confrontati coi valori di valvola aortica naturale (Natural Aortic Valve), e di un lavoro precedente (Schiena Model), in cui era stata utilizzata la tecnica del casting per la produzione di un modello di AV fisiologica. È stato possibile evidenziare una congruenza tra i valori del modello realizzato e quelli della valvola aortica naturale; inoltre il modello realizzato presenta spessori inferiori a quelli registrati nel lavoro di Schiena. È stato possibile concludere che la tecnica proposta di dip-spin coating ha consentito di superare i limiti presenti nella tecnica del casting, dovuti all'utilizzo di stampi 3D.

	Natural Aortic Valve [99]	Schiena Model [2]	Phantom Model
Free Margin Thickness [mm]	0.87 ± 0.27 , 20-59 years 1.42 ± 0.51 , ≥ 60 years	1	0.79 ± 0.03
Belly Thickness [mm]	0.41 ± 0.09	1	0.69 ± 0.02

Tabella 1 Confronto tra i valori medi e deviazione standard relativi allo spessore dei lembi di una valvola aortica fisiologica, di un lavoro precedente e del modello realizzato.

Valvola Aortica Calcificata

Altro beneficio apportato dall'introduzione del presente metodo di produzione è stata la possibilità di includere depositi calcifici nei lembi valvolari, senza compromettere lo spessore delle cuspidi, quindi rimanendo nei range di valori evidenziati dalla letteratura [7]. 8 modelli di valvole calcificate sono stati ottenuti, differenti per tipologia di pattern incluso: pattern radiale (*radial pattern*) o pattern ad arco/arco parziale (*arc/partial arc*) (Tabella 2). La configurazione preliminare del pattern (*preliminary pattern configuration*), consistente in depositi stampati 3D di spessore 1 mm, ha dato risultati in spessore totale del lembo consistenti con la letteratura. I pattern parametrizzati (*parametrized pattern configuration*) sono stati standardizzati nella geometria in modo da migliorare l'adattamento del pattern con la forma della cuspidi e modificare agevolmente il grado di stenosi.

Tabella 2 Esempi di modelli di valvola aortica calcificata.




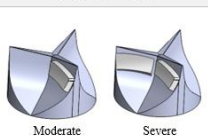
Radice Aortica

I prototipi realizzati di AR hanno potuto validare la fattibilità del processo multi-step presentato. Le configurazioni preliminari e finali ottenute (*preliminary and final ARs*) hanno potuto includere le CAV, il tratto di radice aortica (dall'annulus alla giunzione sino-tubulare, comprendendo i seni di Valsalva), i tratti a monte e a valle della valvola (Inflow and AA tracts) e due estensioni, consentendo la connessione del modello al set-up idraulico. Le dimensioni risultanti per entrambe le configurazioni sono mostrate in Tabella 3 e sono state dimostrate consistenti con la letteratura.

	Preliminary AR	Final AR
Annulus and STJ	23 mm	26 mm
Diameters	(min value from liter.)	(average value from liter.)
VS Maximum Diameter	30 mm	35 mm
AR	16.18 mm	16.8 mm
Inflow + AA tracts	20 mm	70 mm
Total Height of the Model	60 mm	110 mm
Wall Thickness	5 mm	2.5 mm
Commissure Geometry	Rectangular	Triangular

Tabella 3 Confronto dimensionale tra le due configurazioni di AR.

La zona a forma triangolare a livello commissurale nella configurazione finale (Figura 11) ha consentito una più ampia zona di fusione tra i foglietti valvolari e la parete della radice aortica, risultando

	Preliminary Pattern Configuration	Parametrized Pattern Configuration
Radial Pattern	 Moderate Severe	 Moderate Severe
Thickness [mm]	2.34 ± 0.29	Hypothetical 2.58 mm (0.79 mm 1 st dip-coating + 1 mm calc + 0.79 mm 2 nd dip-coating)
Partial Arc / Arc Pattern	 Moderate Severe	 Moderate Severe
Thickness [mm]	2.76 ± 0.10	Hypothetical 2.58 mm (0.79 mm 1 st dip-coating + 1 mm calc + 0.79 mm 2 nd dip-coating)

dunque incrementata la stabilità della struttura. La AR finale ha presentato inoltre tratti a monte e a valle della valvola (Inflow-AA tracts) più lunghi; ciò consente l'impianto di protesi valvolari di differenti dimensioni e designs di TAVI, visto lo scopo per il quale è stato progettato.

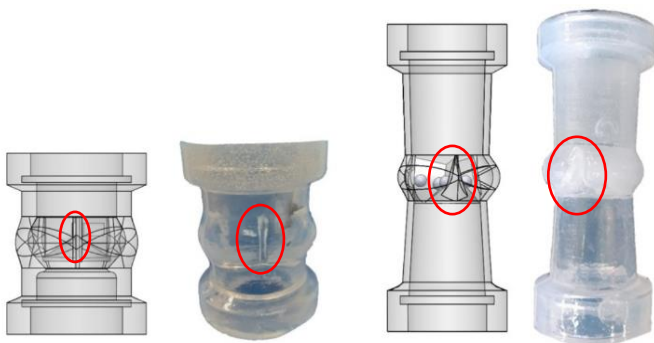


Figura 11 È evidenziata la zona relativa alle commissure nei modelli CAD e siliconici, per AR preliminari e finali.

CONCLUSIONI E SVILUPPI FUTURI

In questo lavoro di tesi è stato sviluppato un protocollo per la realizzazione di un modello polimerico paradigmatico di valvola aortica calcificata, finalizzato alla formazione pratica dei chirurghi interventisti nelle terapie transcatertere, utilizzando materiali e tecnologie di fabbricazione convenienti e facilmente accessibili.

La tecnica di dip-coating ha permesso la realizzazione di lembi valvolari sottili, i cui valori di spessore sono comparabili a quelli

delle valvole naturali e l'incorporazione di patterns di calcificazione progettati ad hoc. Lo Spinning Device progettato ad hoc ha accelerato il processo di fabbricazione, consentendo la produzione contemporanea di 4 valvole e ha fornito un metodo per ottenere valori uniformi di spessore nei modelli di lembi in silicone. L'ottenimento di stampi interni su misura per qualsiasi tipo di modello di calcificazione è stato possibile grazie allo sfruttamento della resina epossidica. La tecnica del casting di silicone ha fornito forme anatomiche flessibili, caratterizzate da geometrie complesse e ha consentito la fusione tra le cuspidi e la radice aortica a livello delle commissure e dell'annulus valvolare.

Tuttavia, tale lavoro ha presentato alcuni limiti. La stabilità dei depositi di PLA nei lembi in silicone deve essere valutata mediante test emodinamici.

La riproduzione delle caratteristiche meccaniche del tessuto valvolare naturale e dei depositi calciferi non era l'obiettivo della tesi, ma il suo adempimento potrebbe ampliare il campo di applicazione del metodo di produzione proposto, anche per il collaudo di nuovi dispositivi o per la pianificazione pre-procedurale.

Sorta Clear 18 ha mostrato una buona visibilità all'interno del modello. Poiché i modelli sono progettati per il training delle terapie transcatertere, è necessario valutare

la compatibilità con le tecniche standard di imaging, come l'ecocardiografia o i raggi X / fluoroscopia. La letteratura ha evidenziato un coefficiente di attenuazione del PLA che lo rende compatibile con l'imaging a fluoroscopia, inoltre un PLA specifico, la cui matrice è arricchita di ceramiche ad alta densità, potrebbe fornire una migliore visibilità ai raggi X.

In conclusione, i risultati ottenuti dimostrano la fattibilità del processo di fabbricazione e il rispetto delle specifiche di progettazione iniziali. Quindi, questo lavoro potrebbe essere considerato un contributo allo sviluppo di modelli di supporto alla formazione interventistica di studenti e cardiologi. Potrebbe essere considerato anche nella pianificazione pre-procedurale, qualora il presente metodo di fabbricazione fosse applicato a geometrie paziente-specifiche.

INTRODUCTION

Valvular Heart diseases (VHDs) contribute to more than 42 000 deaths every year in the US, due to aortic sclerosis or stenosis (AS), mitral valve regurgitation, mitral valve prolapse, mitral annular calcification, rheumatic heart diseases [7].

Aortic stenosis is the most common VHD in the developed countries [1] [8] and it occurs mainly in elderly patients with a prevalence rising from 0.7% in patients aged 18-44 years, to 13% in patients over 75 years [9]. The gold standard as curative treatment of valvular diseases is surgical valve replacement or repair through sternotomy [10]. The promising technologies provide a reduction of the surgical trauma and facilitate the post-operative course [11]; however it implies temporary stop of the heart and the use of artificial heart-lung bypass machine; occurrence of infections and long surgical intensive care stay are also registered [12]. The just mentioned implications of common surgery imply a non-negligible percentage of patients, that are excluded from surgery. The main reason lies in the patient' health conditions, that expose him to high risk of mortality due to the intervention itself. The Euro Heart Survey [8] demonstrated that 31.8% of VHD patients is judged high-surgical-risk because of elder age and presence of comorbidities. The number of high-risk patients it's also rising, because of the projected aging of the population and associated increase in comorbidities [8][13]. Examples of comorbidities that prevent open-heart surgery in case of VHD are: coexistence of coronary artery disease, recent myocardial infarction, left ventricle and neurological dysfunction, extra-cardiac disorders as chronic obstructive pulmonary pathology, renal malfunction, smoking, hypertension, and diabetes.

Transcatheter treatments are a worthwhile option to enable high-surgical-risk patients to undergo cardiac interventions. They consist in the delivery of a therapeutic device by a catheter introduced from venous or arterial access (i.e. femoral artery) under medical guidance, using a delivery system manually controlled. The therapy differentiates from open surgery also because the procedure is performed on the beating heart and there is a different interaction of the implanted device with the cardiac structures. For example, in the treatment of valvular heart diseases with surgery the prosthetic valve is sutured, replacing the calcified leaflets, which are cut out; in transcatheter therapies the device is deployed in the valve septum, anchored through a stent, pushing the calcified leaflets aside, without removing them. These less invasive procedures showed reduced operative durations, less need for blood transfusion and respiratory support and faster recovery periods[14] with respect to the conventional surgical therapies. The first

transcatheter aortic valve implantation (TAVI) for aortic stenosis treatment was performed in 2002 in France[15]. Since then, there has been a revolution in TAVI technology [16]: improvements in the prosthetic valve design led to a simplification of the procedure, reduced complications and improved procedural outcomes, allowing a worldwide diffusion of the approach.

On the other hand, percutaneous techniques still present unresolved complications that limit its application in patients with medium and low operative risk [17]. Severe consequences of a procedural error could be vascular damage, brain stroke, heart attack, coronary obstruction, complications in the device conduction and paravalvular failure of the prosthesis. They could occur due to an incorrect estimation of the device size (when underestimated it can lead to valve regurgitation or prosthesis dislocation, when overestimated to native valve rupture) but also because of the limited vision of the interventional field, since the access to the cardiac chamber is reduced [18]. Hence the need of practical preparation of interventional cardiologists on training devices is required, in order to improve procedure performances [19]. Also norms regulate this need: in April 2004 Food and Drug Administration (FDA) emitted the requirement of developing simulator-based training programs, to develop and demonstrate physician's competence on vascular devices, before approving any therapy [20].

Studies highlighted how a standardized interventional practice, in transcatheter procedures, can lead to an exponential rise in the initial phase of the learning curve, and influence the increasing of technical proficiency, in terms of reduction of intraprocedural times, radiation doses and contrast volumes [2][19]. The relevance of the learning curve cannot be ignored, since studies showed that increasing the training on cardiac devices improved short- and long- term outcomes [21].

In this scenario, artificial simulation models, e.g. synthetic phantoms, emerge as an important tool for the training. It reduces the exploitation of cadavers and animals and improve the performances in the operating room [22]. Learn in a more realistic environment, through a tactile phantom that simulate the pathology, obtained with rapid prototyping techniques, could lead clinicians to a better consciousness of the pathology and to an abatement of the unsuccess due to improper errors [23]. Therefore, phantoms can be so relevant for clinicians practicing because devices and protocols properly engineered can be a cost-effective support to the common training programs, performed directly on real samples [24] with complex geometries.

Two categories of training simulators can be identified: tests benches including biological components (e.g. porcine or bovine organs), or fully artificial simulators. The first type, ex-vivo

simulators, can combine the anatomical similarity with the appropriate functionality, particularly when providing physiological flow and pressure. These models are widely used to test the efficiency of the transcatheter therapies [25]. However, ex-vivo platforms have some disadvantages: challenges in reproduction of pathological conditions (e.g. structural and morphological changes in heart valves in pathology), costs related (generally single use of biological samples), need for specific know-how in simulator management (e.g. difficult connection between artificial components and biological tissue in the bench test) and ethical issues. They also have challenges regarding intra- and inter- species anatomical variability and problems related to logistics, maintenance and disposal [26]. Fully synthetic phantoms can allow to reproduce anatomical structures, in a paradigmatic or patient-specific models, depending on whether the component is designed through general geometric modeling or is obtained from the segmentation of clinical images. Phantoms can be realized in flexible and transparent materials through additive manufacturing techniques (e.g. 3D printing, casting, dip-spin coating), enabling the comprehension of the interaction between the geometry of the phantom and the implantable device, during clinical trainings. Patient-specific models are generally used for pre-procedural planning, because the high fidelity of anatomical reproduction allows to hypothesize operation outcomes (e.g. potential regurgitation flow [27] and prosthetic valve anchoring [28]); paradigmatic phantoms can be optimized in terms of design process and realization work-flow, in order to reduce costs and increase the availability for adequate realistic training, since they allow to simulate the therapy under realistic fluid dynamic conditions, once they are incorporated into test benches and subjected to pulsatile flow. However, at the moment, there is a lack of functional models which feature pathological heart components, in particular aortic valve stenosis [29] and that could be used for interventional cardiologists' training.

The aim of the thesis is the identification of a protocol for the development of functional aortic valve calcified models for application in clinicians training of TAVI procedures. In particular, the work will include the design of pathologic aortic valve silicone models, whose geometry is derived from anatomical data obtained from literature. The method for the obtainment of different grades of stenosis severity is explained, and the rapid prototyping manufacturing technologies, exploited to reach the goal.

This work is carried out in the laboratory of μ BS LAB of the Department of Electronics, Information and Bioengineering of Politecnico of Milano.

The script is divided into 5 chapters:

- **Chapter 1:** heart anatomy and physiology are defined, with particular focus on aortic valve anatomy, pathologies and most common treatments.
- **Chapter 2:** a scenario of the state of art of calcific aortic valve models are presented. Methodologies and technologies used by other authors are analyzed, keeping into consideration pros and cons, in order to outline a course of action for the present work, for the realization of functional pathological aortic valve models.
- **Chapter 3:** technologies and materials needed for the design and the manufacturing of the calcified aortic valve model is illustrated. After presenting a general workflow, the specific protocols for the realization of each component are described in detail.
- **Chapter 4:** presentation and discussion of the obtained models, compared with literature and previous works.
- **Chapter 5:** with respect to the obtained results, conclusions, main limitations, and further developments are outlined.

1. ANATOMICAL AND PATHOLOGICAL BACKGROUND

In this section, general concepts of the heart anatomy are examined. In particular, the aortic valve is investigated since it is the focus of the present work. In conclusion the pathological physiology is described together with the main interventional therapies, focusing primarily on the most innovative treatments.

1.1. Anatomy of the Heart

The heart is located in the thoracic cavity between the breastbone and the backbone. It has four chambers that are separated into right and left compartments by the septum as shown in Figure 12 [30]. Each side has an upper chamber and a lower chamber called atrium and ventricle, respectively. Further, the heart is called dual pump since the two sides of the heart work as two distinct pumps.

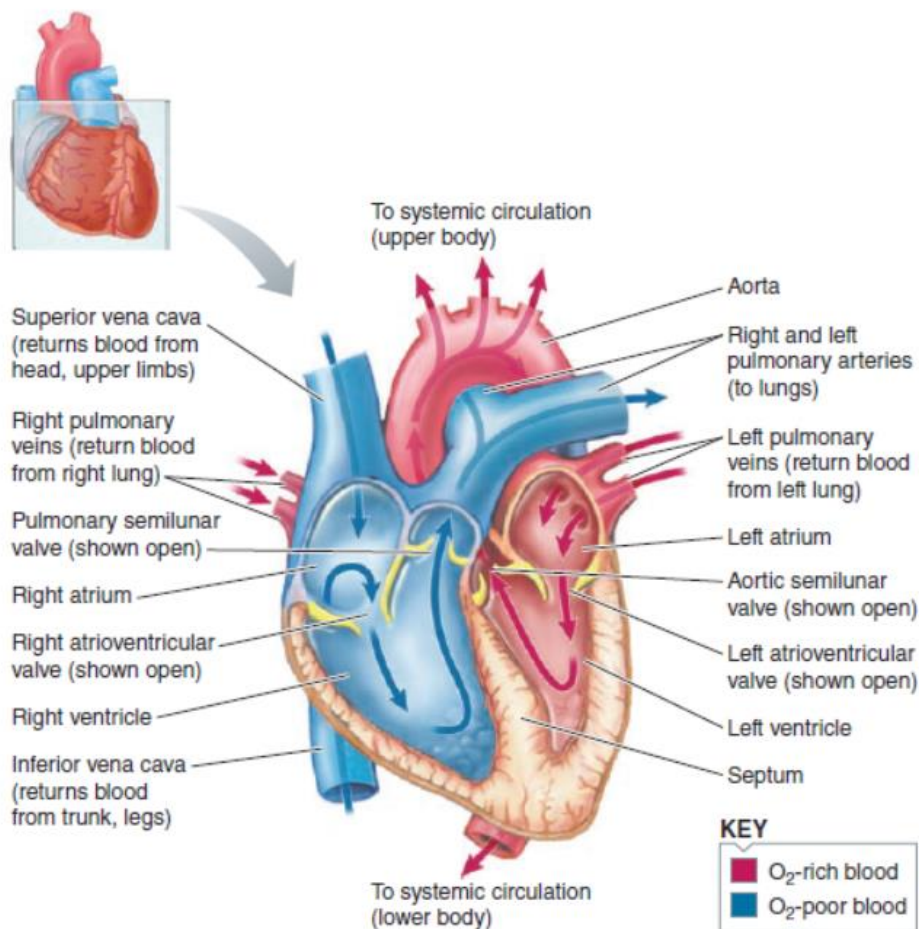


Figure 12 Pulmonary and Systemic Circulation blood-flow ways in the heart [25].

Two are the main functions of the heart: one is pumping of the less-oxygenated blood to lungs, where carbon dioxide and oxygen exchange occurs at the level of capillary vessels and increases the oxygen content in the blood. The second is receiving oxygenated blood to pump to all body organs, in order to deliver oxygen and nutrients. Therefore, these two purposes of heart refer to two main blood circulations in the body: **Pulmonary Circulation** and **Systemic Circulation** (Figure 12).

Pulmonary Circulation includes the right side of the heart, pulmonary arteries, and pulmonary veins. The right atrium collects carbon dioxide dominant blood from superior and inferior vena cava then sends it to the right ventricle [31]. The right ventricle pumps the oxygen-poor blood through pulmonary arteries to the lungs. The pulmonary blood flow has been illustrated in the order of blue arrows in Figure 12.

Tricuspid Valve is one of the atrioventricular valves that is located between the right atrium and right ventricle. When the atrial pressure exceeds ventricular pressure, the tricuspid valve opens and the blood flows into the right ventricle [31]. The valve closes during ventricle contraction and prevents blood to flow back in the atrium [31]. The tricuspid valve is composed of three distinct cusps, three papillary muscles that are connected to the leaflets of the valve with chordae tendineae as observed in Figure 12 and the annulus medially located in the ventricle septum [31]. These three characteristic cusps are named as anterior, posterior and septal.

Pulmonary Semilunar Valve opens when the right ventricle contracts and blood moves to the pulmonary trunk. The closure of the valve occurs when the pulmonary trunk pressure exceeds right ventricular pressure corresponding to the diastole state. Anatomically, the three cusps of the valve have a semilunar shape. The leaflets are attached to the annulus of the valve and these three cusps are named as anterior, septal (left) and right [31].

Systemic Circulation involves, in contrast to the pulmonary circulation, the left atrium and ventricle, pulmonary veins and the aorta. The oxygen-rich blood arrives in the left atrium through pulmonary veins exiting from the left and right side of the lung. Subsequently, the blood flows into the left ventricle where impels the blood to the rest of the body [31]. The red arrows in Figure 12 showed the direction of blood flow on the left side of the heart.

Bicuspid (Mitral) Valve is placed between the left atrium and left ventricle. The valve opens and closes at the same principle as the tricuspid valve does. However, it consists of two leaflets (named anterior and posterior), two papillary muscles, two chordae tendineae and annulus. The chordae

tendineae are a conjunction that attaches papillary muscles and leaflets. Also it prevents the cusps from opening into the atria [30], [31].

Aortic Valve has three leaflets and semi-lunar shape, like the pulmonary valve. The opening is observed when the left ventricle pressure exceeds the aortic pressure and the closure occurs for the left ventricle filling. However, due to the coronary artery existence in the aortic root, the leaflets, attached to the annulus, are named as right coronary, left coronary and non-coronary leaflets [30].

Due to the driving force, generated by the cardiac muscle, the blood can flow within the heart (Figure 12). Therefore, the heart wall is composed of cardiac muscles primarily and has three layers. The inner layer is endothelium; the middle layer is myocardium; the external layer is epicardium[30].

1.2. The Cardiac Cycle

The rhythmical alterations in the electrical activity of cardiac muscle cells are responsible for two phases: systole (contraction and ejection) and diastole (relaxation and filling), also known as the cardiac cycle [30]. The contraction of muscle cells in the heart is provided by electrical excitation of cell membranes, which govern the mechanical events presented in Figure 13.

The mechanical events during the cardiac cycle are explained only considering the left side of the heart. However one should be aware that the same events are equivalent to the right side of the heart, only with lower pressures [30]. There are four main mechanical events in the cardiac cycle: isovolumetric left ventricular contraction, left ventricular ejection, isovolumetric left ventricular relaxation, and left ventricular filling.

Isovolumetric Left Ventricular Contraction: The event occurs once the mitral valve closes and the ventricle systole is triggered. Therefore, it is described as the time interval between the onset of the ventricle systole and the opening of the aortic valve. Due to the unchanged volume but increasing pressure in the ventricle, it is called isovolumetric (invariant volume) [30][32].

Left Ventricular Ejection: When the pressure of the left ventricle exceeds aortic pressure, the aortic valve opens and the blood flows from the ventricular chamber to the aorta. Also, the ejected blood volume during the ventricle contraction is described as the stroke volume [30].

Isovolumetric Left Ventricular Relaxation: Once the aortic valve closes and the mitral valve does not open yet, the ventricular pressure decreases with unchanged volume in the ventricular chamber. The event ends when the atrium pressure exceeds the ventricle pressure.

Left Ventricular Filling: It starts when the mitral valve opens. Therefore, the blood can flow from the atrium to the ventricle. As a result, the ventricle is filled with blood.

Furthermore, the amount of blood that circulates through the pulmonary circulation and systemic circulation is similar. The cardiac output of the heart depends on the heart rate and the stroke volume. In the rest condition, the heartbeat is around 70 beats per minute, and the stroke volume is around 70 ml [30]. Therefore, approximately 5 liters of blood are pumped out from the heart in one minute (Cardiac Output).

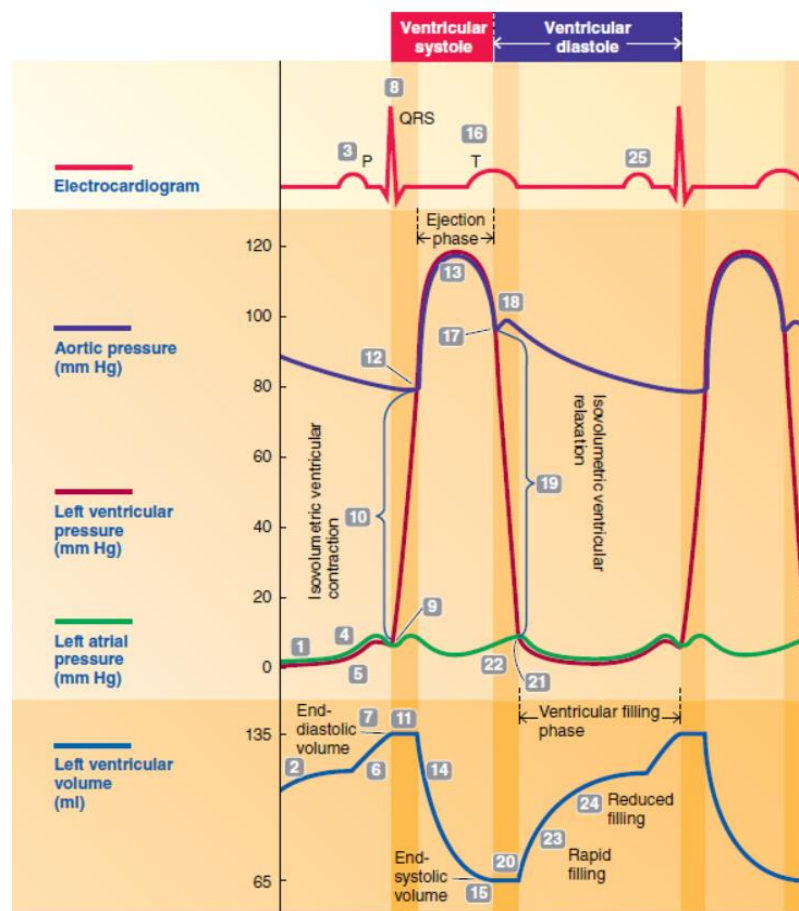


Figure 13 The graph shows the various events which occur simultaneously during an entire cardiac cycle. Three rows are separated concerning changes observed in the electrocardiogram; aortic, left ventricular and left atrial pressures; left ventricular volume [25].

1.3. Anatomy of the Aortic Root and the Aortic Valve

In this section the aortic root (AR) will be analyzed to describe the anatomical, geometrical properties and its purposes in the heart.

The aortic root is defined as connection structure between ascending aorta and left ventricle. The superior border of the AR is determined as sinotubular junction (STJ) and the inferior borderline, called basal-ring, is located in the aorto-ventricular transition level [33]. The predicted length of AR, individuated in the area from basal ring to STJ, measures from 20 to 30 mm. AR comprises of four distinct components: three cusps, three sinuses of Valsalva, three interleaflet triangles and two coronary artery ostia. The AR surrounds the aortic valve (AV) and supports the leaflets [34].

AV provides one-way blood flow from the left ventricle to the ascending aorta. The valve structure is made of three leaflets and annulus. The leaflets are named concerning the existence of coronary arteries: right-coronary, left-coronary, and non-coronary[34].

Sinotubular Junction

STJ is a circular structure of elastic composition, that separates the aortic root from the ascending aorta (Figure 14). It can also be defined as the circumferential integration of leaflets commissures, therefore any enlargement causes impaired valvular opening and closure [34][35].

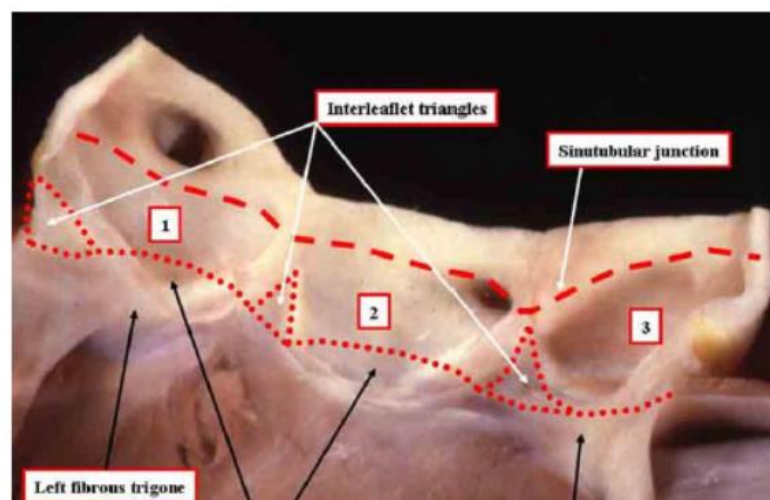


Figure 14 The aortic root has been cut from the fibrous tissue located in between the cusps of the aortic and mitral valve. The level of sinotubular junction has been identified by the red dashed line. The interleaflet triangles and ventriculo-arterial junction has been represented by the red dotted line [29].

Interleaflet Triangles

As indicated in Figure 14, the interleaflet triangles are the continuous fraction of fibrous tissue within the aortic root, grounded from the beginning of the left ventricle outflow tract till commissures, where semilunar fusions of the leaflets are observed primarily [27]. There are three interleaflet triangles between left-noncoronary, right-noncoronary and right-left sinuses. The first triangle has a linkage with a mitral valve leaflet in the fibrous curtain, the second also has the fibrous membrane continuity within the septum however the third one, instead, has the only muscular continuity, which extends to the ventricle [36].

Semilunar Attachment of Leaflets

The leaflets are anchored to the aortic root from the semilunar attachments within the sinuses of Valsalva. As seen in Figure 15, the fibrous tissue spans through the leaflet attachments until its hinge points [27]. However, only two sinuses, which are the origin of coronary arteries, have support of ventricular musculature, instead the non-coronary sinus has fibrous tissue support (Figure 15) [26]. Furthermore, these attachments of leaflets within the sinuses are responsible for the hemodynamic property of the aortic valve [26]. The superior parts of the leaflet attachments are subjected to aortic pressure and the inferior parts of the attachments are subjected to ventricular pressure [26] [37].

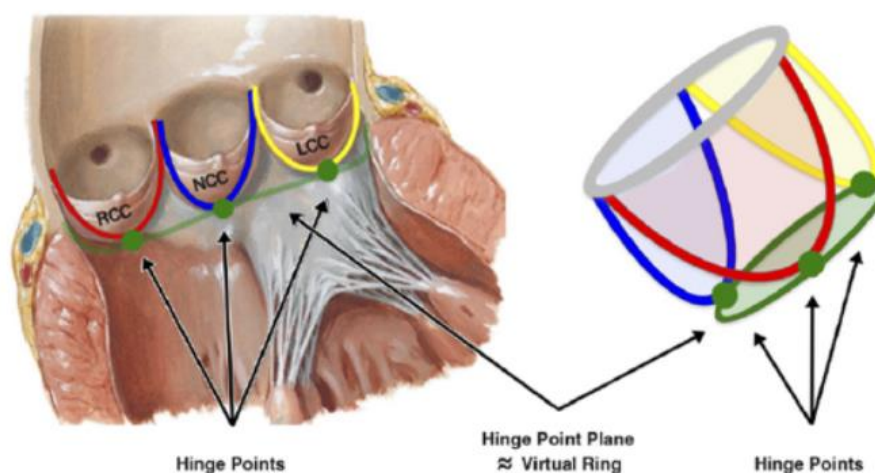


Figure 15 Semilunar shape of aortic leaflets and their hinge points [27].

Sinuses of Valsalva and Coronary Arteries

The sinuses of Valsalva are the pioneer portion of the aortic root as a supportive structure for the aortic valve [26]. Their base captures the hinge points of the leaflets and its musculature tissue reaches till right above the leaflets [27]. As shown in Figure 15, three sinuses have a concave shape, resulting in circumferential enlargement for annulus and are named according to the position of the coronary arteries: Right Sinus, Left Sinus and Non-Coronary Sinus [27]. The blood fills three sinuses of Valsalva during the cardiac cycle, therefore the accumulated blood in the left and right valvular sinuses, is ready to flow through the coronary arteries to deliver blood into myocardium [27]. Furthermore, the wall thickness in the sinus of Valsalva is comparatively smaller than the ascending aorta wall [38] (Figure 16).

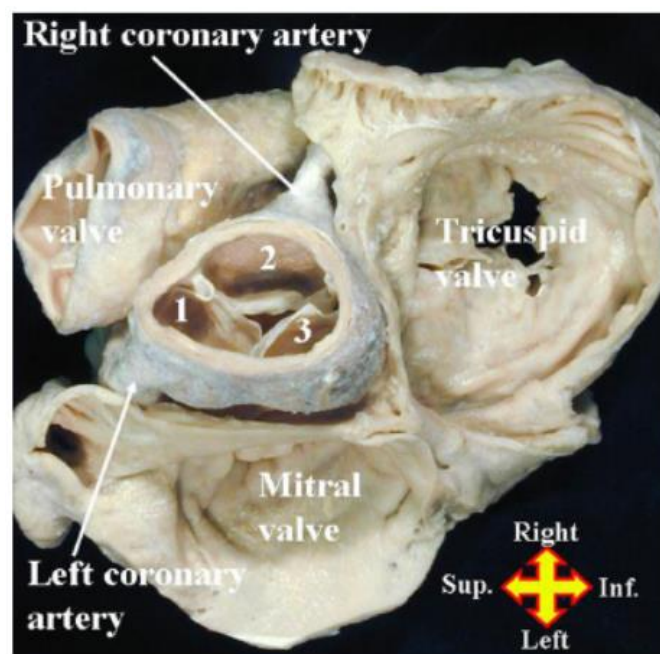


Figure 16 The top view of the transected aortic root from the STJ illustrates which two valvular sinuses are the origin of the coronary arteries and are entitled as the right and left coronary aortic sinuses. The third sinus is called as a non-coronary sinus since there does not exist a coronary artery. Also AV is observed with its closed cusps and named as the same principle with the sinuses [26].

Annulus

Aortic annulus refers to the circular shape between the ventricular outflow tract and the end of the AR[25]. An overlapped area is identified by two virtual rings, as shown in Figure 17. One is called

Ventriculo-aortic junction (VAJ) which crosses semilunar attachments of the leaflets. The second one surrounds the nadir points of the leaflets and called as basal-ring [39].

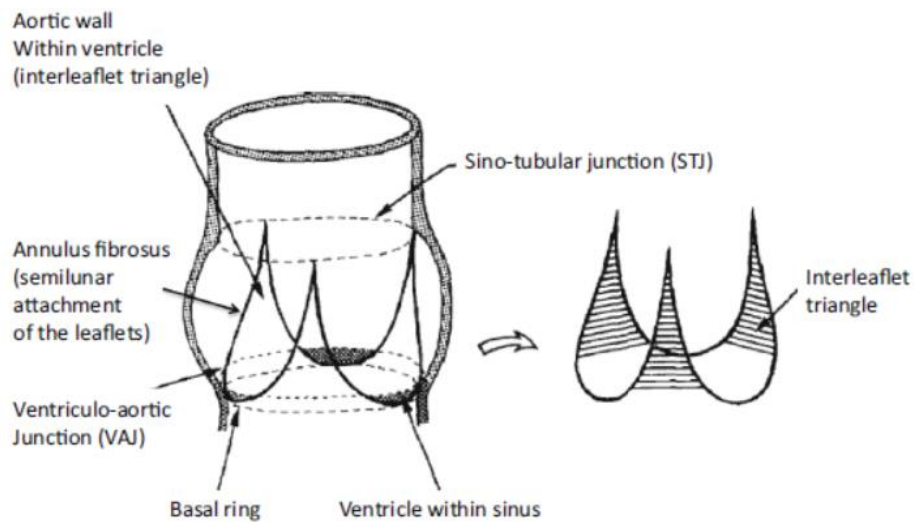


Figure 17 Aortic Root and Imaginary Rings [31].

Geometry

The geometrical definition of the AR can be simplified and described at three levels: aortic valve annulus, sinuses of Valsalva and sinotubular junction [40]. The geometry of these levels can be determined by multislice computed tomography (MSCT) as shown in Figure 18 and from their analysis it is possible to extrapolate the information summarized in Table 4.

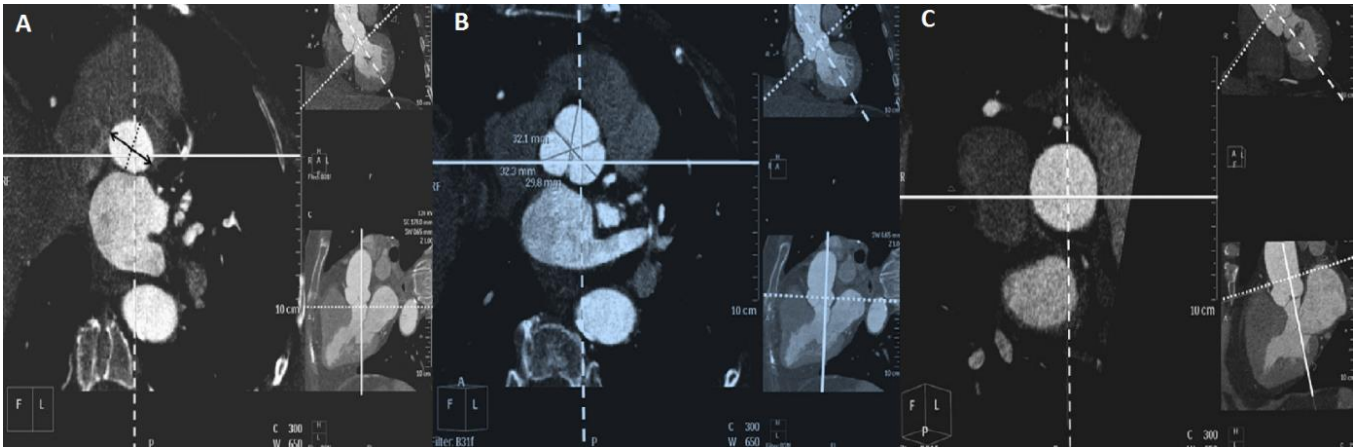


Figure 18 The image of the Aortic Annulus (A), Sinuses of Valsalva (B) and Sinotubular Junction (C) is obtained axial in-plane. In image A, black arrow and dashed lines showed maximum and minimum diameters of the annulus (D_{max} and D_{min}). In image B, the dashed perpendicular line has been ascended to the deepest level of sinuses of Valsalva. Lines are drawn from each commissure till the corresponding cusps. In the image (C), the dashed perpendicular line reached ascending aorta.[35]

Table 1 summarizes the geometry of the physiological aortic root based on medical imaging techniques, such as or on direct measurement.

Articles	[33]	[41]	[42]	[43]	[40]	[29]	[44]
Number of cases	25	50	150	108	52	19	19
Data Acquisition	DM	TTE	MSCT	MDCT	MSCT	DM	DM
Diastole	-	+	+	+	+	-	-
Dimensions							
AV Annulus Diameter [mm]	22.02	22.9±3.9	26.3±2.6	27.05(avg)	24.355(avg)	24.7	26
Max	-	-	-	30.1±3.0	27.85±2.82	-	-
Min	-	-	-	24.0±3.1	20.86±1.81	-	-
STJ Diameter [mm]	20.97	24.0±3.6	28.1±3.1	31.5±3.9	27.78±3.55	23.6	22
VS Diameter [mm]	-	30.7±4.2	32.3±3.9	35.4±3.8	29.87(avg)	-	-
Left	-	-	-	-	29.28±3.23	-	-
Right	-	-	-	-	30.00±3.11	-	-
Non-Coronary	-	-	-	-	30.33±3.02	-	-
Distance between STJ-AV [mm]	-	-	20.3±3.1	-	-	21.8	-
Distance between AV-VS max level [mm]	-	-	17.2±2.7	-	-	-	-
Sinuses of Valsalva Height [mm]							24
Left	17.45						
Right	17.68						
Non-Coronary	19.45						

Table 4 Healthy aortic root dimensions with the tricuspid valve. Direct Measurements (DM), Trans-esophageal Echo (TEE), Multislice Computed Tomography (MSCT), and Multidetector Row Computed Tomography (MDCT). AV: Aortic Valve, STJ: Sinotubular Junction, VS: Valsalva Sinuses. Avg: average value.

1.4. Aortic Valve Pathologies

The prevalence of AS and severe AS among the elderly (over 75 years) is 2.5%, and 13.3%, respectively [45], taking into consideration a study among the general US population. These data are continually rising, since the increasing life expectancy of Western population favors the progression of degenerative cardiovascular diseases [46].

The pathology can be congenital (e.g. bicuspid aortic valve) or it can be acquired during the life.

The etiology of the acquired valvular pathology is mostly degenerative, but can be also due to rheumatic, endocarditis (Acute Articular Rheumatism and Rheumatoid Arthritis), inflammatory or ischemic causes. They can undermine the functional and anatomical integrity of the valves, causing (Figure 19):

- Stenosis: the incomplete valve opening, due to calcification of the leaflets. Other effects are the thickening of the leaflets and the decrease of the effective orifice area (EOA). Also, the blood flow and relative hemodynamics are severely altered, causing a loss in the mechanical performance of the valve.
- Regurgitation: the inability of the valve to maintain competence during diastole, due to tissue dilation, resulting in the dislocation of the cusps and in a backflow of blood through the valve.

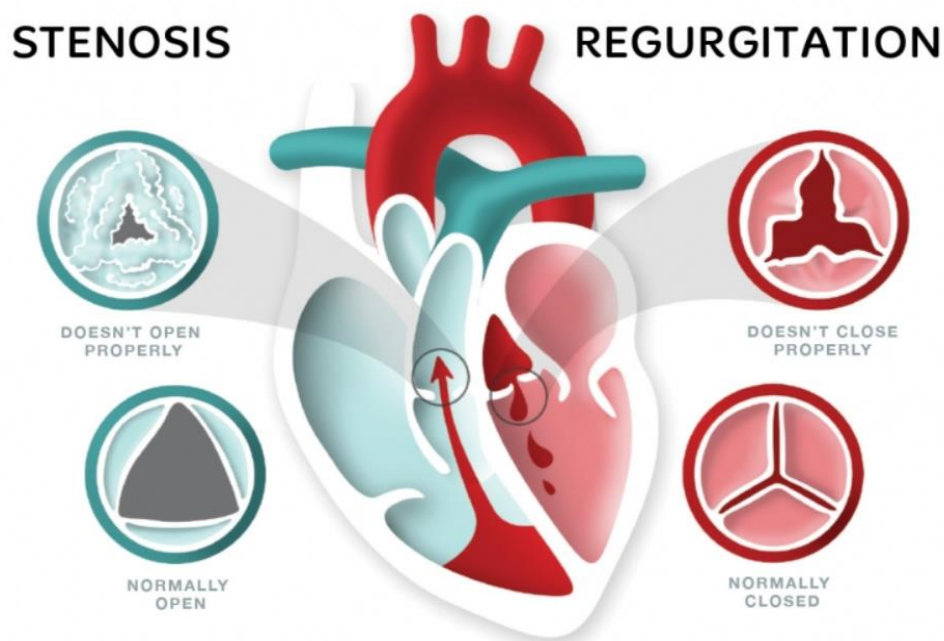


Figure 19 Schematic representation of the main valvular diseases.
www.heartfoundation.org

1.4.1. Aortic Valve Stenosis

Calcific AS is featured by fibrocalcific remodeling process of valve leaflets and annulus. The progressive stiffening of the leaflets can be traced to the combination of two main factors: the chronicle pathophysiological process of calcific depositions, compounded by the mechanical stresses among the valve tissues. The sum of the causes leads up to burdensome aortic valve opening, bigger trans-valvular head losses then in physiological case, hypertrophic response of the left ventricle and aortic insufficiency, which may culminate in heart failure or syncope.

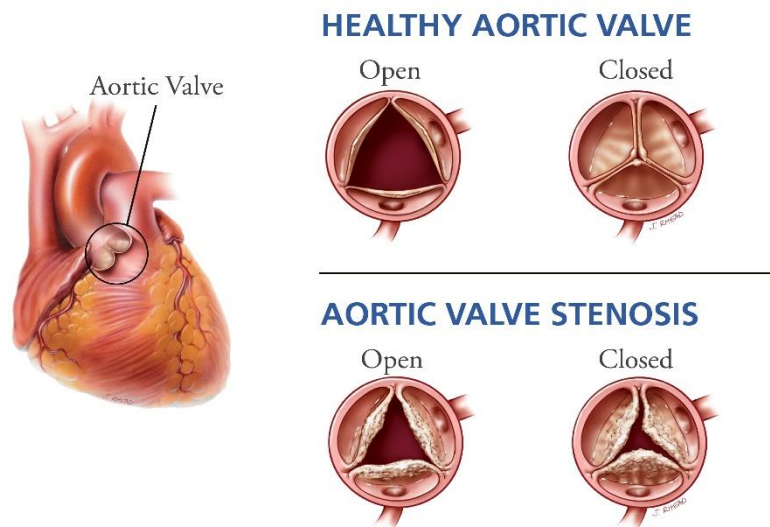


Figure 20 Comparison between the physiological and the stenotic aortic valve in the opened and closed configurations. In the healthy valve, the leaflets are thin and properly sealing. Below the stenotic calcified AV. The tissue is thicker, stiffer and closure is not perfect, resulting in regurgitation during the diastolic phase. www.heartfoundation.org

As it is represented in Figure 20 the physiological valve has a circular orifice and the leaflets can completely open and close. It is evident how the calcified stenotic valve influences the orifice area, hence the increasing pumping power of the heart, in order to provide an adequate cardiac output to the systemic circulation. As consequence, the left ventricle (LV) is overloaded, the ventricular systolic pressure is augmented, and it will lead to heart walls hypertrophy and systolic dysfunction [47]. Instead, in the closed configuration, the valve is not perfectly sealing, allowing regurgitation of blood back in the LV (i.e. insufficiency).

Through the analysis of echocardiographic (ECG) data, it is possible to evaluate the grade of severity of the pathology. ECG shows the stenosis progress, level of valve obstruction and presence of calcification of the cusps. In addition, through eco-doppler techniques is it possible to highlight eventual alterations in the valvular hemodynamics. The most used hemodynamic parameters, that allow to distinguish different grades of stenosis severity [47] are :

- Effective orifice area (EOA=3.0-4.0 cm², in physiological case [48]), determined by using either the Gorlin formula during cardiac catheterization or the continuity equation during Doppler echocardiography [49].
- Mean pressure drop ($\Delta P < 5\text{mmHg}$, in physiological case [48]), determined by plotting the curve that averages the instantaneous transvalvular pressure gradient for each instant of the ventricular ejection period.

- Maximum velocity at systolic peak ($V_{max} = 1\text{m/s}$, in physiological case), determined by eco-doppler as maximum value of the blood flow during systole.

As established by American Heart Association, the assessment of the grade of stenosis can be performed following parameter in Table 5.

Light	EOA > 1,5 cm²	$\Delta P < 25\text{mmHg}$	$V_{max} < 3\text{m/s}$
Moderate	$1 < \text{EOA} < 1,5 \text{ cm}^2$	$25 < \Delta P < 40 \text{ mmHg}$	$3 < V_{max} < 4 \text{ m/s}$
Severe	$\text{EOA} < 1 \text{ cm}^2$	$\Delta P > 40 \text{ mmHg}$	$V_{max} > 4 \text{ m/s}$

Table 5 Schematic resume of the values used to define the grade of stenosis. EOA: effective orifice area, ΔP : pressure drop, V_{max} : maximum velocity at systolic peak.

The pathophysiological process

AS is a chronicle inflammation process, which occurs as the result of a damage of the endothelial layer of the valve leaflets. It is influenced by the complex match between genetics and environment, resulting in gradual accumulation of calcium and lipoprotein deposition in the valve leaflets. This complex cellular process is actively regulated by the valve interstitial cells (VICs)[50] and it is possible to recognize two main phases: the initiation phase and the propagation phase.

As shown in Figure 21, the initiation phase is characterized by a damage of the endothelial layer due to a degeneration of the mechanical stress, called shear stress. It causes the low-density lipoprotein and lipoprotein(a) [Lp(a)] infiltration and deposition in the subendothelial fibrosa layer, where they undergo oxidation. Once oxidized they are cytotoxic and stimulate osteogenic differentiation and fibrocalcific remodeling of the tissues. Also, the recruitment of chronic inflammatory mediators signs the start of the chronicle inflammation: T cells, monocytes and macrophages are involved in the calcific processes of the valve. Early recognition of this phase can reduce the risk of AS, thanks to lipid-lowering drugs. At this point, the propagation phase can be defined. Disorganized collagen is produced, leading to fibrosis, that is a thickening and stiffening of the tissues. The mismatch generated by the different stiffening of the endothelium, brings to increased mechanical stress, cells apoptosis and osteogenic differentiation of the

interstitial cells, which activate osteoblast-like cells. They are responsible of a further generation of calcifying extracellular vesicles, the microcalcification of the collagen matrix.

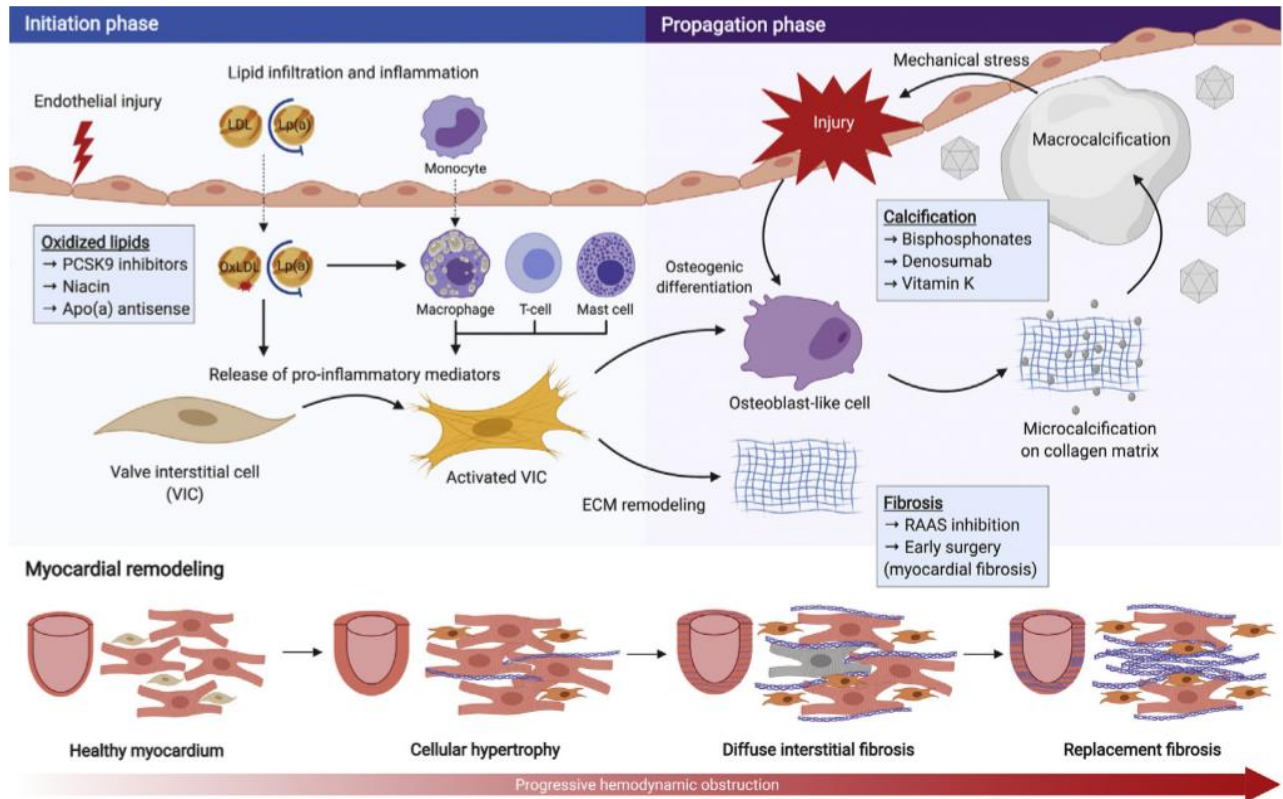


Figure 21 The pathogenesis of Aortic Stenosis (AS) [45]

These processes are demonstrated by PET (Positive Electrons Tomography) /CT (Computed Tomography) imaging of the aortic valve and generally move from the valvular cusps till the body of the leaflets, resulting in a thickening and stiffening of the valve tissue that decrease the orifice area and the opening/closing velocity during the cardiac cycle.

The mechanical stress among the valve

It is known that the hemodynamic load of the circulatory system depends from three fundamental physical components, which are: blood velocity (kinetic energy), heart frequency (pulsatility) and blood pressure (potential energy). The blood flow continuously exercises hemodynamic forces, called wall shear stresses (WSS) sensed by the endothelial layer. A laminar shear stress promotes the release of factors that inhibit coagulation and leukocyte migration; a low shear stress ($Re=200$) causes turbulent flow, hence influences the activation of platelet-derived transforming growth factor- $\beta 1$ (TGF- $\beta 1$), a cytokine that induces fibrosis and calcification [51]. A turbulent flow

generated in the area of greater mechanical stress (between the leaflet and the aortic wall), can lead to the formation of calcific deposits, when genetically prone.

4D flow magnetic resonance imaging and fluid-structure-interaction simulation (which apply mathematical models to the macroscopic behavior of the couple tissue-blood) can show the turbulent flow, which is generated between aortic wall and leaflets (Figure 22).

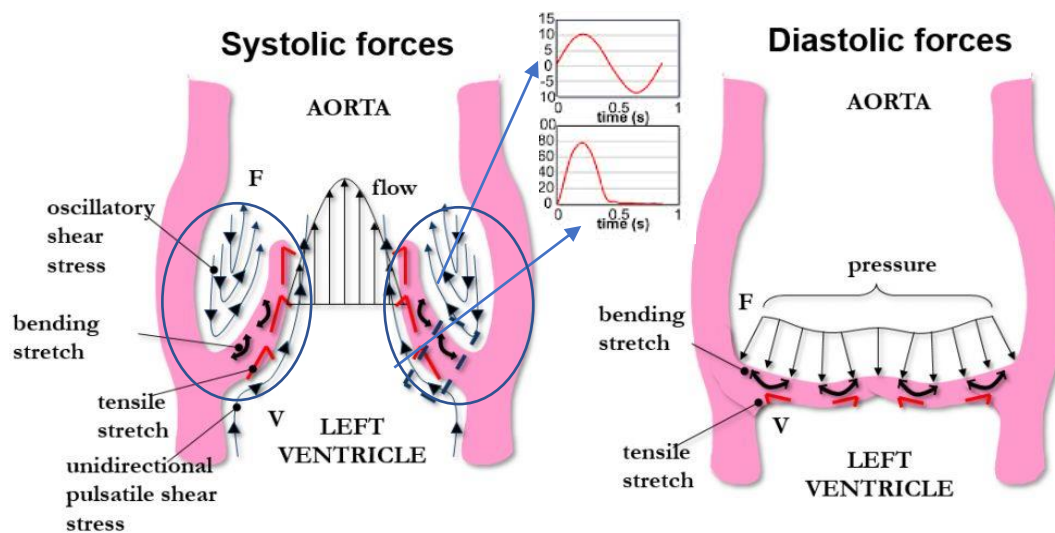


Figure 22 The drawing schematizes the shear wall stresses acting in the region of the aortic valve [46]

The occurred damage led to the cellular response explained before, hence to a progressive stiffening of the leaflets' tissues. The decreased orifice area would hinder the correct outflow of blood into the aorta: to maintain a sufficient cardiac output and an aortic pressure around 80-120 mmHg, intraventricular pressure inside the left ventricle (LV) increases. As shown in the graphic Pressure-Time above (Figure 23), during ejection there is a great difference in pressure between the left ventricle (LVP) and the aorta (AP); in this example, LVP is 200 mmHg (physiologic conditions ~120 mmHg) and the AP is reduced from 120 to 110 mmHg [52]. Normally the pressure gradient across the aortic valve during ejection is very small, just a few mmHg, but in case of severe stenosis can become quite high (>100 mmHg). The magnitude of the pressure gradient is determined by the severity of the stenosis and the flow rate across the valve.

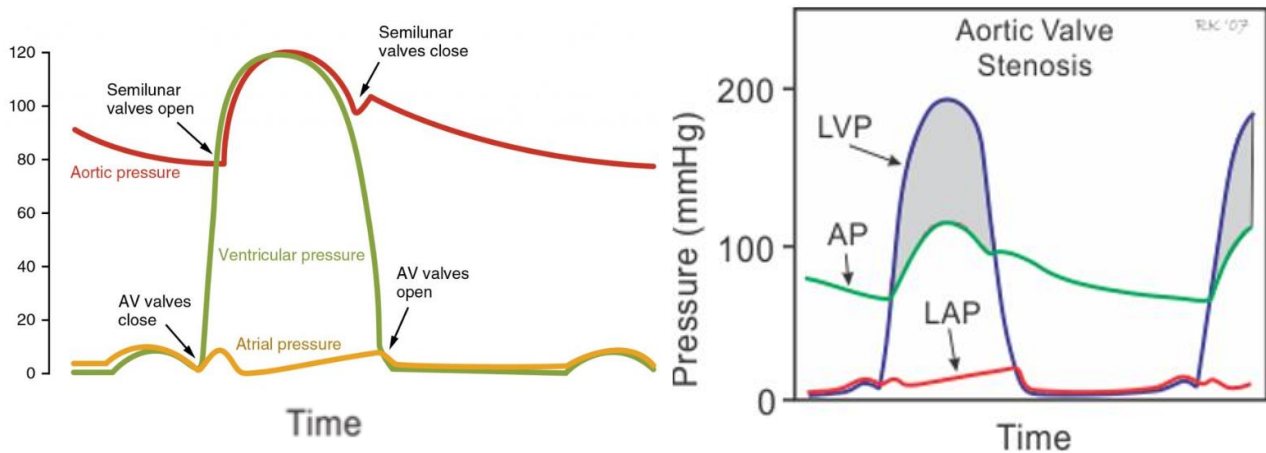


Figure 23 Graphics showing the different values of pressure in the physiological case (on the left) and in the pathological case of AVS (on the right). LVP: left ventricular pressure. AP: Aorta pressure. LAP: Left atrium pressure [49].

Calcification patterns

A study carried by Thubrikar M. et al. [5] demonstrated that 87% AVS patients, in the analyzed cohort, had a specific pattern of calcific deposits while 13% had either an unrecognizable pattern due to heavy calcification or no pattern. The author identified two common types of repeatable patterns, both associated by the fact that grew in areas of the leaflets that are more subjected to shear stresses, since the calcium deposition is result of an aging pathophysiological process accelerated by mechanical stresses. The mentioned pattern and their occurrence:

- Radial Pattern (20.5%, Figure 24): it occurs as progressive fusion of nodules of calcium deposits along the basal attachment. This area is subjected to maximum cyclic flexion due to cusps rotation and bending during the heart cycle, hence it's the more exposed zone to mechanical injuries and activation of the propagation phase of the pathophysiological process. From the attachment line, the pattern gradually spreads radially to the free edge, as it is possible to see from radiographs in Figure 25.



Figure 24 Radial pattern [5].

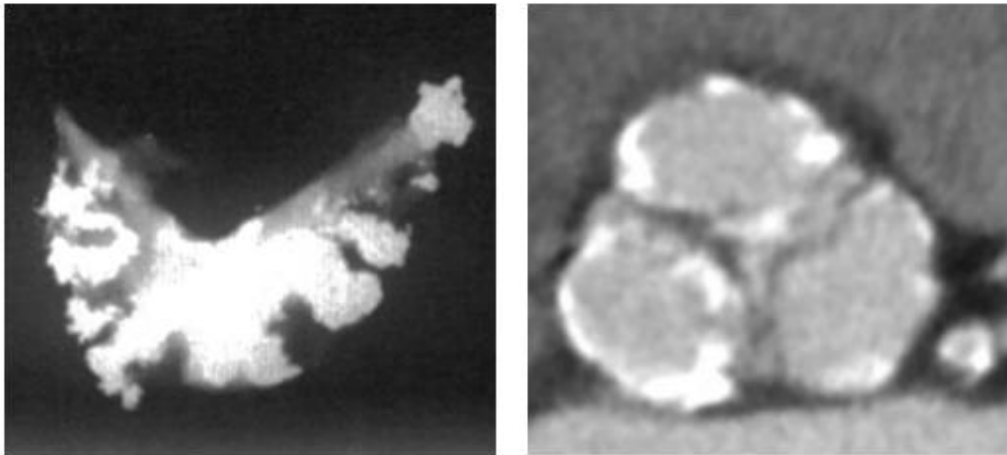


Figure 25 First type of calcification: radial pattern. On the left frontal view radiograph of the aortic valve cusp from the study of Thubrikar. Heavy calcific deposits are visible, starting from the attachment line and diffusing through the belly radially. On the right, top view of multiple large spots of calcifications, at the base of the leaflets (moderately calcified aortic valve). [50]

- Arc/Partial Arc Pattern (53% and 26.5%): presence of calcific nodules starting from two points in the attachment line and proceeding along the line of cusps coaptation (Figure 26). It represents the area under the free edge (i.e. nodulus of the valve), which is exposed to secondary flexion in the valve movement. Calcific deposits focus on eventual creases of the leaflets, generated by the hemodynamic forces Figure 27.



Figure 26 Arc Pattern) [5].

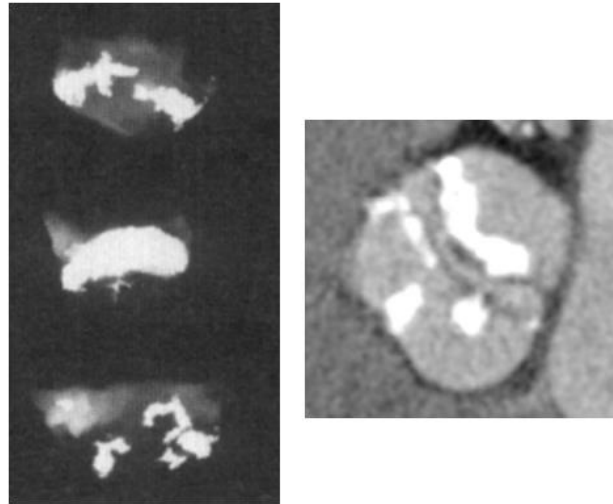


Figure 27 Radiographs of stenotic aortic cusps from Thubrikar studies with clear patterns. On the left frontal view of severe stenosis due to arc shape and partial arc. On the right top view of the same pattern, at moderate grade.

- In the case of bicuspid valves (Figure 28), the degree of flexion is increased, due to the pathological geometrical configuration, on the region of cusp attachment. The presence of a fibrous raphe increases bending stresses [53].



Figure 28 Calcification pattern in bicuspid aortic valves. [53]

Calcification pattern formation was divided by Halevi et al. into three stages [6]:

1. Formation of separate nodules, primary along the attachment line, later on in the center of the belly.

2. Growth of the nodules toward each other, in order to form a complete arc. In some cases it is possible to recognize a circle shape, when arc and radial patterns are combined. When they fail to complete the growth, it is found a partial arc or partial circle.
3. Volumetric growth of the formed pattern.

1.4.2. Bicuspid Aortic Valve

The Bicuspid Aortic Valve (BAV) is the most common congenic cardiopathy, since its incidence involves 1%-2% in the general population with 2:1 male-female ratio [54]. Its genetic history is characterized by association with many other valvular (as insufficiency, stenosis and endocarditis) and vascular pathologies (dilation and aneurysms) [55].

The patients who suffer of BAV show an unnatural fusion of two of the three AV leaflets, hence they present a valve composed of two abnormal leaflets, usually of different dimensions due to inadequate fibrillin-1 production during valvulogenesis [56]. In some cases BAV is strictly bicuspid, in others it presents a ‘raphe’, which is a malformed commissure in the conjoined area of the two underdeveloped leaflets [57].

The patients who suffer of this pathology are more subjected to aortic valve stenosis than other people. The explanation is attributable to the morphological conformation of the valve: the geometry of the two cups leads to abnormal hemodynamics, hence to increased mechanical stresses among the leaflets’ tissues [58].

The most common BAV classification [54] considers the morphologic aspects evident during the echocardiographic exam and it highlights three phenotypes of fused cusps (Figure 29) and their frequencies in both raphe presence and absence:

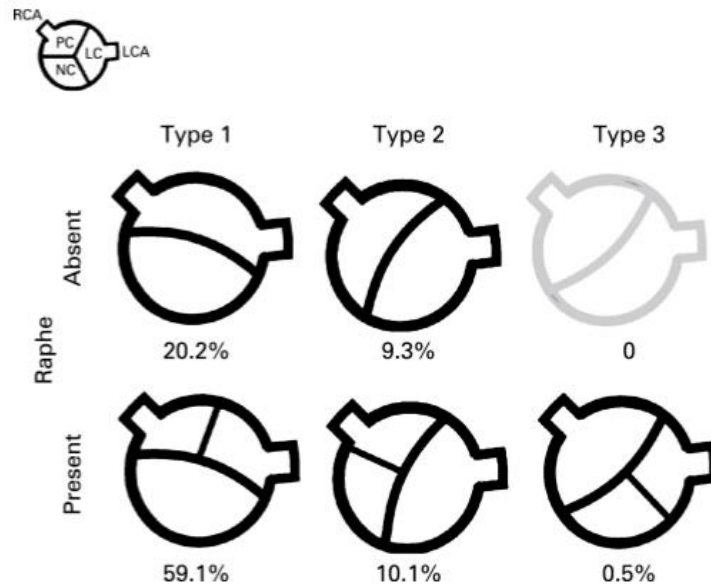


Figure 29 Schaefer classification of the BAV morphology, as seen from a parasternal short axis view on echocardiography and their prevalence [44]. RCA: right coronary artery, LCA: left coronary artery, RC: right coronary cusp, LC: left coronary cusp, NC: non coronary cusp.

Type 1 (60%): congenital fusion between right and left coronary cusp (also called anterior-posterior BAV).

Type 2 (10-15%): congenital fusion between right and non-coronary cusp (also called right-left BAV).

Type 3 (5%): congenital fusion between left and non-coronary cusp.

1.5. Transcatheter Therapies for Aortic Stenosis

In the last decades transcatheter techniques are becoming more popular as an alternative to open heart surgery especially in patient with high surgical risk. The conservative open-heart surgery is handled by cutting the anterior wall of the thorax, in order to expose the interior organs, dissecting the native valve to repair it or substitute it with a prosthetic one. It requires the cardiac arrest and so the exploitation of the extracorporeal circulation. The transcatheter intervention is called TAVI (Transcatheter Aortic Valve Implantation) [59]. It is an endovascular procedure consisting in the incision of a peripheral artery (e.g. femoral artery, subclavian artery) to guide via catheter into the aortic root a valve stented into a small profile. Once the annulus is reached, the prosthetic valve is

deployed onto the native valve, pushing the calcified leaflets aside, without removing them (as is done in conventional surgery). Since the access to the cardiac chamber is reduced, the lack of direct visualization of the interventional field [18] is supported by peri-procedural imaging fluoroscopy or 3D transesophageal (transthoracic) echocardiography for procedure guidance and real time diagnosis of potential complications (tamponade, coronary occlusion, aortic dissection/regurgitation) [60].

Although a decade has passed since the first TAVI implantation in France, it is yet to penetrate most of the developing countries in a major way [24], radically transforming the way to operate high risk or inoperable AS patients. Studies [61] showed that, in Europe and North America, approximately 290000 elderly patients are at high- or prohibitive- surgical risk and should be treated with minimally-invasive procedures. This number is continually rising, since the rapid increase in life expectancy. The spreading of the therapy should be supported by a structured training program for interventional cardiologist [24], in order to decrease the occurrence of severe outcomes (e.g. vascular damage, brain stroke and coronary obstruction). As a matter of fact, learning curves demonstrate the correlation between cumulative experience and success rate, in terms of reduction of collateral outcomes and intraprocedural times [2][19]. TAVI educational programs generally consist in computer-based simulations, mainly used by medicine students; conversely, educational courses on physical phantom simulators and proctorship for first implantations on humans, are addressed to interventional cardiologists [62]. All the programs could offer different ways of teaching the wide range of existing TAVI products.

It is possible to identify two generations of TAVI devices [59].

The first generation includes the FDA-approved SAPIEN and SAPIEN XT valves (Edwards Lifesciences, Irvine, CA) and the CORE valves (Medtronic, Fridley, MN).

- SAPIEN (Edwards Lifesciences, Irvine, CA) (Figure 30): it is composed of bovine pericardial tissue, PET (polyethylene terephthalate) sealing cuff and chromium cobalt alloy frame and it's balloon-expandable [47][63]. It was introduced in 2006 and became the first TAVI system to acquire CE mark approval, with a success rate of 75% [16].

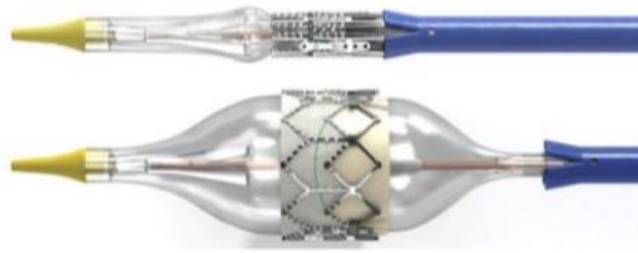


Figure 30 SAPIEN valves, Edwards Lifesciences, Irvine, CA [42].

- CORE (Medtronic, Fridley, MN) (Figure 31): it is composed of porcine tissue and a nitinol frame and it is the first self-expandable device[47][64]. The procedural success rate is 77.6% [16].



Figure 31 CORE valves, Medtronic Fridley, MN [42].

These devices belong to an old generation, because of some problems related to paravalvular regurgitation, vascular complications, strokes and conduction disturbances. Their use was replaced from a newer generation devices, which apport some benefits, such as: reduction in size of delivery apparatus and sheath diameter more controllable deployment mechanism, lower risk of valve mobility and embolization, decreased paravalvular regurgitation (PVR) and bleeding [59]. Because of these reasons, the new generation of TAVI is enhancing the possibility to apply percutaneous techniques also to young and low-risk patients [59][16][65]. Some of the more innovative examples, available since 2014, are:

- Edwards SAPIEN 3 (Edwards Lifesciences, Irvine, CA): it has a smaller crimping profile, it presents the addition of a PET cuff in the inflow portion of the valve, a longer cobalt-chromium open cell stent frame and increased number of sizes (20-23-26 mm), that allows a reduction in severity of PVR [66]. A more flexible delivery system allows an easier deep placement of the valve and less vascular damages. (Figure 32)



Figure 32 Edwards SAPIEN 3 [16]

- ACURATE neo (Boston Scientific, Marlborough, MA): it is a self-expanding valve implanted by trans-femoral and trans-apical approaches. Porcine tissue leaflets are arranged among a nitinol frame whose structure provides high stability during the procedure. A PET skirt is provided to decrease PVR. The procedural success rate is around 90.4% [16]. (Figure 33)

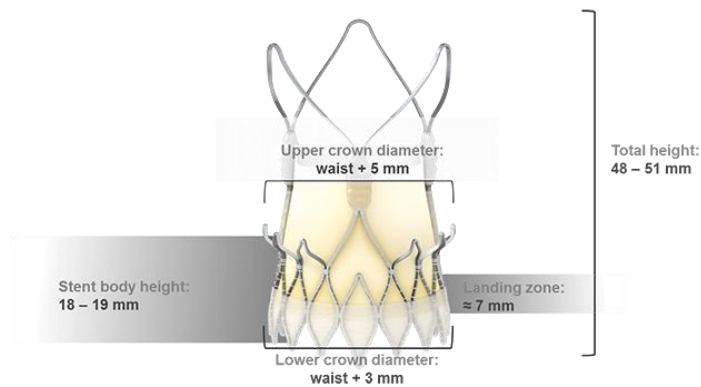


Figure 33 ACURATE TA™ prosthesis. [16]

- CoreValve Evolut™ R System (Medtronic, Minneapolis, MN) is an improvement of the old CoreValve, in order to provide a safer profile. The leaflets are produced with an anti-calcification technology. A better fitting in angulate anatomies is reached through a shorter frame and the higher radial forces optimize the sealing at the annulus. The procedural success rate is around 86% [16]. (Figure 34)



Figure 34 CoreValve Evolut™ R System. [16]

- Portico™ valve (St Jude Medical, St. Paul, MN, bought by Abbot Vascular): its three bovine pericardial leaflets mounted on a nitinol stent frame, with the presence of a pericardial tissue skirt to decrease PVR. The procedural success rate is around 84% [16]. (Figure 35)

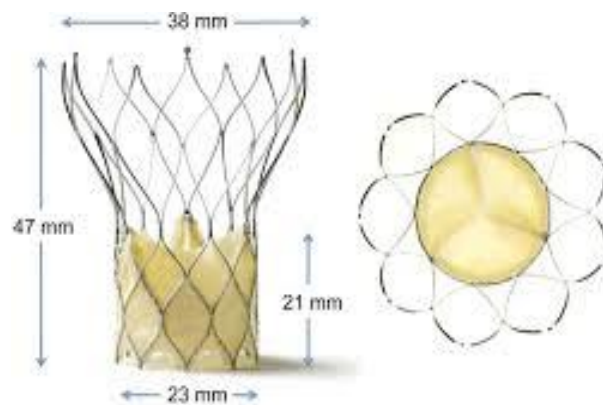


Figure 35 Portico™ valve. [16]

- CENTERA (Edwards Lifesciences, Irvine, CA) is a self-expanding valve, made of three bovine pericardial tissue leaflets. The short stent frame allows a facilitates the fitting and a motorized delivery system provide the deployment. The mortality rate of 1.0% is very low, but it is reported a moderate PVR (4%) [16]. (Figure 36)



Figure 36 CENTERA valve. [16]

A chronological representation of the TAVI devices is in Figure 37.

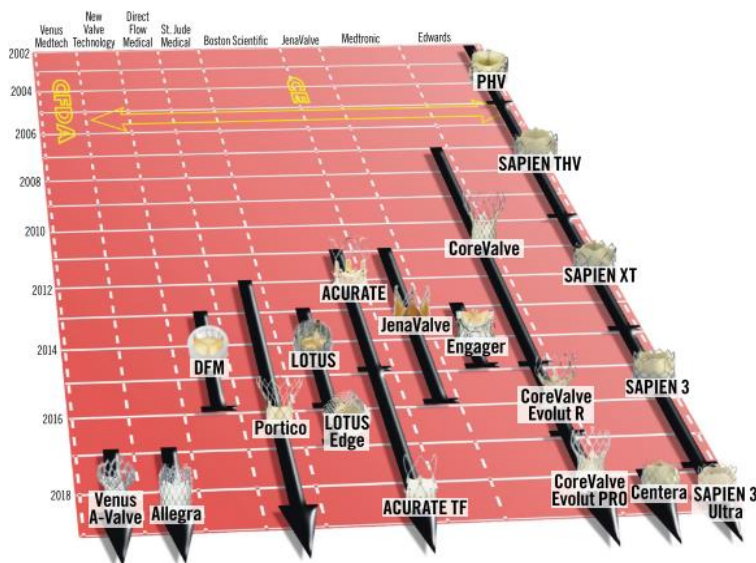


Figure 37 Evolution of TAVI approved by CE mark or China Food and Drug Administration approval. They are represented with respect to the date of regulatory approval. [16]

2. STATE OF ART

The increasing population aging and the rising number of high risk patients, due to the presence of comorbidities, enhanced the need of percutaneous operations and consequently the necessity of a standardized clinical training for operation room's team [67][68]. Indeed it was showed that pre-operation training provides more favorable outcomes[10]. Moreover, Food and Drug Administration (FDA) in April 2004 emitted the first mandate where entails the medical industry to provide simulator-based training programs when introducing a new medical device[69]. Taking into consideration training necessities, the methodologies for realization of physiological and stenotic cardiac valve models used in the laboratory have been disclosed in this state of art.

Furthermore, the analysis of stenotic cardiac valve model classification in the literature revealed that hands-on training can be performed in small mammalian in vivo models, large mammalian ex vivo models and totally artificial in vitro models.

Large mammalian ex vivo models are useful in the case of severe aortic stenosis, since percutaneous interventional treatments need practical experiments. According to the literature, the method of recapitulating stenotic condition on a biological aortic valve was injection of a chemical solution which causes tissue rigidity [70] or insertion of printed stiff materials by glue [18]. In spite of their advantages, the use of biological components can bring to lots of limitations, as shown from Anderson's acute swine models [70]. However, the concept of stiff material insertion was a feasible and realistic approach to replicate calcifications on biological aortic valves. Therefore, this aspect was taken into account as a realization methodology of a standard calcification model.

The manufacturing processes of totally artificial models for stenotic cardiac valve cases were also considered. Due to similar biomechanical characteristics of rubber-like and rigid materials used in 3D printing technology, it is possible to rapidly produce totally artificial patient-specific stenotic cardiac models concerning CT images[71][72][73][74][4][75] . However the technology used to produce these artificial models was expensive and not standard.

The casting manufacturing was exploited based on the literature review as another rapid prototyping technique[76][22]. This technique allowed to produce parametric synthetic models, which represent a general anatomic morphology compared with in vivo and ex vivo alternatives.

In the following chapter the literature review regarding manufacturing technologies for physiological and stenotic cardiac valve models were briefly analyzed. In particular, an ex-vivo

model, parametric and patient-specific artificial models were examined in order to capture the improvements in the field of phantom realization for interventional cardiology training. They were classified as non-functional and functional models, depending on whether their behavior can be tested under dynamic conditions.

2.1 Non-Functional Models

Non-functional models of heart valves represent well their anatomy which can be also a patient specific one. They can be employed for procedural planning i.e. to test the outcomes derived from the interaction between implantable device and anatomy of the specific patient. However, these studies are limited by the lack of testing under hemodynamic conditions.

2.1.1. Maragiannis et al., Aortic Stenosis Model, 2014 [71]

Maragiannis et al. performed tests of 3D printed calcific models only for the specific case of aortic stenosis (AS), since this pathological condition is widely known to cause relatively immobile valve cusps, hence a limited hemodynamics.

A set of patients affected by severe stenosis were selected to replicate anatomical models, collecting data about aortic annuls diameter, calcium distribution, Doppler AVA, number of functional valve cusps and baseline echocardiographic left ventricular stroke volume. Therefore, CT DICOM images at midsystole of 8 patients were obtained and successively elaborated through anatomic modeling software (Mimics, Materialise, Belgium). The elaboration consisted in: segmentation of the relevant zones (valve cusps, left ventricular outflow tract, ascending aorta, calcified tissues) and reconstruction into a stereolithographic file (.STL). The computer aided designed structures were 3D-printed (Objet260 Connex Printer, Stratasys) using fused dual-material 3D printing technique:

- Calcified zones printed in rigid material (VeroWhitePlus RGD835, Objet)
elastic modulus (E)= 2000 to 3000 MPa
- Soft tissue structures in rubber-like material (TangoPlus FLX930, Objet)
E= 0.146 MPa at 20% strain

A summary of the followed steps is represented in *Figure 38*.

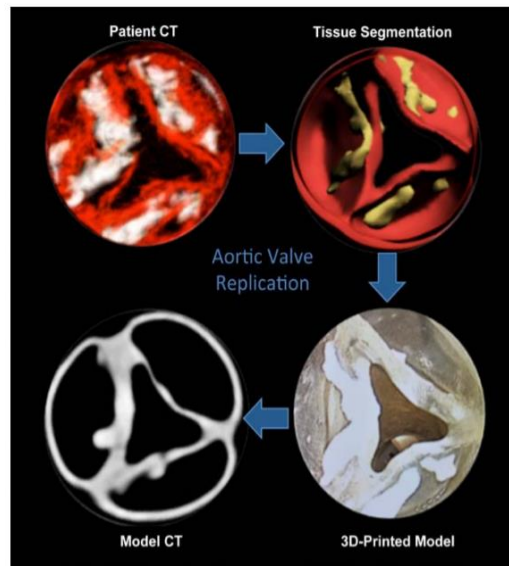


Figure 38 Phases of realization of patient-specific models. CT DICOM data converted in CAD-STL file, exported to a 3D printer to create concrete 2 material fused construct. Final CT of the model to compare the orifice area with the anatomical one [71].

The authors assessed the geometric accuracy through static multidetector 64 slice CT to compare with the clinical CT images the measurements of the regional calcium deposition and AVA (Figure 39)

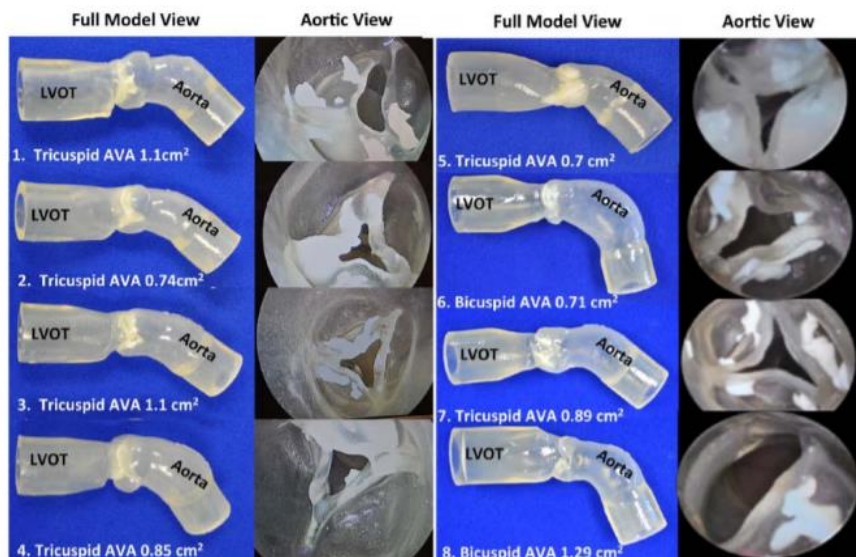


Figure 39 Patient specific 3D models. The models are shown from the views of the aorta long axis and aortic valve area, to evidence the calcium distribution [71].

Mechanical tests were carried to verify the correct reproduction of the mechanical properties:

- Calcified zones (cylinders of 2mm) underwent compression tests, registering $E = 62$ MPa.

- Soft tissues (strips 2x4mm) underwent tensile tests, registering $E=0.4$ MPa.

A relevant limitation of the model is the range of application: it can be applied only in the case of severe stenosis, because of the relatively fixed cusps, since the designed models are obtained from CT imaging data, which represents only a single moment of the cardiac cycle (mid-systole). Therefore, this model cannot be used to represent functional constructs or to permit a simulation of pathological hemodynamic conditions.

2.1.2. Weber et al., Fibrin Aortic Valve Model, 2015[72]

The authors demonstrated the efficacy of a multi-step injection molding process, for the realization of Tissue-Engineered heart valves.

The material employed was a scaffold of fibrin, because of the autologous origin, rapid polymerization, tunable degradation and possibility to manufacture in 3D geometries, thanks to the property of crosslinking with other polymers, without the need of glue or stitches.

The innovative method consisted in the realization of combinable molds: the ventricular stamp (male mold), the vascular stamp (female mold) and two external shells, as depicted in Figure 40.

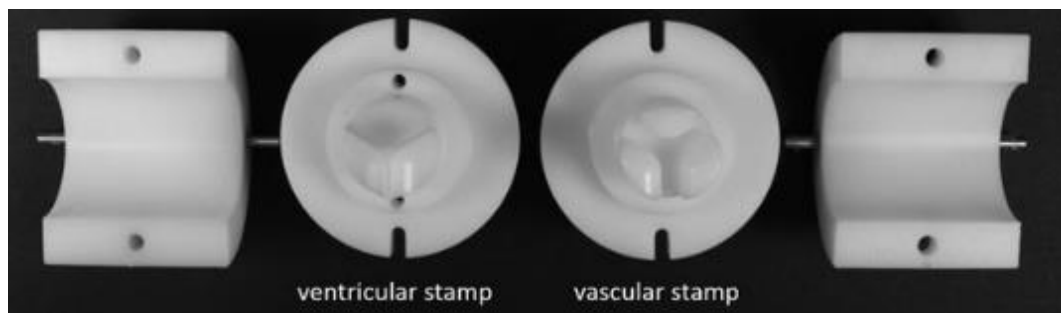


Figure 40 Mold components: ventricular and vascular stamps, and external shells[72].

A layer of fibrin gel was positioned in the space between the ventricular stamp and the vascular one. After the time required for the polymerization of the gel, the external shells were put around the assembly (ventricular stamp/layer of polymerized fibrin/vascular stamp). Successively, another quantity of fibrin gel was inserted into the assembly through a hole in the external shells, and the total construct was left to polymerize before demolding. This procedure was repeated to realize a second layer of fibrin gel, upon the first one (Figure 41)

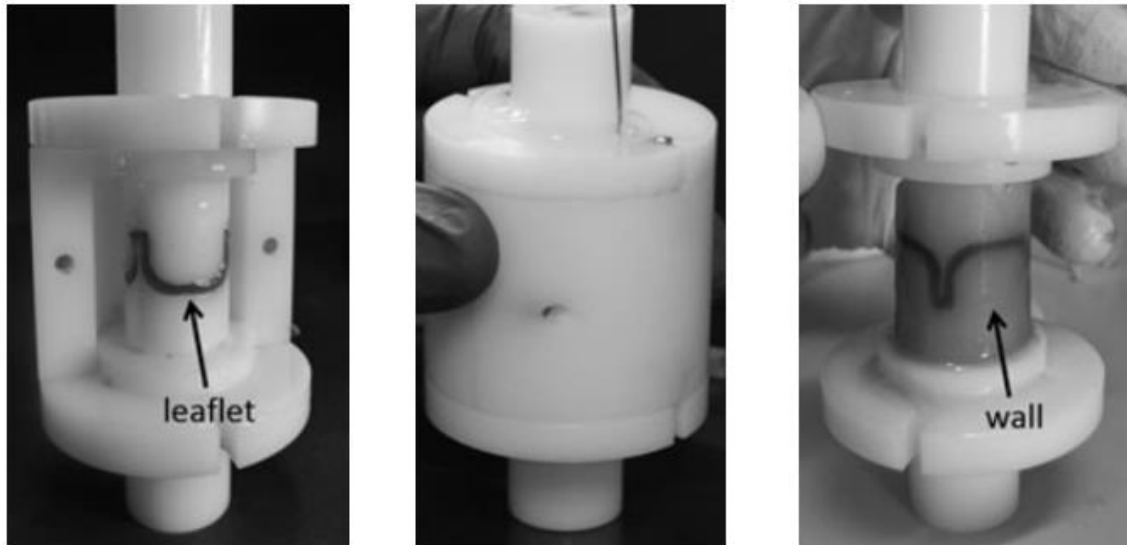


Figure 41 Molding procedure:

- *A layer of fibrin gel positioned between ventricular and vascular stamps*
- *Closure of the assembly with the external shells*
- *Injection of fibrin gel through the hole of the external shells. [72]*

The work strength is the manufacturing method, while the limit is the purpose of project: the model was designed to provide a scaffold for cells cultures embedding, and this functionality was tested by valve opening/closing cycles in a bioreactor and with continuous stimulation over 2 weeks.

2.1.3. Ripley et al., Aortic Root Models, 2016 [76]

The aim of Ripley's work is to reproduce patient specific 3D printed aortic root models in order to test TAVR and predict paravalvular aortic regurgitation (PAR). They managed to provide 3D realistic visualization models for pre-operational planning, in order to visualize how the prosthetic valve will adapt in situ and to highlight eventual failures in circumferential sealings.

The study tested prosthetic balloon-expandable Edwards Sapien valves, as TAVR technique. The dimensions of the artificial valves were determined from pre-procedural cardiac computed tomography measurements of the patient's annulus, performed by volumetric electrocardiogram-gated multiphase acquisitions. The analysis of peak systolic phase intervals allowed to define the maximum valve opening. The blood pool of aortic root, annulus and left ventricular outflow tract have been segmented, transformed into stereoligraphic (STL) mesh file and exported into computer aided design software called 3-matic Materialise. Annular calcium was realized by indentations in the segmented blood pool at the sites of calcium, a 2mm thick wall was extruded

from the blood pool, and finally to get a lumen, the inner blood pool was subtracted. The model was finally 3D printed: aortic root models in a clear flexible resin through Fromblab 3D printer, valve models in hard plastic material through Printrobot printer.

The valve models, compatible with specialized prosthetic valve sizes (23, 26 and 29mm), were implanted in the level of annulus[8] and paravalvular leaks have been analyzed on each patient's 3D printed aortic root model (Figure 42) through light transmission tests.

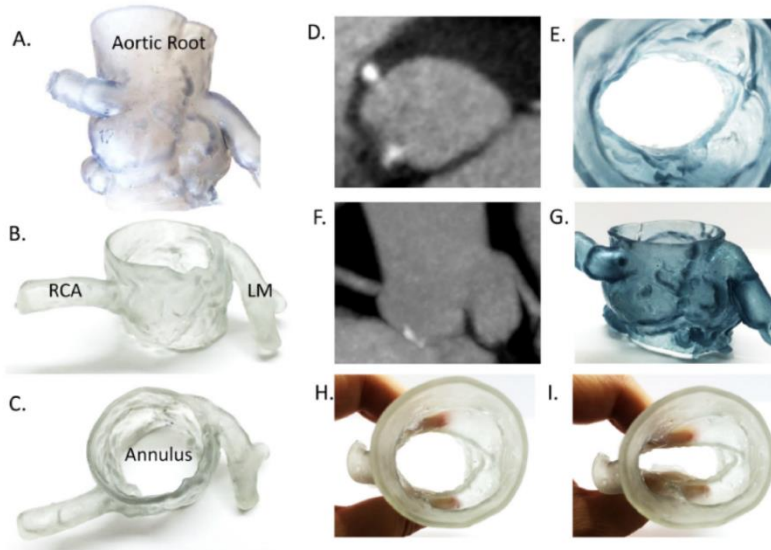


Figure 42 Patient Specific 3D printed aortic root models, including right coronary artery RCA, left main artery LM (A,B,C). The figure represents CT images of annulus (D) and its 3D resin realization (E). There are also figured the scan of sinuses of Valsalva (F) and its 3D resin model (G). Also the final 3D models in elastic materials to mimic the tissue properties of the aorta are pictured (H-I). [76]

Although the 3D technique is promising in the field of operational predictions, there are some limits, as an incomplete incorporation of elements of the valvular complex (such as leaflets and calcium deposits) and a non-perfect correspondence between the elastic modulus of the aortic wall (between 3-9MPa) and the used flexible material.

2.1.4. Schmauss et al., Calcified Porcelain and Flexible Ascending Aorta Model, 2012 [77]

In the article, the team explained the rapid prototyping technique used to fabricate 3D replicas of anatomical structures of a 70 years old's man, died due to ischemic event. 128 slice CT data were obtained from the stenotic aortic valve and from the complete calcified ascending aorta (porcelain aorta) to assess the interventional aortic valve replacement procedure, through transapical access. Diagnostic findings indicated that the patient received a 26-mm Edwards SAPIEN valve by transcatheter aortic valve implantation. The CT datasets were imported into image processing

framework and segmented. The 3D surface was transformed to .STL file and 3D printed (Spectrum Z 510; ZCorporation, Burlington, MA). The printer was able to print, injecting layer-by-layer a liquid binding on the powder plane, two different materials: rigid or flexible.



Figure 43 Rigid physical model of the porcelain ascending aorta (A) and Flexible 3D printed model of ascending aorta (B) [76].

Therefore two different replica models were printed: a rigid model of the porcelain ascending aorta (A) and a flexible calcified ascending aorta model, where test TAVI intervention (B) (Figure 43). The intervention experiments allowed the identification of problems in the aortic anatomy and the opportune technique to be used. Smaller, stiffer and inflexible/inelastic aortic root and Sinuses of Valsalva were observed in the severely calcified aorta. This characteristic implies efforts providing a perfect fit between the annulus and the prosthetic valve. Aware of this thanks to the 3D replica, the authors decided to implant the prosthetic valve at the deepest level of the aortic root model, in order to avoid occlusion of the sinuses of Valsalva.

The work showed how relevant it is the assessment of aortic annulus dimensions, in order to implant a correct size valve in complex aortic anatomies. A concrete representation of the aortic annulus and the spatial relation with coronary arteries is fundamental to minimize perioperative complications, such as: paravalvular aortic regurgitation, valve migration and ischemic events.

2.2 Functional Models

Functional models faithfully reproduce a realistic valve anatomy, both a general one, in the case of parametric models, or a patient specific one, derive from CT images. They also allow a simulation of the dynamic behavior of the modelled component, once set in test benches with the proper fluidynamic condition generated by hydraulic simulators. Rapid prototyping and additive manufacturing, as 3D printing, allow the realization of sophisticated anatomical replicas; they are useful to visualize complex anatomies, plan operations, provide informative methods to test new devices and accurately perform treatments on a patient's anatomy before actually performing the procedure [73][28]. Many are the improvements in the last decades to replicate patient-specific models thanks to the combination of high-spatial resolution computed tomography technologies, computer-aided design software and fused materials 3D printing.

Here are collected some of the most relevant examples for the reproduction of aortic stenosis, which lead us to the choice of the production technique, the materials and the prototype designs.

2.2.1 Maleki et al., Stenotic Aortic Root model, 2014 [74]

The model presented by the authors was ideated for preliminary in vitro testing of percutaneous therapies, using synthetic materials instead of biological samples. Their aim was to present a reproducible model of both ascending aorta and stenotic valve, where to implant transcatheter valves and test the performance under realistic physiological conditions.

The authors started from Labrosse' study [78] about the anatomy of natural aortic valve in dynamics, and applied pathological features from a computational study about a metric for the stiffness of calcified aortic valves [79]: in the Computer Aided Design (CAD) model they increased the leaflets' thickness (2mm), as happens in atherosclerosis process, and during the manufacturing they used stiff shore materials (65 durometer-Digital MaterialsTM combination of TangoPlus and VeroPlus materials).

After the conversion in STL. File, the model was obtained through fused deposition technique (Figure 44), and installed in ViVitro cardiac simulator (ViVitro Labs Inc., Victoria, BC, Canada) to assess the hemodynamic performance during prosthetic valve implantation (EDWARDS-SAPIEN 26 mm balloon) (Figure 45). The assessment involved the measurement of pressure upstream and downstream the stenotic valve, transvalvular flow rate, effective orifice area using

continuity equation, peak and transvalvular pressure gradients using Bernoulli equation; the obtained data confirmed a well reproduction of clinical situation and in-patient observations.

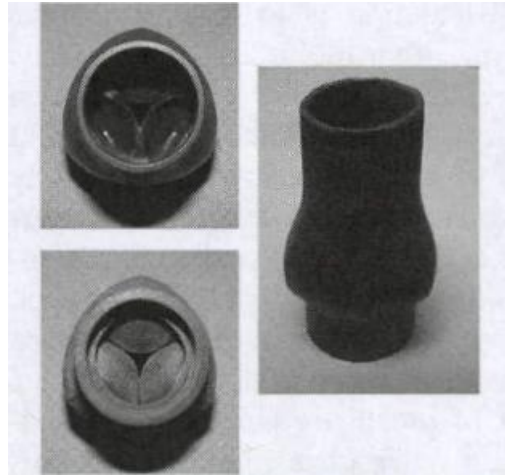


Figure 44 Top, down and side view of the physical model of ascending aorta and stenotic valve. [74]

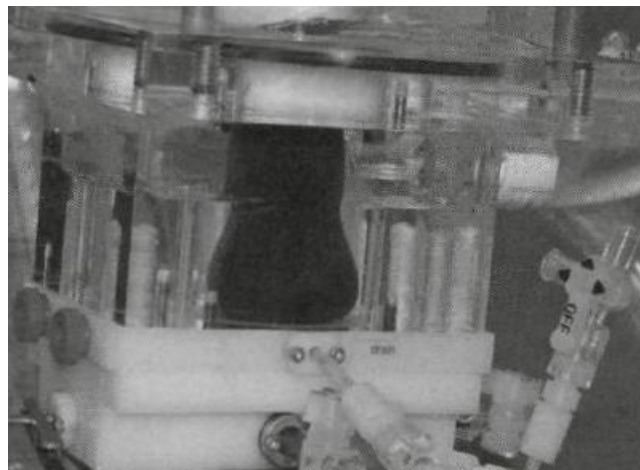


Figure 45 Physical model installed in ViVitro pulse duplicator system. [74]

A limitation highlighted from the authors is a lack of inclusion of coronary ostia, that can allow a connection of the model into an in vitro test of coronary arteries flow. It is also to stress about the fact that the modeled stenosis is obtained only conceptually, through a modification of the mechanical properties of the valve tissue, which is stiffened and thickened. As a matter of fact, the model doesn't reply the realistic shape and aspect of a pathologic valve, since it doesn't include calcific deposits on the leaflets (Figure 46).

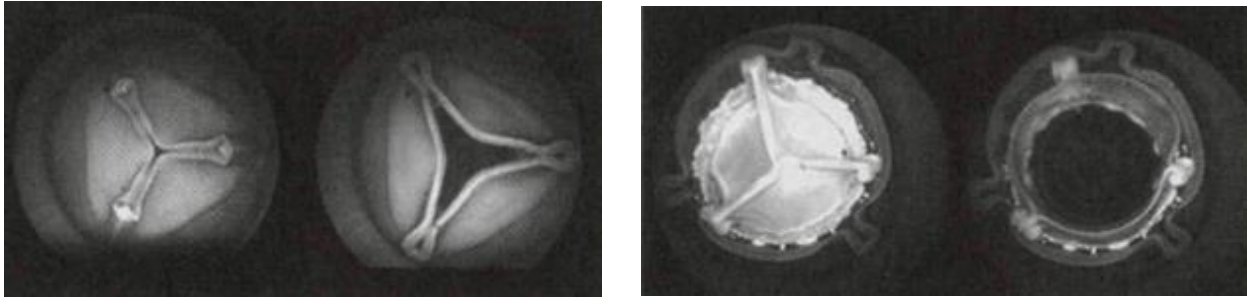


Figure 46 Both closed and opened configuration of stenotic aortic valve model on the left, and transcatheter aortic valve on the right, recorded by high-speed camera.

2.2.2 Sacco Model, Politecnico di Milano, 2015 [18]

The work was aimed to model a stenotic aortic valve. It was obtained combining a sample of biological aortic valve and a calcification pattern, whose morphology is standardized. The author designed the pattern from Thubrikar[5] study: calcific deposits follow a radial distribution, occurring as multiple spokes radiating from the cusp attachment toward the center of the cusp, as in Figure 47.

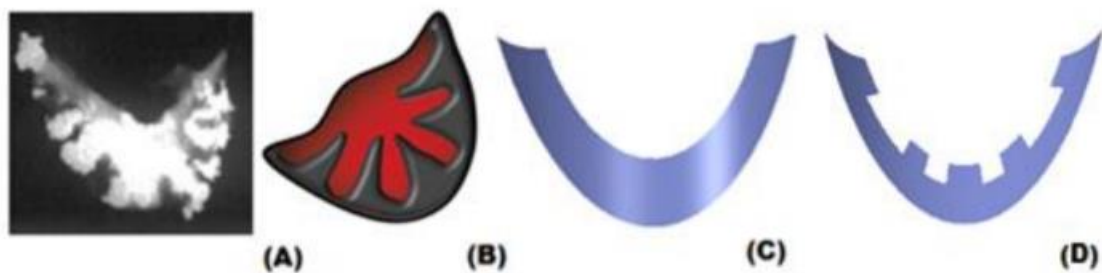


Figure 47 From the CT images of Thubrikar's study (A), calcification pattern is chosen (B) and then realized through 3D-printing technique (C-D). [18]

Sacco realized the pattern in PLA (polylactic acid) through 3D-printing technique (printer DeltaWasp 2040) and adapted it for three grades of stenosis, increasing the pattern extension in radial direction and hence reducing the valve orifice area. PLA calcifications were then positioned on the three leaflets of the porcine aortic valve, through a specific designed holder (Figure 48) and manually glued.

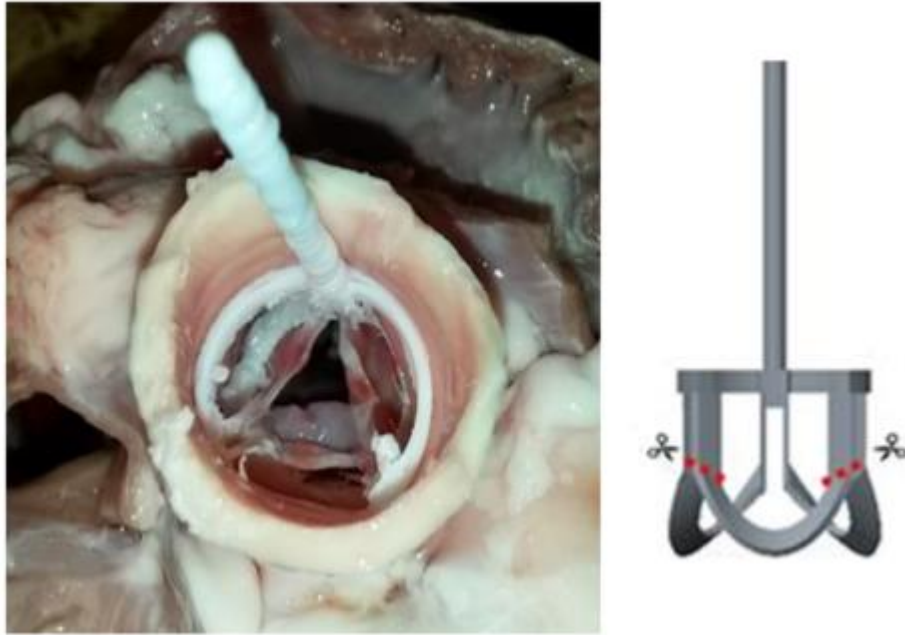


Figure 48 Calcifications accommodation on the porcine leaflets through specific support on the left. Design of the centering support on the right. [18]

The functionality was assessed in stationary and pulsatile flow tests, from which the repeatability of the method was verified.

From the pulsatile flow test it turned out a relevant limitation. The mechanical sealing between calcifications and biological leaflet is not satisfactory: the calcific patterns glued to the biologic leaflets define the technique as operator dependent both in the choice of the quantity of glue and in its homogeneous distribution. Furthermore, the methodology adopted is studied to be applied on native biological valves, hence it implies all the negative aspects of the inclusion of biological components in clinical training simulators, as the inter/intra specie-variability (less standardized anatomical conditions), the differences from the human organs and also the biological deterioration.

2.2.3. Izzo et al., Calcified Mitral Valve Model, 2016 [78]

The goal of the work was the accurate 3D printing of a mitral stenotic valve to test TMVR procedure. The authors put attention on a particular concern: provide an objective method to assess whether an implanted valve is sufficiently supported by the annulus and leaflets. The 65-years old woman was unsuitable to SAVR, with a predicted mortality risk of 25% (based on Society for Thoracic Surgeons database, STS score), since she was suffering at the same time of some

comorbidities, as severe mitral stenosis, mild-to-severe aortic stenosis, atrial fibrillation, renal disease, hepatitis C and breast cancer has been artificially manufactured.

Diagnostic and anatomic data were gathered from transthoracic echocardiogram (TTE), transesophageal echocardiogram (TEE) and variable pitch electrocardiograph (ECG) gated CT angiography. They were also useful to acquire volumetric data to generate 3D printed models. The obtained image data from mentioned scans were analyzed in a 3D visualization software called Toshiba Vitrea 3D Enterprise Suite. The process flow of the data acquisition is illustrated in Figure 49.

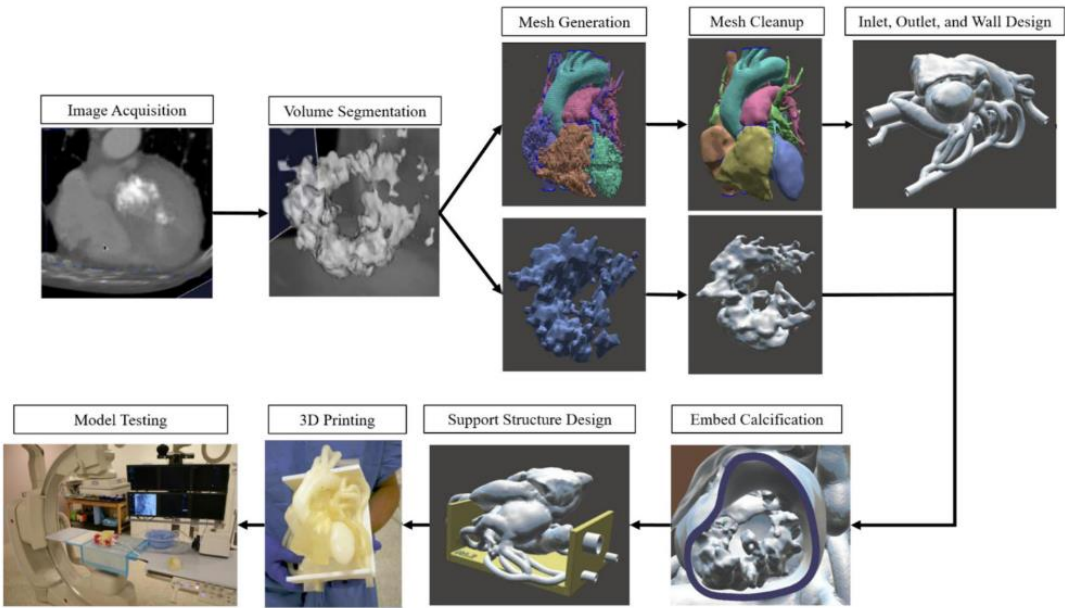


Figure 49 Software process flow of 3D printed heart phantom models. [80]

In the study, to be sure of the mitral calcification identification, the anatomy of the patient was divided into 2 parts to be segmented by Vascular Modeling Toolkit (VMTK): one dedicated to heart vasculature (four heart chambers, aorta, superior and inferior vena cava and pulmonary arteries); the second is mitral valve calcification. 3D image scan files were cleaned up to repair the meshes and eliminate artifacts problematic for printing and successively they were converted into stereolithographic (STL) files, in order to be 3D printing by Object 500 Connex3 Polyjet 3D printer system. The 3D printer was able to print 2 different materials at the same time (Figure 50):

- For the anatomic structures: materials with properties to mimic vascular tissue (Tango+, Shore: 26-28)

- For the calcific deposits: stiff material, which mimics bone tissue (DM_9770, Shore:68-72). The parts were also coated of tantalum powder and superglue to mimic the radio-attenuating properties of the calcified valve.

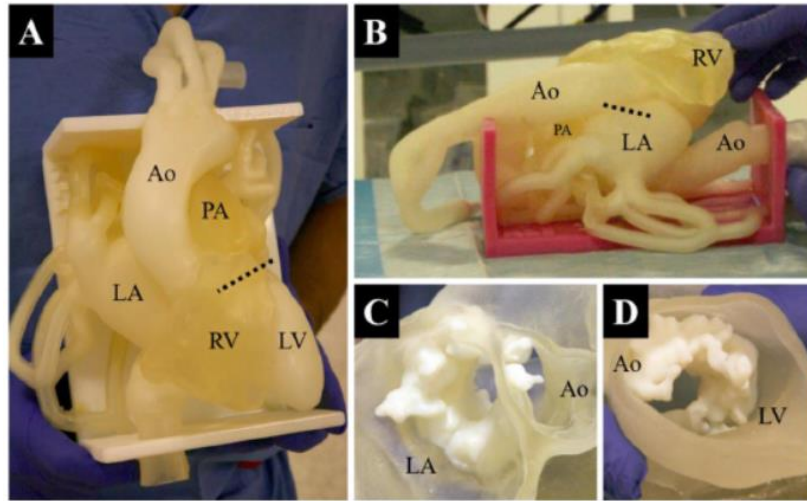


Figure 50 Cardiac Phantom (A, B) and Calcified Mitral Valve(C, D). [80]

The phantom was tested, placing it on the angiography table and connected to a pulsatile pump (Harvard Apparatus, Holliston, MA) and a solution glycerol-water was left circulating through the phantom, in order to simulate blood flow viscosity [is it enough to be considered functional model?). Two different size valves were tested (20mm SAPIEN 3 and 23mm SAPIEN XT from Edwards Life-Sciences, Irvine, CA), in order to decide which one best fitted the patient's anatomy to minimize Left Ventricular Outflow Tract (LVOT) obstruction. Therefore, the real operation ended with the results predicted from the experimental study.

2.2.4. Schiena Model, Politecnico di Milano, 2018 [4]

The work consists in the design of aortic and mitral valves, obtained through additive manufacturing techniques and casting of synthetic polymeric materials, to be used within a ventricular structure for clinical training.

The aim of the author was avoiding the exploitation of biological components within the artificial hydraulic test benches already existent in literature. A completely synthetic simulator prevents from the intra/inter-specie variability and provides a more standardized instrument to test new trans-catheter therapies for heart valve diseases.

Schienna started from the CAD design (Software Solidworks, 2016-2017 Student Edition, Dassault Systems) of male and female molds, which replicate the anatomical shape of the heart valves and aortic roots, on the basis of anatomical studies carried by Labrosse [29]. He improved the design of the valves' anatomy, adding a curvilinear free margin profile in order to have more realistic wider leaflets and coaptation surface (Figure 51).

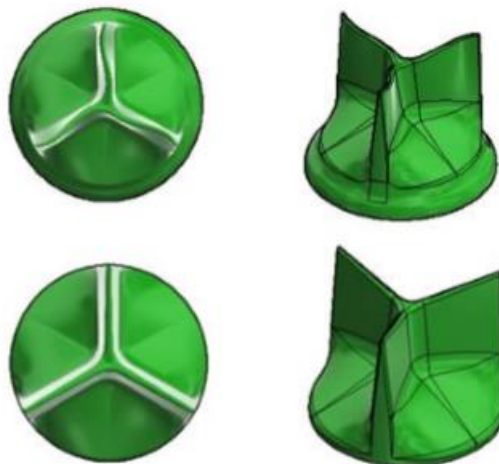


Figure 51 Free margin profiles. On the top the new designed curvilinear one, on the bottom Labrosse's linear one. [4]

Afterwards, the author realized PLA-molds (Figure 52, Figure 53) through 3D-printing technique (Ultimaker 3D-Printer), where casting silicon rubbers (GLS-50 and GLS-20PRO, Prochima, Calcinelli di Saltara, PU, Italia).

Materials to be casted were chosen with respect to their mechanical properties, such as: casting property, room temperature polymerization; after polymerization, the materials have to be flexible, fatigue and tensile resistant and stay in a certain range of shore (around 20).



Figure 52 In blue, silicon (GLS-20PRO) casted inside of the PLA-mold, in black. [4]

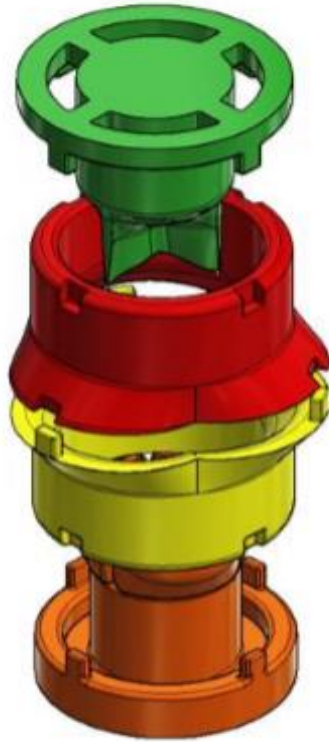


Figure 53 CAD assembly of the molds for aortic valve and aortic root support. [4]

The characterization tests consisted in compliance evaluations and trial sessions conducted in steady and pulsatile settings (set-up ISO 5840) to simulate physiological conditions and evaluate the fluid-dynamic performances (opening-closing functionality, transvalvular head losses, eventual reflux).

The stationary set up (Figure 54) involved a hydraulic circuit made of: centrifugal pump (P, BM04APP, Savino Barbera s.r.l, Brandizzo, Italia), reservoir (R) and valve holder (V). The anterograde/retrograde flow was imposed and registered thanks to a flux-meter (F, HT110R Transonic System 102 Inc.), to quantify pressure drops across the valve. Pressures were measured through piezoelectric transducers (P_{monte}-P_{valle}, PC05D series, Honeywell Inc., Morristown, NJ).

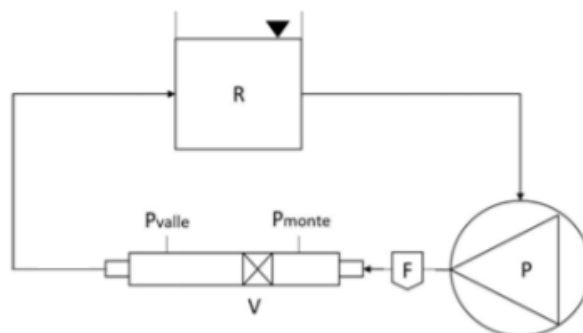


Figure 54 Stationary test set up. [4]

The pulsatile set up (Figure 55) comprised a ventricular chamber where to connect aortic and mitral valves. The aortic valve was after-loaded (I) and the mitral valve was pre-loaded (R). The hydraulic set-up was activated by a pulsatile cylinder-piston pump to provide systolic and diastolic waves, in order to establish backflow volume, transvalvular pressure drop and Effective Orifice Area (EOA).

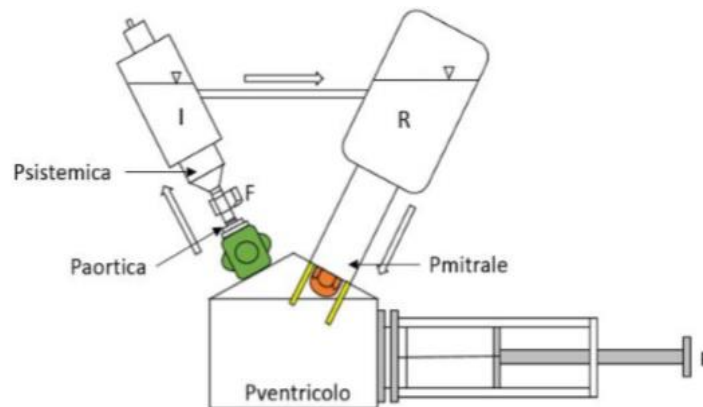


Figure 55 Pulsatile tests set up. [4]

Evident limitation is the lack of visibility with diagnostic imaging tools, very important for the percutaneous training they are aimed. For this reason, the materials, which are colored, should be changed in order to use the prototypes with echo and fluoroscopy.

Furthermore, the presented model has no pathological aspects, providing polymeric models which perfectly simulates physiological fluidynamic performances. The development of pathological models can be useful to evaluate efficiency and efficacy of a therapy in pathological conditions.

2.2.5. Rotman et al., Replicator model, 2018 [75]

The work is relevant, as the authors realized Replicator, an accurate patient-specific benchtop which models the human upper body vasculature (iliac arteries to left ventricle) to test transcatheter aortic valve replacement (TAVR). The authors explained the higher reliability of their benchtop, rather than the common left heart simulators (LHS), due to a faithful patient specific aortic valve and aortic root in situ. They highlighted that common anatomical-idealized bench tests (e.g. non calcified leaflets, straightened elastic ascending aorta) can be enough to compare baseline performances of prosthetic valve devices, but they would lack the realistic post-procedural outcome. The reported pulse duplicator, called Replicator, is based on realistic patient's anatomy and can show eventual complications or consequences of TAVR.

Aortic root and valves were provided by Vascular Simulations LLC (Stony Brook, NY, USA). The factory got anatomical data from CT scans of patients, and it realized the models by additive manufacturing technique: at first CT scans were converted in .STL files and 3D-printed (Stratasys Dimension Elite 3D Printer) in plastic material. The obtained mold was dipped into silicon, put on zero gravity to get a uniform distribution and cured into oven. A xylene bath was needed to melt the plastic core, to get the silicon replica of the exact patient geometry. To replicate the severe stenotic valve, the authors applied calcific deposits on the silicon models provided by the factory. (Figure 56)

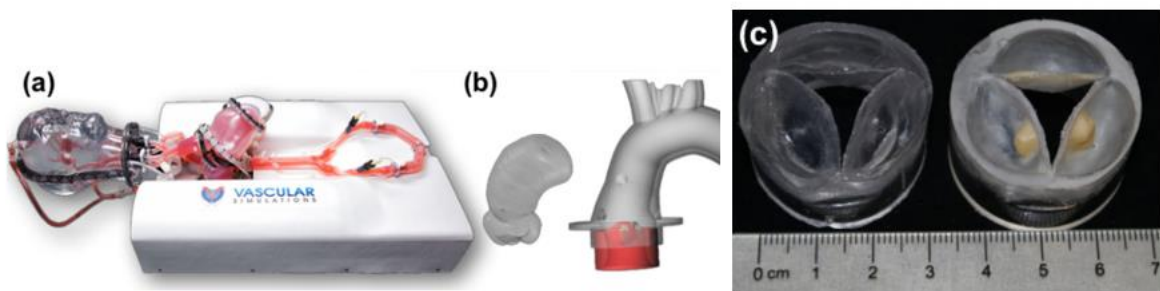


Figure 56 In the figure are shown:

- a) the Replicator, upper body bench test of Vascular Simulations
- b) reconstruction of ascending aorta and aortic root
- c) moderate (Shore 30) and severe stenotic (Shore 50) aortic valve. [75]

Following ISO 58403, hydrodynamic tests were carried out in the Replicator, through Windkessel mechanism (compliance and resistance) to recreate physiological flow and pressure conditions across the valve, updating during the operation. An active feedback mechanism allowed to keep under control possible arteries' occlusion or wrong positioning of the catheter. However, the optimal results presented in the work are limited by the necessity of the products provided by Vascular Simulations LLC.

2.3 Aim of the study and objectives

TAVI is providing an alternative to open heart surgery due to the rising population of high-risk patients affected by moderate-severe stenotic aortic valve. In spite of its advantages mentioned in Chapter 1.5, intra-procedural errors of TAVI procedure, caused by the confined perspective in the interventional field, can cause life-threatening consequences. Therefore, it is a requirement for interventional cardiologists to practice on a realistic anatomy model. In this scenario this work is placed.

The models collected in the state of the art were critically analyzed, to understand which aspects are to take into consideration to realize a pathological valvular model that can be aimed for interventional cardiologists training.

The goal of the thesis was the development of a polymeric model of stenotic aortic valve. From the analysis of literature, information about the manufacturing technologies are highlighted: rapid prototyping as 3D printing and multistep casting. The exploitation of rubber-like materials, in particular photopolymers, emphasized the possibility to directly print cardiac components, obtaining models with biomechanical characteristics similar to the real ones. The main limitation lies in the use of very expensive technologies.

An alternative to this technology is given by the casting production method. An easy strategy that involves the realization of a 2 parts mold: inner mold, which gives the internal surface geometry of the piece and outer mold, responsible for the external conformation. In the interspace between the two components, is casted the liquid material and let to cure. This methodology provides flexible models, with accurate shape, controlled in geometry both internally and externally.

In addition, the studies carried by Schiena and Weber highlighted the possibility to carry on casting techniques through a multistep protocol. This methodology can allow a multistep addition of components realized in different times and materials and merged together.

The main disadvantage of this production process highlighted from Schiena's work [4] lies in the difficulty of the realization of a thin structures (leaflets), hence an improbable anatomical fidelity. The present work wants to provide a solution to the problem, taking into account the mold-dipping technique used by Rotman et alia [75] to have thin silicon films. On this purpose a specific device is realized, to increment the productivity and the quality of the results.

The literature shows different approaches that can be followed for the reproduction of the stenosis pathology: although simultaneous 3D printing of two materials reproducing both calcific and valvular tissues gives benefits with respect to perfect anatomical reproduction, once again it proves to be a too expensive technology. The study carried by Sacco [18] showed the possibility to glue 3D printed calcification above ex vivo valves. However, the need of a standardized attachment between calcific pattern and leaflet emerged.

With respect to the reproduction of the geometry of the valves, two different approaches are proved by literature: general geometry or patient specific one. A model based on general geometric configurations seems to be the most effective to analyze the impact of common pathologies.

From literature also emerged the necessity to guarantee the material compatibility with the main imaging techniques, in order to keep monitored the transcatheter procedure. In the mentioned works, almost all, were at least transparent to allow the view with the naked eye.

In conclusion this work wants to go over the limitations highlighted in the state of art, proposing a manufacturing method for the realization of parametric calcific aortic valve models aimed to interventional cardiologists training of transcatheter therapies. In particular, the realized phantoms are realized with the following specifics:

- Exploitation of cost-effective technologies, that allow the realization of multiple models in a fast way.
- Standardization of the manufacturing protocols, to avoid inter operator dependence.
- Mechanical properties that could allow a realistic interaction between phantom structures and devices.
- Transparency or compatibility with imaging techniques.
- Duration of use appropriate to the training procedures for which they are intended.

3. MATERIALS AND METHODS

In this chapter are described materials and methods necessary to obtain polymeric cardiac structures, goal of the present work of thesis: aortic root, leaflets and calcifications. After a brief introduction about technologies, instruments and materials used, the methodology for designing and manufacturing molds and polymeric models are described. Design specifications, geometries exploited, and protocols followed for the models' realization are shown.

3.1. Technologies and Tools

Polymeric models designed in the present thesis work are obtained through three manufacturing methods: dip-spin coating technique for the leaflets, embedding for the calcification and casting technique for the aortic root.

Dip-spin coating methodology is the combination of dip-coating and spinning techniques. Dip-coating is a manufacturing method in many industrial areas because of its easy, inexpensive, and reproducible capacity [81], [82]. This technique consists in depositing the coating solution onto

the mold surface by immersing it into the liquid coating and withdrawing at a fixed celerity [81], [82]. The process includes four essential steps, as shown in Figure 57: *Immersion* of the mold that has to be covered with the liquid coating, slow *Withdrawal* of the object, *Consolidation Drying* and *Curing Sintering* of the liquid coating [83].

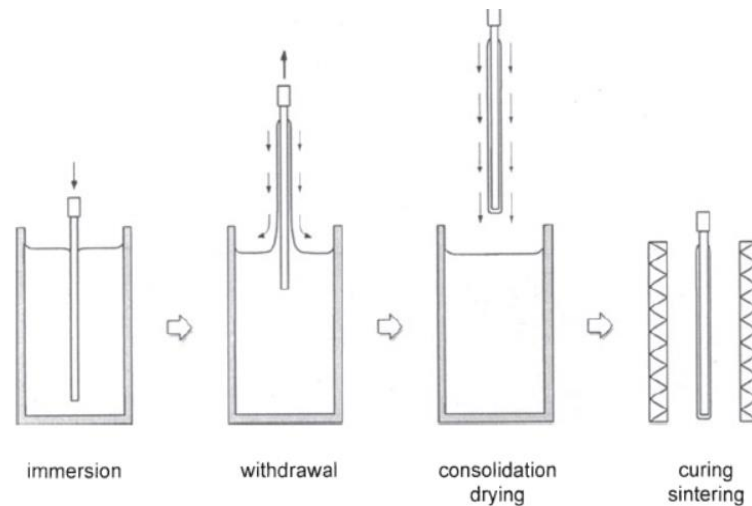


Figure 57 The Essential Steps of Dip Coating. [83]

In the thesis work, the just mentioned *Immersion* step was done in an ad-hoc designed *Dipping Container*, tailored on the geometry of the mold that has to be dipped, in order to avoid waste of material. It is shown in Figure 58, and its geometry is better declared in Appendix B.

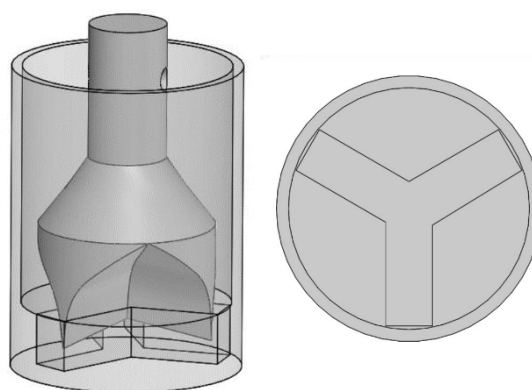


Figure 58 Dipping Container front view during the mold dipping and top view.

Curing Sintering step was facilitated through spinning procedure. This technique involves that the object covered by liquid coating is set into a *Rotational Device*, and the centrifugal forces allow a homogenous and thin distribution of the coating around the surface of the covered mold during the curing time. In the present work, 3D printed molds (PLA, poly-lactic-acid) were immersed in a

container of polymeric coating solution (Sorta Clear 18) and cured using an ad-hoc designed *Spinning Device* and described in paragraph 3.3.

Embedding technique is the process of inserting a specimen in the mass of a liquid coating, in order to provide structural support for the specimen [84]. In this work, polymeric patterns (PLA) were embedded into silicone medium (Sorta Clear 18).

Casting technique is the manufacturing process where a polymeric solution is injected into the interspace of two complementary molds and it is let to harden due to polymeric reaction (Figure 59).

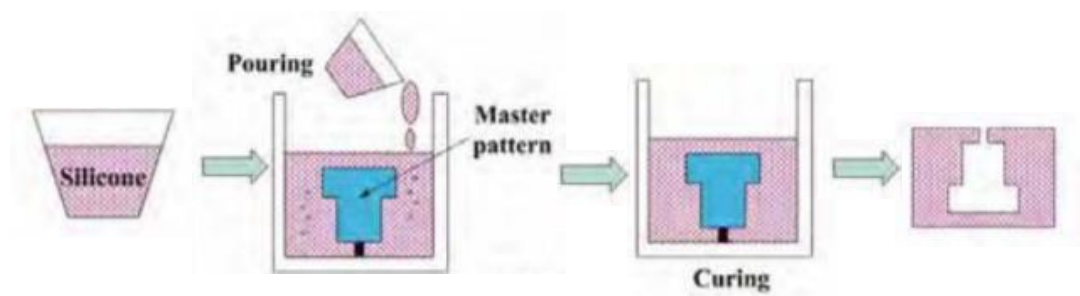


Figure 59 The essential steps of casting technique. Silicone is shown as example of polymeric solution that is poured into an assembly of outer and inner molds. Once the silicone is cured, it can be extracted, obtaining a silicone model.

In this thesis the casted material was a silicone rubber (Sorta Clear 18) that once polymerized corresponded to the desired phantom.

The molds were realized through polymer (PLA) 3D printing and they were defined as inner and outer molds, since they respectively gave the internal and external shape of the phantom. Varying the reciprocal dimensions of the two molds it was possible to control the interspace both in geometry and thickness. It has to be noticed that both inner and outer molds are the assembly of many sub-molds, as shown in Figure 60.

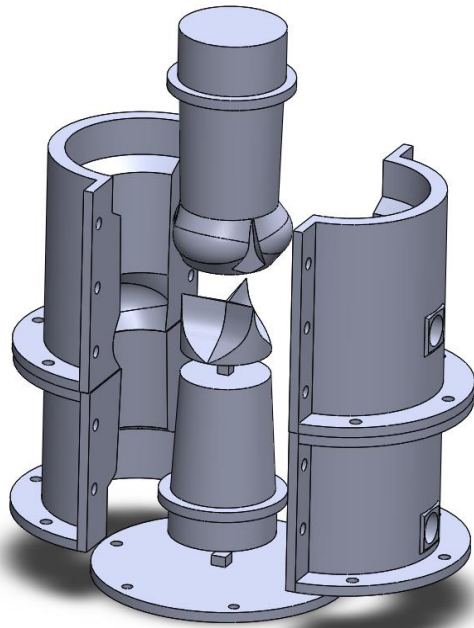


Figure 60 Outer and Inner molds, composed by many sub-molds.

The **rapid prototyping** manufacturing process from the design to the obtainment of the models consisted in the following steps (Figure 61):

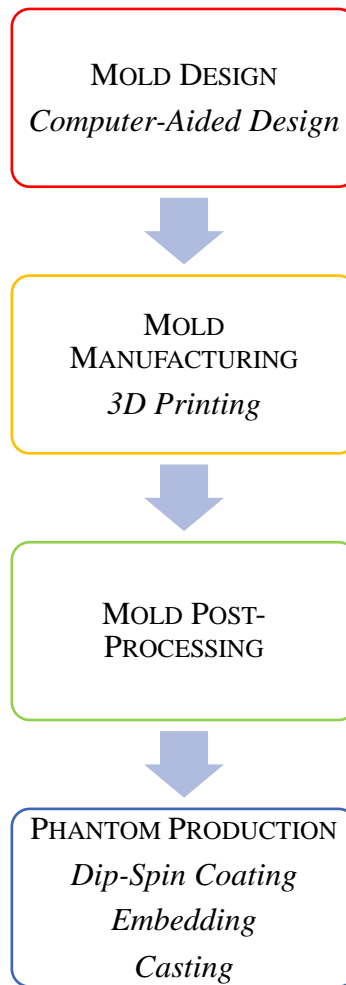


Figure 61 Iter of the manufacturing process for the obtainment of the silicon model

Starting from the analysis of the literature ([29] and Table 1), a parametric model of the biological structures of interest was defined. This model was used to design in *SolidWorks* software, a CAD technology, inner and outer molds (Molds Design). Once the design-phase was completed, the molds CAD models can be converted into mesh models and rendered compatible for 3D printing (Mold Manufacturing). Once obtained the 3D printed molds, they have to undergo manual processing in order to improve the surface quality (Mold Post-Processing). Further, molds were exploited to realize the phantoms by 3 production techniques (Phantom Production). Different production techniques were used with respect to the anatomical part they represent:

- Dip-Spin Coating to obtain the silicone leaflets. The valve mold was dipped into silicone coating and set curing in the Spinning Device.
- Embedding of 3D printed patterns into silicone coating, to reproduce the calcification of the cusps.
- Silicone casting into the assembled 3D printed molds, in order to obtain the aortic root.

3.1.1 Software

Software exploited during the process of realization of the molds are:

- SolidWorks 2019-2020 Student Edition (Dassault Systèmes) (Figure 62): software of solid modeling computer-aided design (CAD). It allows to design 2D and 3D projects of solids and surfaces, thanks to a customizable parametric system. It is possible to realize technical drawings, objects and assemblies of the parts. Through the software it is possible to export an .STL file, that is the assignment to a tridimensional object geometry of a mesh and a set of vectors normal to the surface.

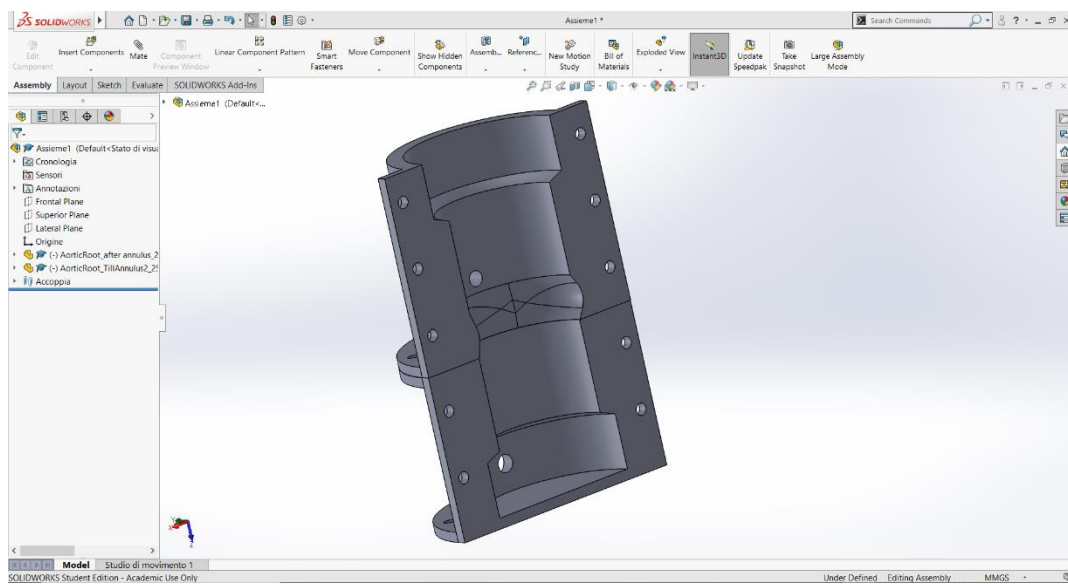


Figure 62 Graphical user interface of SolidWorks.

- Netfabb Standard (2019 Autodesk, Inc.) (Figure 63): it is a software application used to repair mesh models, check printability and slicing, before additive manufacturing processes and rapid prototyping as 3D printing. It can detect some typical errors occurred during CAD files conversion to STL. It ensures that the mesh is valid, closed, oriented and does not contain any self-intersection, that brings to holes onto the surface, redundant elements and overlapping surfaces.

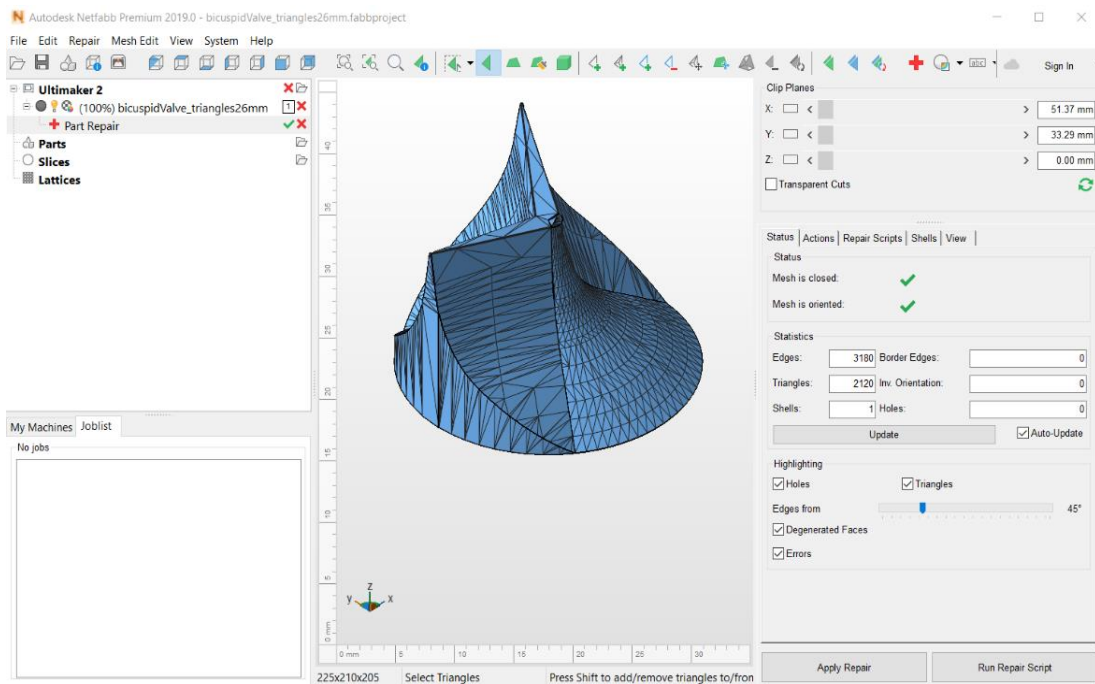


Figure 63 Graphic user interface Netfabb Standard.

- Cura 4.2.1 (Ultimaker, Netherlands) (Figure 64): open source software useful for the optimization of the parameters' setting before 3D printing a CAD model. Once set all the printing parameters, it provides a preview of the final printed object, estimates time of printing, quantity of material needed, and it suggests the addition of support material, to give more stability and better surface quality to the printed model. It works on the input .stl file and gives as output a .gcode file, which is readable by the 3D printer. The final exported file contains all the needed printing information, in particular the position of the extruder during the work execution. The parameters that can be adjusted before printing and the specific values set for the realization of the molds are summarized in Table 6.

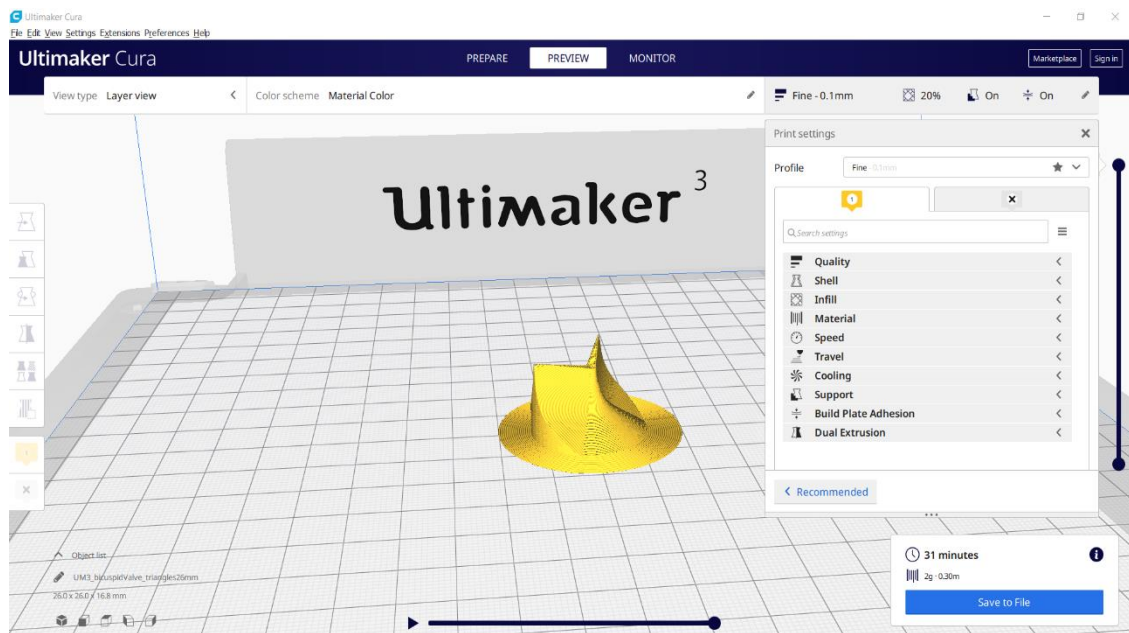


Figure 64 Graphic user interface of Cura.

Parameter	Description	Influence on the printing	Standard Value	Higher Quality Value
Quality				
<i>Layer Height [mm]</i>	Height of each layer of material deposited by the nozzle.	Spatial resolution. Time of printing.	0.2	0.1
Infill				
<i>Infill Density [%]</i>	Percentage of the inner volume filled by the filament.	Quality in terms of mechanical resistance. Time of printing.	20	20
Material				
<i>Printing Temperature [°C]</i>	Heating temperature of the nozzle. It depends on the used material.	Quality in terms of mechanical resistance, adhesion between the layers and presence of bubbles.	210	210
<i>Build Plate Temperature [°C]</i>	Heating temperature of the build plate. It	Quality in terms of solidification time.	60	60

	depends on the used material.	Adhesion of the object to the plate.		
<i>Speed</i>				
<i>Printing Speed [mm/s]</i>	Nozzle movement velocity.	Time of printing. Quality of the extruded filament.	70	60
<i>Support</i>				
<i>Support Placement</i>	Type of support material extruded to sustain the hanging parts.	<i>Touching Build plate</i> , support from the plate. <i>Everywhere</i> , support from the object.	<i>Everywhere</i>	<i>Everywhere</i>
<i>Support Overhang Angle [°]</i>	Inclination angle of the printed object with respect to a vertical plane, beyond which support is generated.	Smoothness of the protruding surfaces.	60°	40°
<i>Support Density [%]</i>	Density of the extruded support.	Easiness in support removing. Quality of the protruding surfaces.	15	25
<i>Build Plate Adhesion</i>				
<i>Build Plate Adhesion Type</i>	1 st extruded layer of material on the Build Plate.	<i>Raft</i> , strong base support for high plate adhesion of the object. <i>Brim</i> , good compromise between plate adhesion of the object and printing time. <i>Skirt</i> , improve the fluidity of material extrusion.	<i>Brim</i>	<i>Brim</i>

Table 6 Main parameters to be set before printing.

3.1.2. 3D Printer

3D printing is a Solid Freeform Fabrication technique, that allows rapid prototyping manufacturing: starting from digital models obtained from CAD, they build layer by layer 3D objects.

Additive Manufacturing technologies differ for method of deposition of the layers and the type of material used; the main typologies are powder bed sintering through carbon dioxide laser beam (*Selective Laser Sintering*), crosslinking of a liquid photopolymerizable resin via UV laser (*StereoLithography Apparatus/PolyJet*) and extrusion of melted material (*Fused Deposition Modeling*, Figure 65).

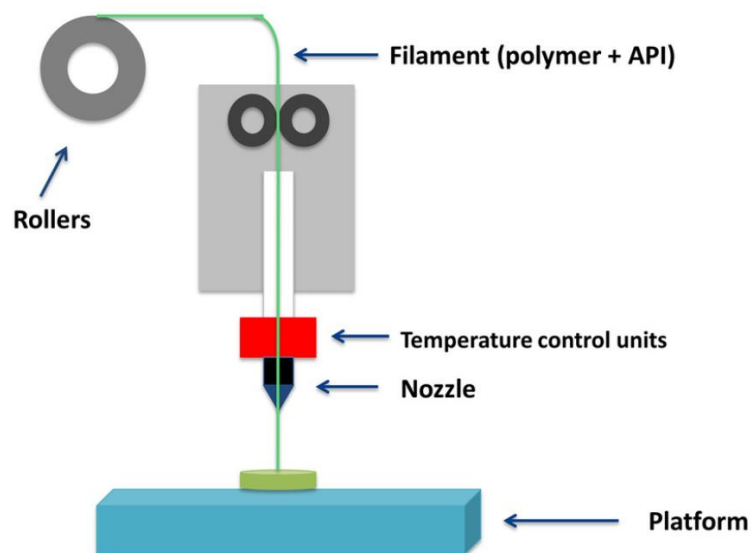


Figure 65 Scheme of the process of Fused Deposition Modeling. [81]

To the last category belongs Ultimaker3 3D Printer, available in the laboratory μ BS LAB of the Department of Electronics, Information and Bioengineering (DEIB) of Politecnico di Milano. As mentioned before, it works by squeezing from the nozzle a filament of thermoplastic material, at its softening (melting) point. The filament is deposited on the Build Plate of the printer, and kept above its solidification temperature to allow the complete fusion with the next layers [85].

Ultimaker3 is the 3D Printer used in the present work of thesis to realize the parametric models. The main components of the machine (Figure 66, [86]) are:

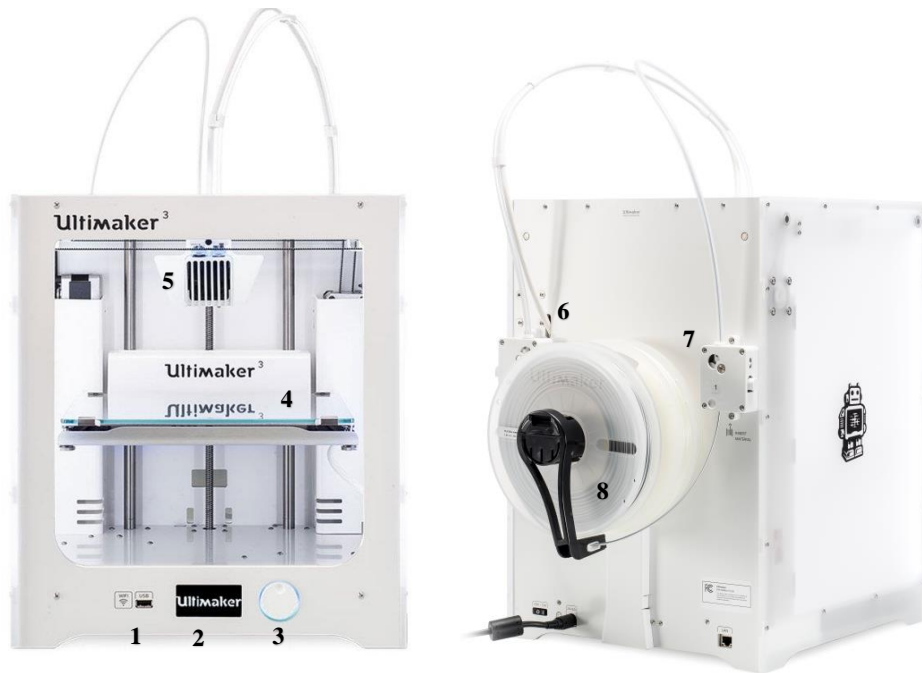


Figure 66 Ultimaker3 3D Printer. [82] The main components are:

1. USB key
2. User display
3. Knob to select settings
4. Build plate
5. Print head
6. Feeder 1
7. Feeder 2
8. Coil of material with NFC scanner

- **Interface Display:** it allows an intuitive user interaction with the machine, in order to set machine parameters and import .gcode files through USB key.
- **Print Head:** it allows a dual extrusion of materials. It gives the possibility to extrude a combination of build materials and water-soluble supports (ex PLA/PVA), in order to obtain complex models. In the head a fan system is included to optimize the cooling, hence obtaining smoother surfaces. The maximum extrusion temperature is 280°. The nozzle is swappable with respect to the material to be printed, changing diameter as 0.25, 0.40 or 0.80 mm. The diameter of the nozzle influences the feed rate of the filament, hence the resolution of the print.
- **Build Plate:** it is made by heating glass, which assure high material adhesion. The light and stiff design reduces vibrations.

- Live Camera: to keep monitored every stage of the printing, also by remote position.
- Dual Geared Feeders: to apply more pull action on the filament and avoid heat exposure from the motor. To upload new material, it is possible to manually insert the filaments through a lever function. An integrated NFC material scanner, through RFID chip, identifies the loaded filament and verifies the correspondence of the material selected by the user. A wide range of materials are printable: PLA, ABS, PVA, PC, PP, TU 95A and Nylon. PLA and ABS are the most used materials; they differ [84] for prices, ABS is cheaper, and extrusion temperature, higher in ABS, hence deriving greater propensity to deformation of the in-progress printing.

3.2. Materials for Mold Production

3.2.1. PLA

To 3D print all the molds and the calcification patterns of the present work, filaments of PLA (Poly-lactic-Acid, 3D Italy, Rome, Italy) were selected. This thermoplastic polyester is nowadays the most common and versatile [84] 3D printing material, because of its low threshold for high temperatures and cost-effectiveness. Furthermore, it is obtained from renewable resources, hence it is biodegradable. Its specifics are summed up in Table 7 [87] .

PLA FILAMENT SPECIFICS	
<i>Diameter</i>	2.85 mm
MECHANICAL AND THERMAL PROPERTIES	
<i>Melting Temperature</i>	145-160°C
<i>Glass transition Temperature</i>	~ 60°C
<i>Tensile Strength</i>	59 MPa
<i>Elongation at break</i>	7 %
<i>Modulus of Elasticity</i>	3500 MPa
PRINTING PROPERTIES	
<i>Extrusion Temperature</i>	210-215 °C
<i>Build Plate Temperature</i>	60 °C

Table 7 Summary of the properties of interest of PLA.

PLA was chosen to reproduce the properties of calcific deposits, also due to its similarity, in mechanical properties (Table 8, [88]) , to the very used in literature VeroWhitePlus™ polymer (RGD875, Stratasys, MN, US). As already mentioned in the State of the Art ([89][90][91][92]), it is used to realize calcification patterns embedded into polymeric phantoms of cardiac valves. This polymer, belonging to Vero™ family, is a rigid opaque material, most widely used for visual models and engineering prototypes thanks to its light functional testing property. VeroWhitePlus™ was discarded in the present work, since it has to be printed by PolyJet 3D Printers.

VeroWhitePlus MECHANICAL PROPERTIES	
<i>Tensile Strength</i>	50-65 MPa
<i>Elongation at Break</i>	10 %
<i>Modulus of Elasticity</i>	3000 MPa

Table 8 VeroWhitePlus™ Mechanical Properties. They were compared with PLA properties.

3.2.2. XTC-3D®

XTC-3D® (Smooth-On, Macungie, PA, US) is a protective coating for smoothing and finishing 3D printed parts, that fills cavities and print striations without melting the surfaces where it is deposited.

This coating was used in the post-processing phase of every 3D printed component, brushed after the use of sanding paper (Figure 67, on the left), in order to decrease the roughness of the surfaces that were in contact with the casting material. Indeed, studies demonstrated [3] the efficacy of protective mold coatings in the improvement of the surface uniformity and transparency of the silicone models. The complete datasheet is collected in Appendix A.



Figure 67 Molds undergoing Post-Processing phase: rubbing down process via sanding paper on the left and brushing XTC-3D coating on the right.

3.2.3. E-30 Epoxy Resin

E-30 Epoxy Resin (Prochima, Calcinelli di Saltara, Italia) is a transparent thermosetting polymer, that crosslinks at room temperature. It is obtained by mixing two liquid components: the natural resin derived from bisphenol F, and a hardener obtained from cycloaliphatic amine. Their reaction is exothermic.

Calcifications embedding process was characterized by a difficult control of the resulting thickness. Epoxy turned out to be the solution for the obtainment a replica of the calcification pattern: it was poured above the calcified leaflets contained in a specific silicone mold. Once cured, the epoxy custom mold of the aortic valve is obtained. It was used as valve-tailored inner mold during the aortic root casting process. This technique is easy, fast and free from operator dependence. The data sheet is reported in Appendix A and a detailed usage protocol is related in Chapter 4.

For the preparation of the epoxy resin, it is necessary to adhere to the following procedure:

- Merge together part A and part B in the mixing ratio by weight 100:60.
- Slowly mix with a spatula with an elongated blade, trying to remove the product around the walls and on the bottom of the container, in order to obtain a homogeneous mix throughout the mass.
- Wait a few minutes for deaeration before pouring. In the event of bubbles persistency, vacuum degassing into the de-airing hood.
- After pouring, check for the presence of bubbles, and if necessary, facilitate their release by puncturing with a toothpick.
- Wait for the total hardening: 72 hours, at 25° C.

Particular regard to:

- Performing all the steps within the Pot Life: 40 minutes.
- The surrounding temperature: hot temperature speeds up hardening process, due to the thermosetting nature of the material

3.3. Material for Flexible Structures

3.3.1. Silicone

To realize the polymeric cardiac components, materials with particular properties are needed, in order to fulfill the project specifications mentioned in section 2.3. :

- **Flexibility** after complete material vulcanization, in order to simulate mechanical behavior of the tissue when subjected to pulsatile flow conditions (e.g. valve leaflets opening and closing).
- **Transparency**: in order to allow a visual feedback. Since the model is designed to train interventional cardiologists in the implant of transcatheter devices, it is important to allow a good direct visibility of the procedure.
- **Compatibility with imaging techniques** to monitor through standard live imaging methods (i.e. Fluoroscopy, Echocardiography), as highlighted from the State of Art [89] [3][93][76].
- **Easily available and cost-effective.**

The material's requirements related to the exploited techniques are:

- **Pourable Property**: it is necessary that the material maintains its liquid state at room temperature, in order to be easily casted or used to dip/embed materials at room temperature. The vulcanization at room temperature is required also because the material has to be used combined with PLA, whose Glass-transition Temperature is very low (Table 7).
- **Resistance to fatigue, tensile strength and break** also when the realized model presents very thin thickness. It is the case of the valve leaflets: they have to resist extraction from the molds and hydrodynamic conditions during training sessions.
- **Pot-life time**, sufficiently long in order to have the chance to carry out the necessary preparations for the manufacturing processes (i.e. for the material casting: vacuuming, syringes loading, injection times).
- **Viscosity** sufficiently low to permit an easy extrusion of the material from the syringe (casting technique): a low resistance to flow of the fluid, prevent from bubbles generation and decreases procedural times. Viscosity property is also relevant in dip-spin-coating technique, since the parameter influences the thickness of the coating fluid.

For the choice of the casting and dipping material the above-mentioned characteristics and the materials highlighted from literature, analyzed in Chapter 2, were taken into consideration.

TangoPlus (FLX930, Stratasys, MN, US) emerged from the State of the Art, as golden standard for imitation of biological cardiac tissues [92][94][73][89][90][95][74], but it has to be printed by the expensive PolyJet™ photopolymerization Technology.

Therefore, the TangoPlus was compared with other materials available on the market, considering cost-effectiveness, transparency and with mechanical properties, such as Shore Hardness, Modulus of Elasticity, Tensile Strength and Elongation at Break. In the group of the accessible materials, the rubber-like category is favorable with respect to Poly-vinyl-alcol cryogels, due to their easier processing and better performances in terms of less shrinkage effect (<0.1%) [74]. Silicones are elastomers based on high molecular weight linear polymers, available in different Shores values, vulcanizable at room temperature and with negligible shrinkage. Sorta-Clear™ Series rubbers (Smooth-on, Macungie, PA, US) and Pro-Lastix 20 (Prochima, Calcinelli di Saltara, Italia) were selected for a preliminary comparison, as shown in Table 9.

MECHANICAL PROPERTIES				
	<i>TangoPlus</i>	<i>Sorta Clear 18</i>	<i>Sorta Clear 40</i>	<i>Pro Lastix 20</i>
<i>Tensile Strength [MPa]</i>	1.5	2.9	5.5	4.9
<i>Elongation at Break [%]</i>	220	545	400	500
<i>Tear Strength [kN/m]</i>	20	14	16	14
<i>100% Modulus of Elasticity [MPa]</i>	0.3	0.24	0.62	unavailable
<i>Shore Hardness [Scale A]</i>	24	18	40	20
<i>Viscosity [mPa*sec]</i>	No interest	21000	35000	7000 ± 2000
<i>Color</i>	Translucent	Translucent	Translucent	White

Table 9 Mechanical properties comparison between TangoPlus [92] and other promising available silicones. Silicones' values are taken from their data sheets, in Appendix A.

The main properties taken into consideration were: *Tensile Strength*, as the maximum amount of tensile stress the material can take before failure; *100% Modulus of Elasticity*, as characteristic of the material, it defines the ratio between stress and deformation in the case of monoaxial load for elastic materials; *Shore Hardness*, stiffness classification; *Viscosity*, since the amount of friction between adjacent layers of a fluid influences both casting and dipping, as explained before; Color, since a good visibility inside of the silicone phantom is a functional prerogative. Comparing the materials with the properties of TangoPlus (Table 9), Sorta Clear 18 was the one that fits better the parameters of interest, with respect to both mechanical properties and transparency. It is an elastomeric silicone that allows a faithful reproduction of the mold's details, since it vulcanizes inside the molds at room temperature through polyaddition reaction, via platinum catalyst addition in ratio 100A:10B. For further details, in Appendix A is the datasheet of the material.

For the preparation of the silicon rubber, it is necessary to adhere to the following procedure:

- Merge together in a container part A and part B (for the selected SortaClear 18 the mixing ratio by weight is 100A:10B).
- Slowly mix for 3 minutes, paying attention to scrape sides and bottom of the mixing container.
- Vacuum degassing into the de-airing hood. Place the container containing the mixture inside the machine. Apply vacuum (-1 bar), interrupting with slowly air discharging to come back to atmospheric pressure. Repeat till the complete absence of bubbles into the silicone, assessable by the naked eye. Keep attention to the increasing level of material inside of the glass, since the vacuum induces the silicon overflow from the container.
- Extra produced material can be saved in freezer, slowing polymerization reaction.

Particular regard to:

- A complete degassing of the silicon. Eventual presence of bubbles originated during the parts mixing can compromise the mechanical properties of the silicon structure. Making sure to leave sufficient room in the container to allow a proficient volume expansion of the silicone, hence less time necessity to complete the degassing process.
- Performing all the steps within the Pot Life time (for SortaClear 18 is 60 mins).

3.4. Spinning Device

This section presents the design and the manufacturing of the Spinning Device (SD) to assist the dip-coating process, in order to obtain a homogenous coating-material distribution as well as speeding up the fabrication process, producing multiple aortic valves.

The fundamental principle was based on the transmission of the axial rotation of a motor to the aortic valve molds that are inserted in the machine, in order to spin them around their own axis. The objective of this spinning device is to allow a homogeneous distribution of the thickness of the coating among the valve molds. The goal was reached, not only through the rotational movement, but also through the inclination of the plane, where the molds were turning, hence reducing the amount of the coating material on the molds using the gravitational force.

As a summary, the two essential design criteria for the realization of the SD were:

- I. The transmission of the rotational movement from motor to four molds, in order to have a multiple production.
- II. The adjustment of the inclination of the motor-plane, in order to exploit gravitational force in the achievement of the right coating-thickness.

To allow the transmission of the rotational movement, the mechanical design of Planetary Gear Systems (PGS) was exploited. This technology, composed by spur gears, allowed the transmission of the movement from a Sun Gear (connected to the motor), to Planetary Gears where the valve molds were positioned. The gears were kept together by an outer constraint, provided by a Ring Gear. More stability was achieved by application of covers (Cover for RG, Cover for SG, Figure 68).

Furthermore, motor was fixed on a plate parallel to the PGS (Concentric Connector Plate, Figure 68), and they were aligned with four M6x10mm screws. After the assembly was completed, the hollow cylindrical carriers (Valve Carriers, Figure 68) were inserted into the gears of the PGS, to hold the valve molds. Finally, the device was adjusted on a support to be able to give the desired inclination. The components of the SD are shown in Figure 68.

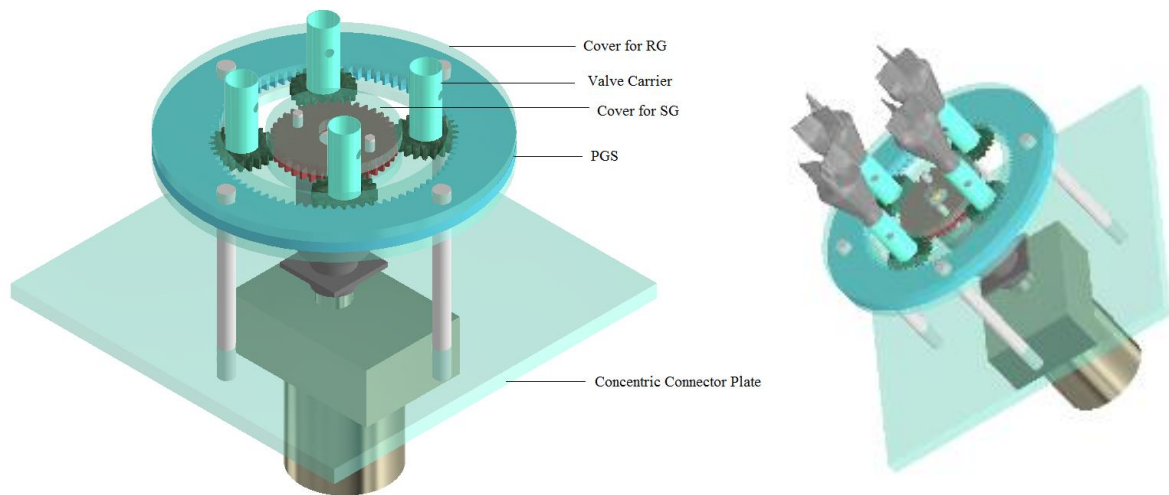


Figure 68 On the left explanation of the CAD components of the SD: RG: ring gear, SG: sun gear, PGS: planetary gear system. On the right demonstration of the inclined SD, including valve molds.

PGS Design and Assembly Procedure

The components of PGS were spur gears, in particular Sun Gear (SG) located in the center, four Planet Gears (PGs) that turned around the sun gear, and a Ring Gear (RG) which surrounded the other components as it is presented in Figure 69. In general, the design constraints of PGS were assigned by input and output rotations. In this case, the input rotation was provided by a motor connected to the SG, and the output rotation was obtained from PGs. RG supported SG and PGs in a fixed position.

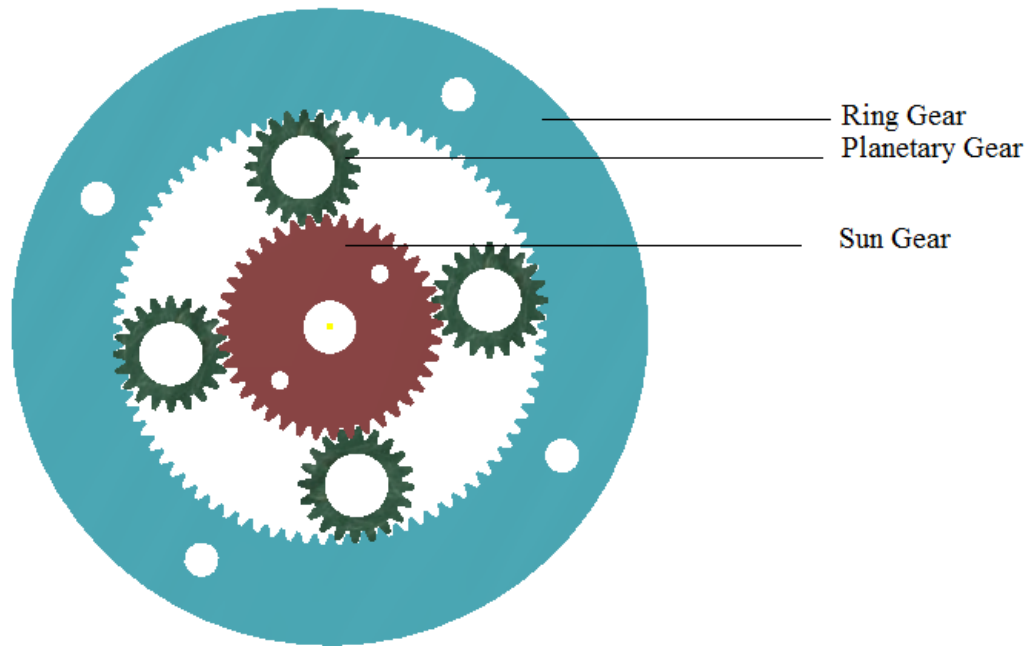


Figure 69 The Planetary Gear System Configuration and its components. The sun gear has input rotational speed (w) and the planetary gears have output rotational speed (w). However, the ring gear has a fixed position meaning that $w=0$. The figure is designed in Inventor Autodesk Software.

Taking into account all the design parameters for the spur gears, the CAD files were generated in Inventor, Autodesk Software by using its Spur Gear toolbox feature, shown in Figure 70.

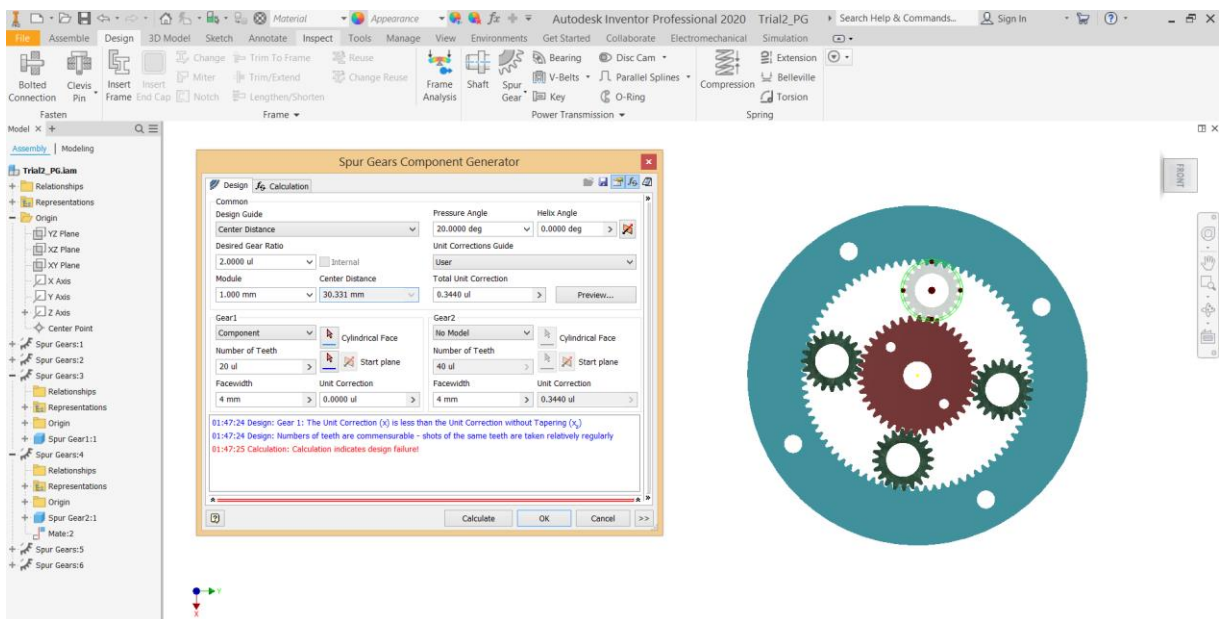


Figure 70 Spur Gear Component Generator and Design Parameters presented in Inventor Software.

The gear sizing of the PGS was made working on the relations between Planetary Gears, Sun Gear, and Ring Gear. The parameters are gear ratio, module, number of teeth, and face width, shown in Figure 71.

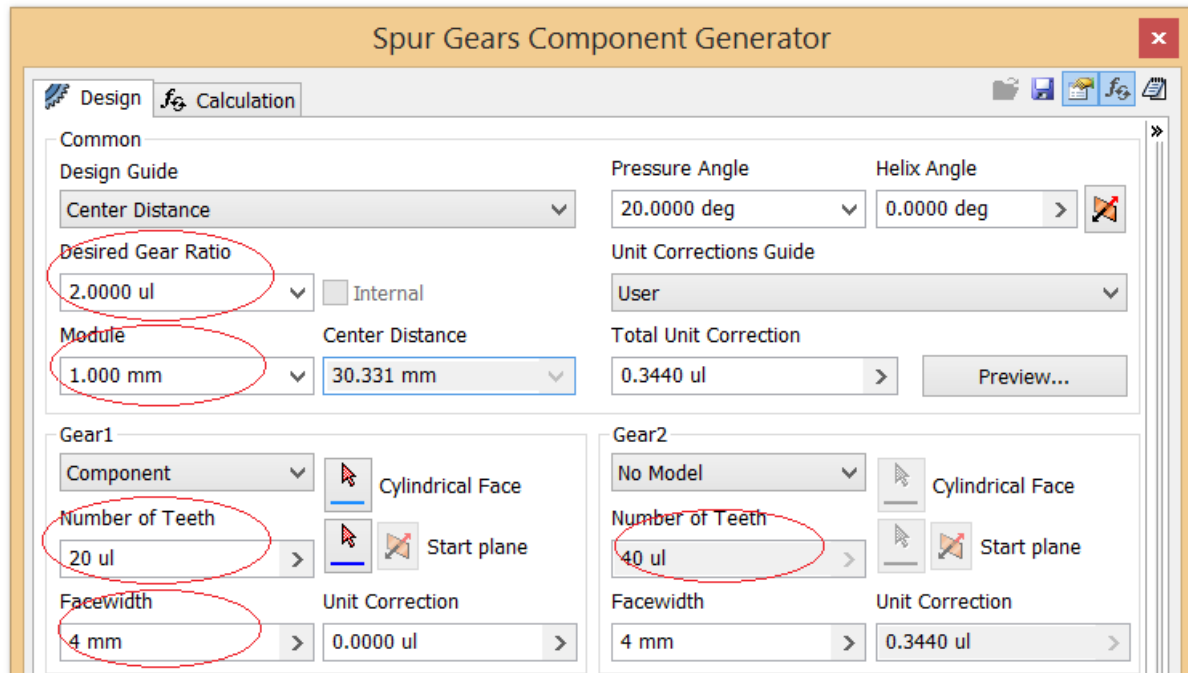


Figure 71 Design parameters of spur gears.

Over and under the SG and RG were positioned covers, in order to assign more stability to the structure. All spur gears and PGS covers, shown in Figure 73, were cut from 4 mm thickness PMMA plate by Universal Laser printer, through Adobe Illustrator Software.

Valve Carrier Design and Assembly Procedure

In order to insert the aortic valve molds into the Spinning Device, other CAD designs were made to be 3D printed: Valve Carriers (VCs) and Shaft Supports (SSs) for the aortic valve molds. VCs and SSs were basic cylindrical structures, designed to be joined together and fixed through M3 screws (Figure 72).

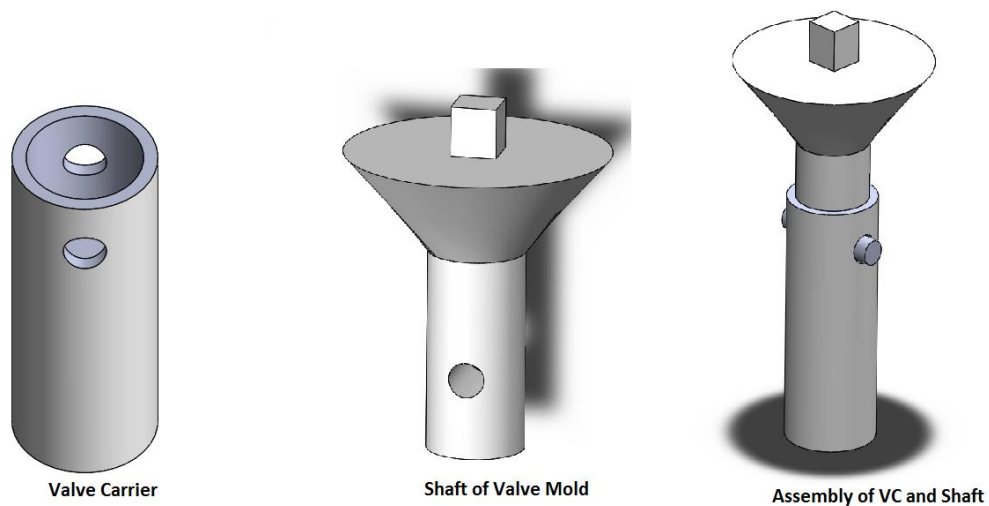


Figure 72 Valve Carrier, Shaft of the Valve Mold, and their fixation assembly that allows the rotational transition to the valve mold.

VCs were glued on four PG, achieving the final configuration of the SD shown in Figure 73.

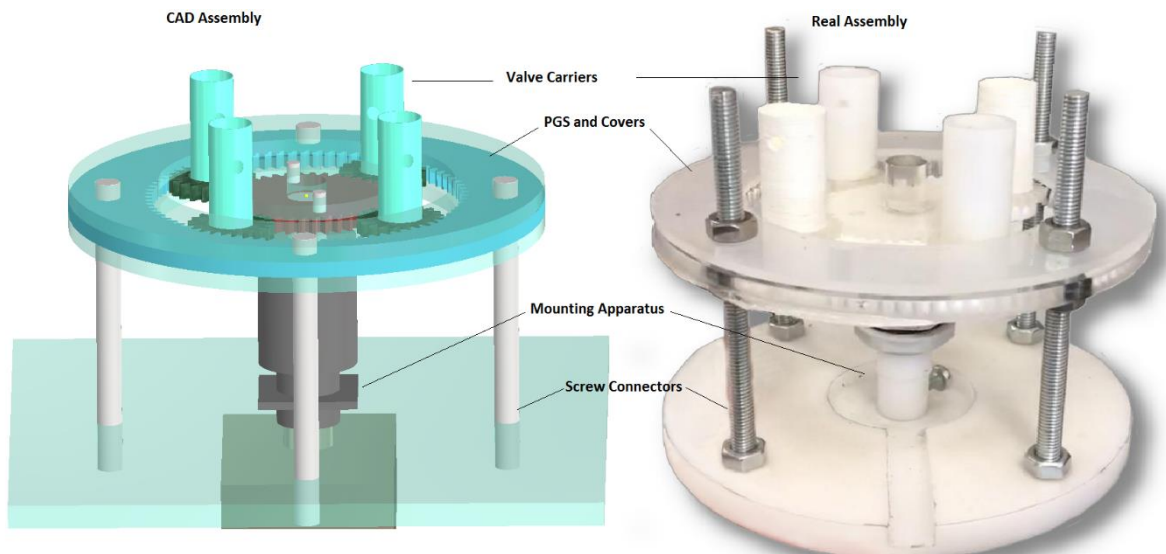


Figure 73 On the left CAD assembly, on the right the real assembly of the Spinning Device.

Inclined Support Design and Assembly Procedure

Furthermore, a support was used to give an inclination to the spinning structure. Three different angles (40° - 60° - 80°) were assigned during the preliminary manufacturing of polymeric aortic valves. The satisfactory leaflet thickness has been achieved at 40° , and the support (inclined plane) was adjusted, respectively.

The manufacturing process of SD has been finished when it was positioned to the inclined support and it is presented in Figure 74.

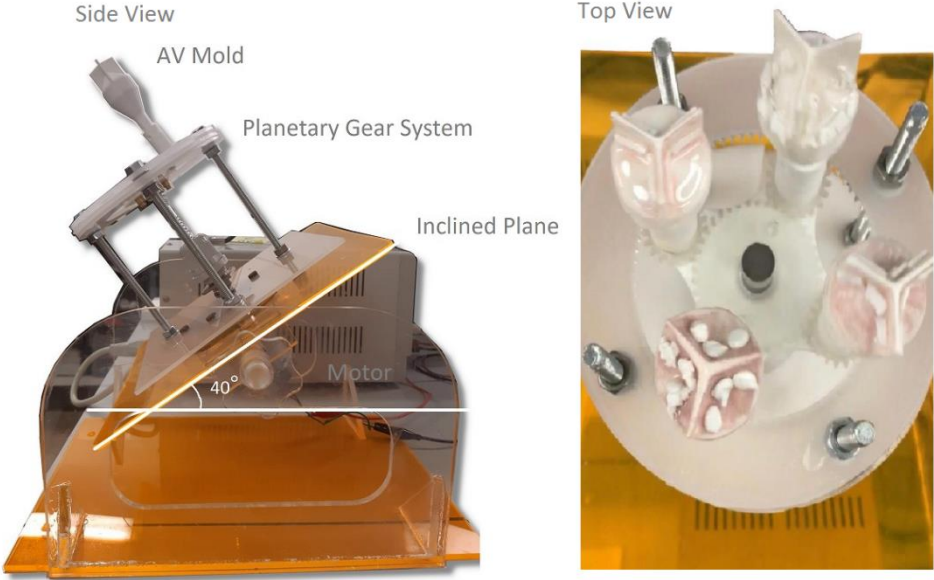


Figure 74 Spinning Device inclined at 40°, on the left, uploaded of the aortic valve molds into the VCs on the right.

3.5. Workflow of the Manufacturing Process

The manufacturing process developed in the present work of thesis was the combination of three protocols aimed to the production of the calcified leaflets and a tailored inner mold, that are needed for the obtainment of the whole aortic root.

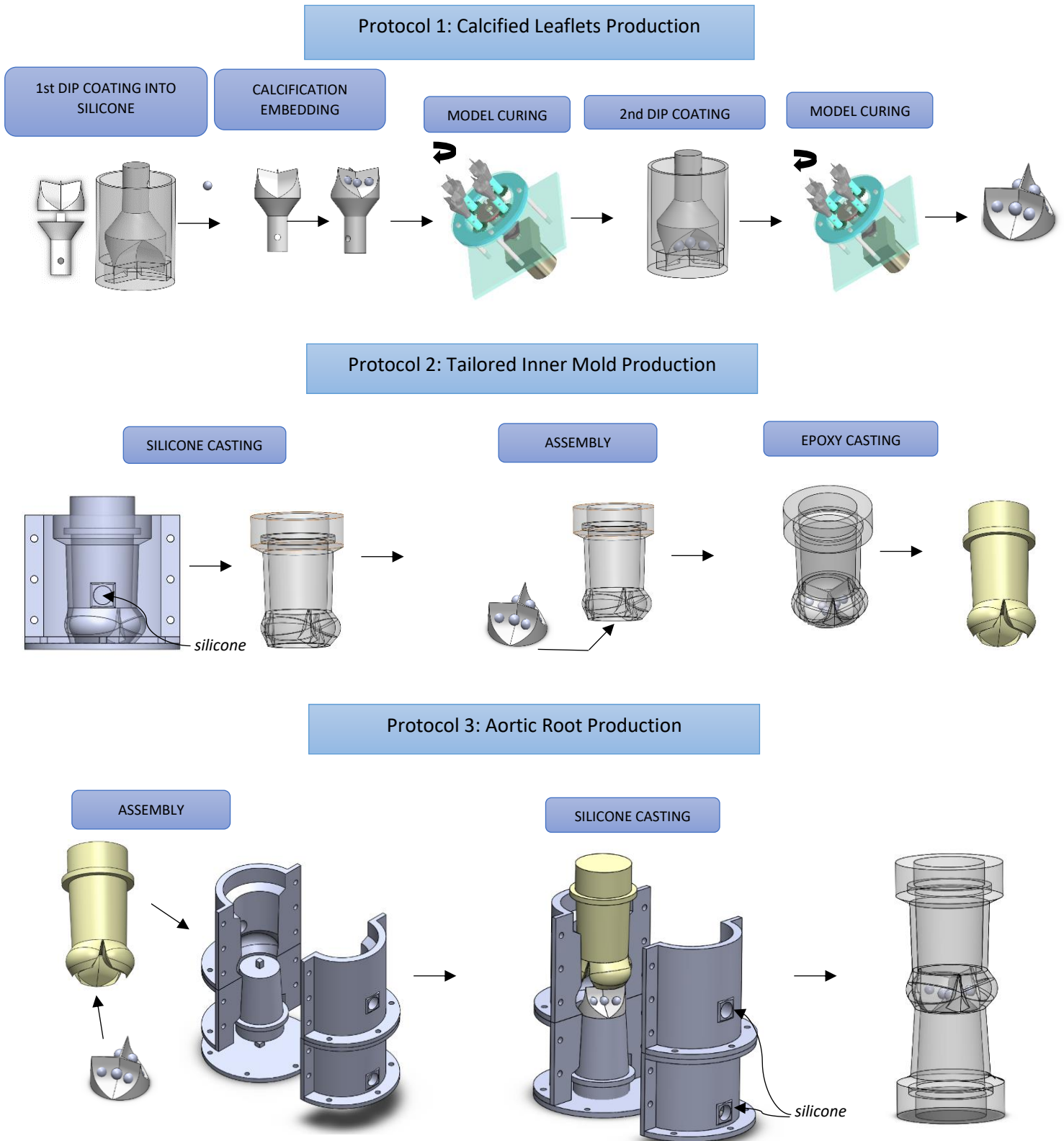


Figure 75 Representation of the three protocols developed for the silicone model manufacturing.

3.6. Molds Design

The manufacturing protocol presented in the work of thesis required different types of molds, as it is shown in Figure 76.

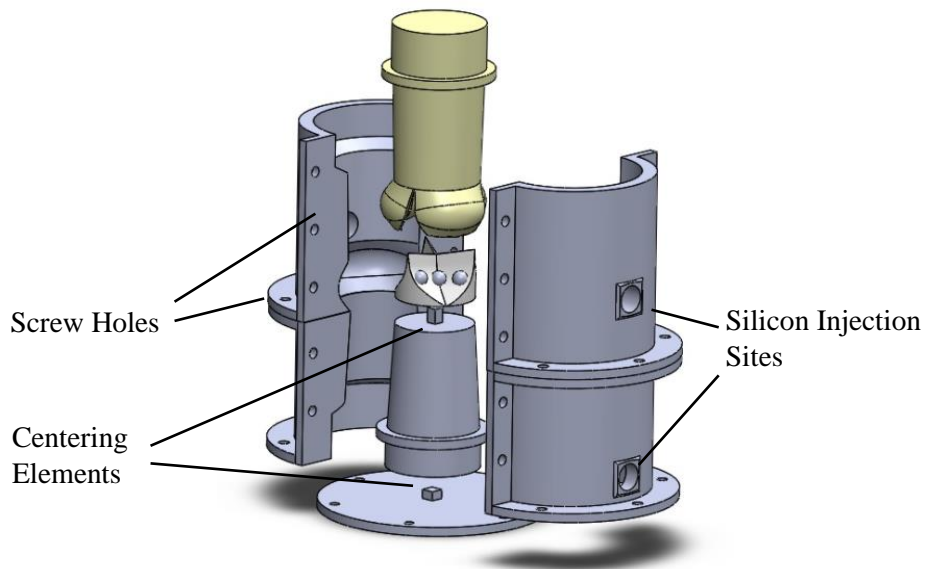


Figure 76 CAD assembly of some of the designed molds.

They can be classified as inner and outer molds:

Inner molds defined the internal geometry of the silicone model. Some of them were standardized for every produced model and 3D printed: they are the tricuspid/bicuspid valve mold, that defined the leaflets geometry and internal configuration of the AR, and the mold representing the Inflow tract. Conversely, the mold representing the ascending aorta (AA) tract was ad-hoc produced in epoxy resin and tailored on each valve.

Outer molds were responsible of the external conformation of the final model. They represent an external predefined shape of the AR, extending through the Inflow and AA tract. They were 3D printed. In the primary design, outer molds consisted in two unique sides; later they were subdivided into four tracts, in order to facilitate the disassembly of the molds, without breaking the silicone model. A basal outer mold was used to inferiorly seal the structure. Outer molds are characterized by:

- Centering elements between inner molds, and the basal mold. They avoided movements during the injection of silicone, keeping controlled the interspace dimension.
- Sites for the silicon injection through syringe.
- Screw holes to keep closed together the external molds.

For each mold, first of all an analysis of the anatomical structures they refer is carried out, in order to highlight the **geometry of each component**. Successively the **molds designed** for the models manufacturing, are presented.

3.6.1. Tricuspid Aortic Valve Mold

To produce polymeric calcified AVs, first of all, the physiological AV (PAV) geometry must be modeled. AV leaflets and annulus dimensioning was derived from the literature analysis (Table 1, Chapter 1) and mainly from studies carried by Labrosse [29] and Schiena [4]. The models were realized following the parameters mentioned in Figure 77.

Some assumptions were considered in order to design the tricuspid AV model, as shown in Figure 77:

1. The three cusps of the valve are identical in dimension and features. H was chosen 16.9 mm. They were modeled as a three-lobed epicycloid uniformly spaced around an axis every 120° .
2. Diameter of the annulus (D_b , Figure 77) range size is from 22mm to 27mm. It was chosen 23mm.
3. Diameter of the Sino-Tubular Junction (D_c , Figure 77) range size is from min 20mm to max 31.5 mm. It was chosen 23 mm.
4. Valvular leaflets thickness was set 0.6 mm thick, and their height was 16.8 mm.
5. Arantius Nodulus, in closed configuration, was set 3 mm (X_s , Figure 77) below the Sino-Tubular Junction.
6. The nominal angle α (Figure 77), between the valvular base and the tangent to the belly of the leaflet was 30° .

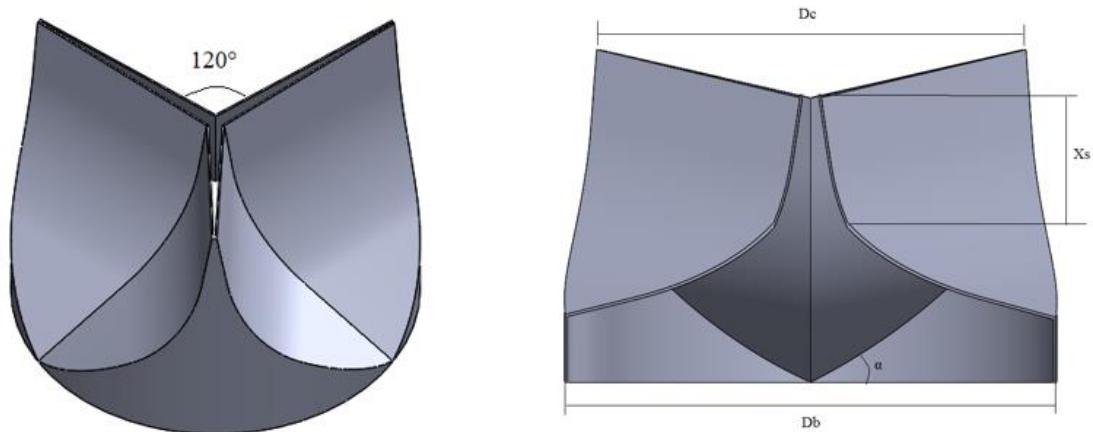


Figure 77 On the left, the free edge of the leaflet angle was demonstrated. On the right, aortic valve geometry parameters: D_b , the base diameter; D_c , the commissure diameter; X_s , the height of the coaptation of leaflets in the center; α , the angle of the leaflet in the closed configuration.

From the geometrical parameters of the AV model, AV molds were generated: Preliminary Design and Final Design.

Preliminary Design

The preliminary design (Figure 78) satisfied the main parameters identified in Figure 77, but it was not able to replicate realistic anatomical geometry. It was created for a preliminary verification of the efficacy of the dip-coating manufacturing process. The results were analyzed with respect to the measurements of the thickness of the resulting leaflet.

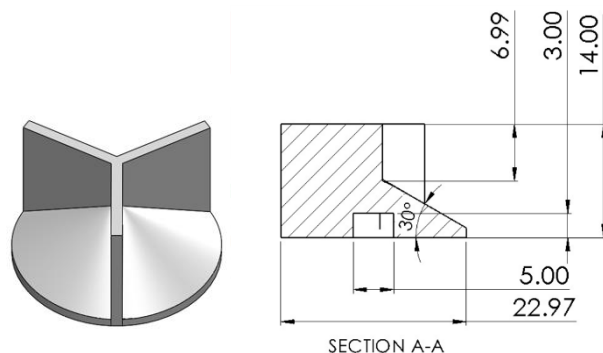


Figure 78 CAD model of Preliminary Design

Final Design

In the final design, improvements in the reproduction of the physiological conditions were reached not only in terms of dimensions but also of anatomical shape. Therefore, the achievements of the final design, shown in Figure 79, were:

- Realization of interleaflet triangles.
- More realistic curvature of the belly surface.
- Surface continuity between belly and nodulus areas of the valve.
- Arantius Nodulus.
- Sino Tubular Junction.

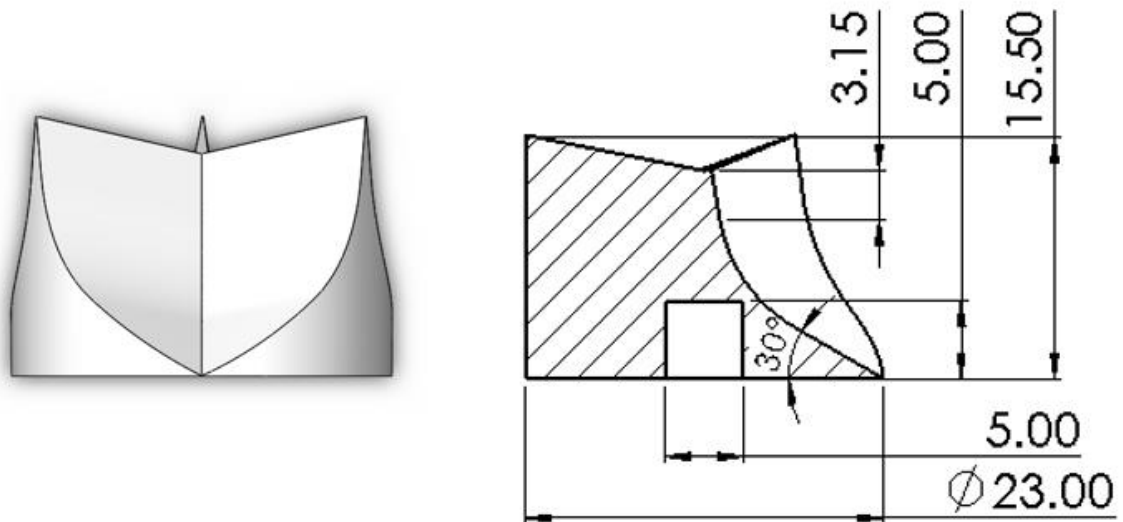


Figure 79 Final CAD model of the more physiological valve mold.

3.6.2. Bicuspid Aortic Valve Mold

To reproduce the bicuspid valve, the most common congenital aortic valve abnormality, as already described in Chapter 1, it was decided to eliminate one of three free edges. The remaining free edges replicated a general BAV condition since two cusps were merged comparing to the tricuspid aortic valve.

The mold in SolidWorks (Figure 80) was generated starting from the tricuspid valve final geometry, described in previous paragraphs, hence all dimensions were maintained the same. Then, it was

differentiated through the fusion of the two cusps. It was done applying the function “Revolved Cut” of 120°.

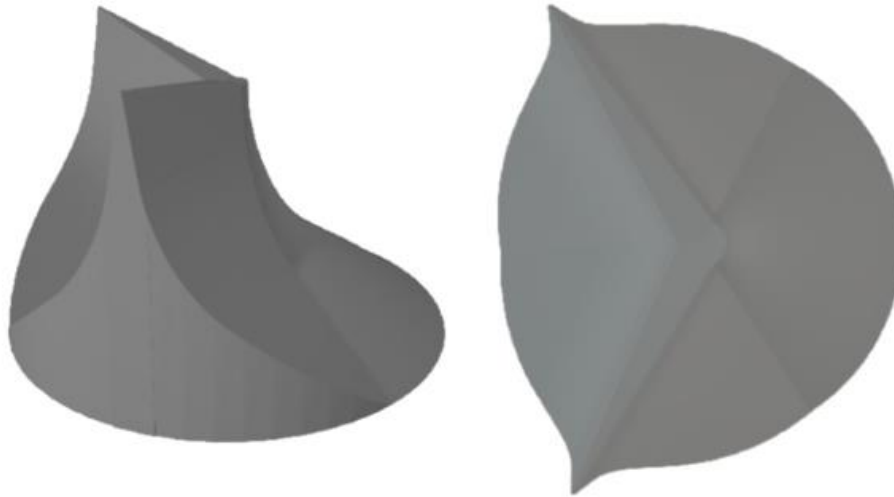


Figure 80 The CAD model of BAV

3.6.3. Aortic Root Molds

AR was designed to provide the AV stability, by its integration with Aortic Valve commissures and annulus, in order to resist the diastolic load without going through the collapse of the structure. AR was modeled as the area between annulus and STJ, comprising Valsalva Sinuses (VS) to obtain more realistic results and better functional simulation of the compliance of the structure [4]. Inflow and AA tracts were also considered in order to provide the space necessary to connect the model to a hydraulic testing circuit, through connectors described in literature [96].

Assumptions followed for the parametric AR configuration are:

1. The three Valsalva Sinuses have identical sizes and features. They were modeled as a three-lobed epicycloid uniformly spaced around an axis every 120°.
2. The height of the sinuses is determined by AV model height, in order to be compatible.
3. The wall thickness is set 5 mm.
4. Extension-portions upstream and downstream the AR, that allow a connection with hydraulic test benches.
5. Annulus and STJ diameters respect AV dimensioning.

Since two CAD models were designed for Aortic Valves, also two corresponding Aortic Roots are designed: preliminary and final one. Therefore, they differ for values of annulus and STJ diameter and for the shape of the area corresponding to the commissure profile of the leaflet (rectangular for preliminary AR, triangular for final AR). The final model was improved with respect to the preliminary one, also through the extension of the inflow and AA tracts. This enhancement should allow an easier connection of the phantom to the hydraulic testing circuit, through the use of connectors mentioned before [96].

CAD models of Aortic Roots phantoms are shown in Figure 81.

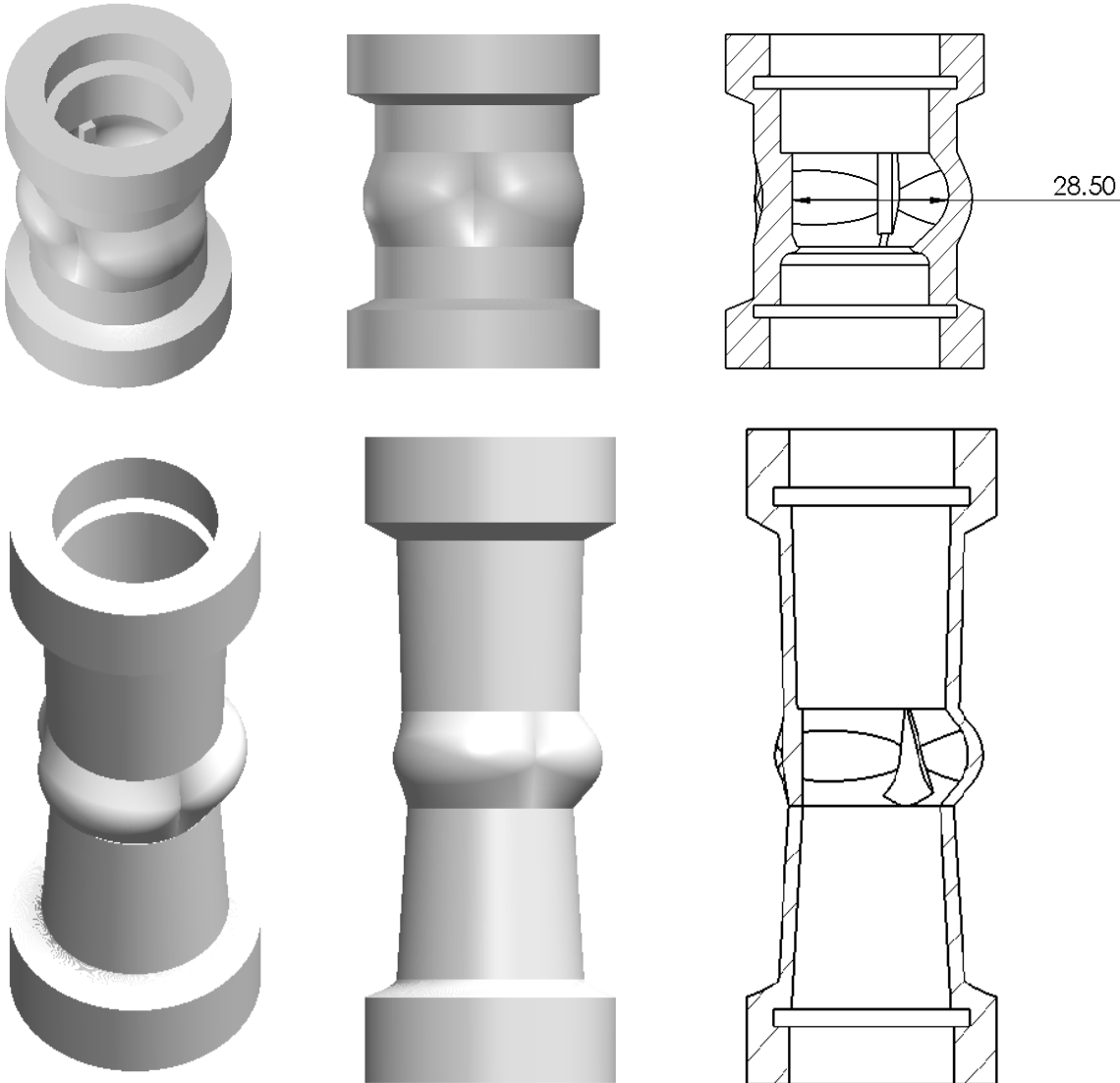


Figure 81 Preliminary (on the top) and final (on the bottom) configurations of the Aortic Root. From the left the two views of the CAD drawing, on the right the technical drawing to focus the attention on the commissures' area: rectangular for preliminary design and triangular for the final one.

The molds to realize the two AR configurations are shown in Figure 82. They are constituted by Outer and Inner molds, in order to create an interspace where to cast the silicone. Different section's dimensions were blended through *Loft* feature, hence maintaining the real diameter values extracted from literature. The Final Mold was improved, compared to the Preliminary one, because each external mold was divided into two sub-molds, in order to facilitate the opening. Furthermore, each sub-mold had its own injection hole positioned at the bottom (not on the top, as for Preliminary Mold), to allow better air escape during the casting process.

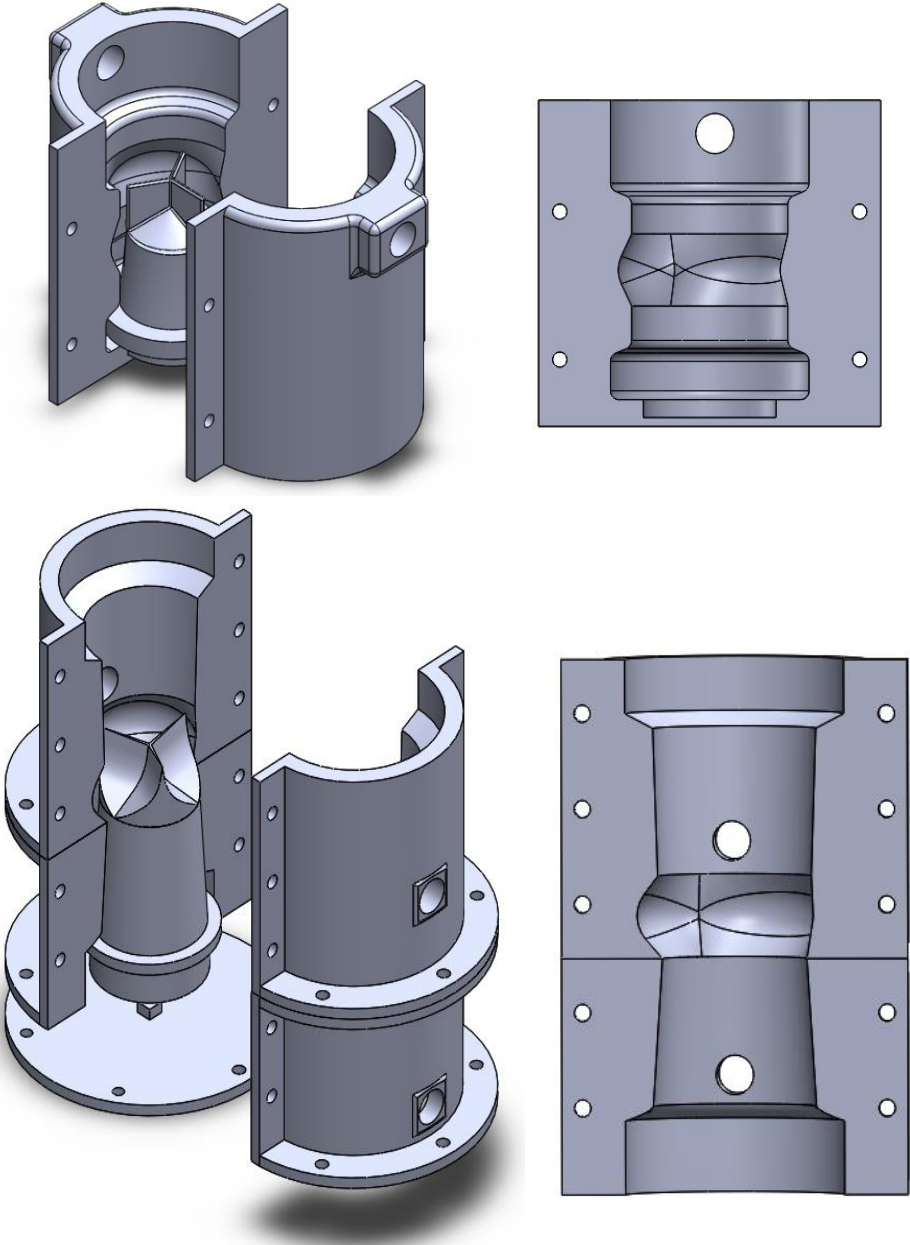


Figure 82 Aortic Root Inner and Outer Molds. On the top, the preliminary molds, on the bottom the final molds.

3.6.4. Custom Inner Mold

A Custom Inner Mold proved necessary in order to be positioned above the inner mold of the Aortic Root. The peculiarity of this mold is that it was tailored for every silicone valve, since it had on the bottom the cavities corresponding to the core of the calcific pattern the valve is carrying. It also gave the shape of the AA tract. A CAD example of Custom Inner Mold is shown in Figure 83.

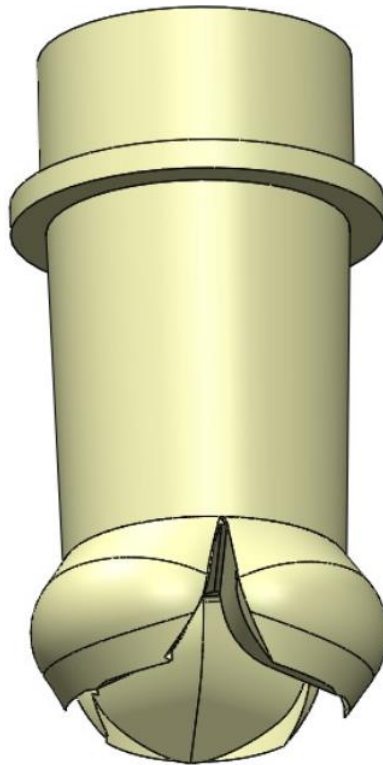


Figure 83 Example of Custom Inner Mold.

A Silicone Mold (SM) is needed, where to cast epoxy (Figure 84) in order to obtain the custom inner mold. Since the resin doesn't merge with silicone rubbers, it was decided to realize the mold in Sorta Clear 18, in order to allow an easy extraction of the cured epoxy. Two SMs are designed, in order to be used for the two versions of Aortic Root, preliminary and final.

The final SM differed from the preliminary since it was decided to take into consideration only from the annulus up.



Figure 84 Silicone Molds. On the left, the preliminary one, on the right the final one.

To obtain the SMs, outer and inner molds were necessary, and they were called Silicone-Casting Molds (SCM). They were 3D printed, in order to cast inside the silicone. They are shown in Figure 85.

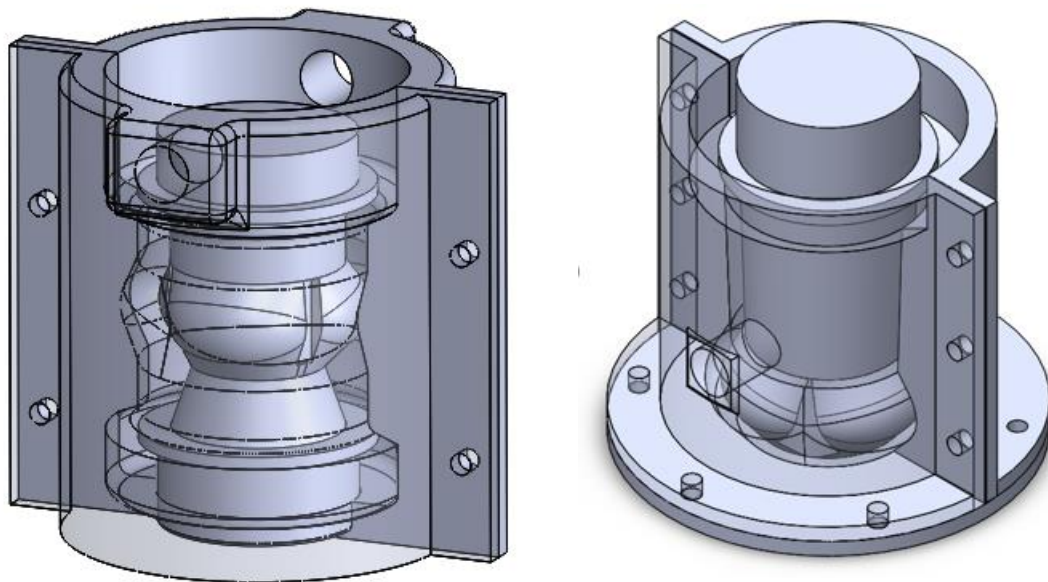


Figure 85 Silicon-Casting Molds. On the left the preliminary one, on the right the final one.

3.7. Calcification Pattern

To realize the pathology of AV stenosis, the present work of thesis suggests as solution the incorporation of 3D printed calcification patterns into the silicon phantom.

3D printed patterns were designed in order to simulate:

- *Most recurrent morphology and location* underlined by literature.
- *Thickness* comparable with respect to biologic aortic valve and wall. The thickness was reproduced by modifying the CAD design volume, as showed in Halevi work [6] .

Calcific deposits' **morphology** was designed based on the following assumptions:

- Only moderate and severe stenosis entities were considered. The reason of the choice was the established need to perform TAVI training for moderate and severe stenosis, that are the main cases when this technology is used.
- Of the three stages of calcification growth process (Chapter 1), it was taken into consideration only the last one. Since aortic valve disease is asymptomatic in the early phases, TAVI is performed mainly at advanced stage.
- PLA was used as preliminary material for calcified aortic valve manufacturing, for the reasons described in Chapter 3.
- Regarding the morphology of the calcific deposits, the present work of thesis took the inspiration from the patterns identified by Thubrikar [5] and confirmed from many subsequent studies [6] [97], [98] (Chapter 1).

Pattern 1- Radial: progressive fusion of nodules of calcium deposits along the attachment line, area of maximum cyclic flexion, and progressively spreads radially to the free edge.

Pattern 2 – Arc/Partial Arc Shape: presence of calcific nodules starting from two points in the attachment line and proceeding along the coaptation line of the cusps giving origin to an arc or partial arc.

Both the patterns are designed for moderate and severe stenosis grade. The transition from moderate to severe stenotic grade was reached by increasing the **surface area** of the calcific pattern and its **thickness**. An increase of the surface area of the calcific pattern is considered responsible of the decreasing in effective orifice area of the valve [74]. It was decided to cover with the 3D printed calcific pattern 33% of the total surface of one cusp in the case of moderate stenosis, and 45% in severe stenosis, as highlighted from Halevi study [6]. The augmented thickness of the pattern is accountable for a challenging opening and closure of the leaflets, which brings to higher pressure gradient across the valve.

To reproduce the calcification patterns, preliminary 3D printed modelled depositions were employed, varying only the surface area. They were useful to assess the feasibility of the manufacturing method. Successively, parametrized ad-hoc patterns were designed, in order to have a better fitting between calcification and silicone valve, and to standardize the shifting from moderate to severe stenosis, changing design parameters (both thickness and surface area). Parametrized patterns could be employed in further studies.

Pattern 1-Radial

The pattern realized in *preliminary model* is shown in Figure 86.



Figure 86 Ad-hoc 3D printed PLA preliminary pattern.

As mentioned before, these patterns are 3D printed as calcific deposits prototypes. The range of natural valve thickness is between 0.87 ± 0.27 mm (value of aortic cusps thickness under healthy conditions [99]) and 4.8 mm (maximum thickness value of calcification [6]), hence for the patterns alone the thickness was set 1 mm. The patterns were realized in PLA filaments for the reasons explained in Chapter 3. To increase the grade of severity, an expansion of surface is done: 38 mm^2 for moderate stenosis (Figure 86, on the left) and 63 mm^2 for severe stenosis (Figure 86, on the right).

Successively, the *parametrized model* was designed. SolidWorks CAD model of the aortic valve was used as starting point (Figure 87, A). “Extruded Cut” of a circle was applied from the center of the valve, concentric to the valve annulus, whose diameter is D_{circle} (Figure 87, B). The valve volume underwent Boolean subtraction of the area of the circle. A crown-shaped model was obtained (Figure 87, C), and the surfaces selected in blue constitute the pattern of the calcific deposit. It was necessary to isolate the blue pattern, to create a part-file that can be meshed and 3D

printed. It was generated an assembly-file: it had to contain the crown-shaped structure and an empty part. Selecting the empty part in the assembly, “Edit Component” and “Copy Surface” (this command is obtained putting $d = 0.0\text{mm}$ in “Offset Surface”), it was possible to save the surfaces of interest (the blue surfaces) as a part file. At this point the thickness was increased of 1 mm for moderate stenosis and 1.5 for severe stenosis. The obtained calcific entity can be applied to each cusp (Figure 87, D) since the three inter-commissural distances were supposed to be equal, hence the three cusp were identical. Technical drawings were recorded in Appendix B.

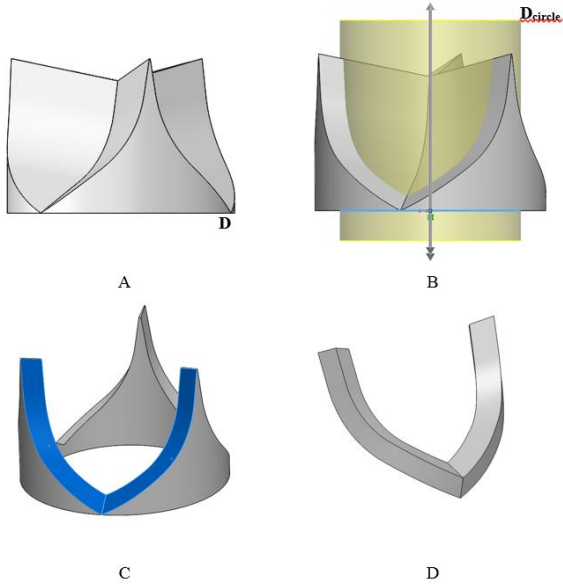


Figure 87 Representation of the CAD process of realization of the calcific pattern 1

To increase the grade of severity of the stenosis, it was possible to decrease the area of the circle (diameter D_{circle}), that identifies the geometric orifice area (GOA, described in Chapter 1, Figure 87, B), anatomical area of the aortic valve orifice, defined by American Heart Association as an alternative for the estimation of stenosis grade. To verify the assessment of the stenosis grade of the designed patterns for the valve of annulus-diameter $D = 23\text{mm}$, the ratio D_{circle} / D was compared with literature values [18] (Table 10):

Literature value D_{circle}/D	Designed value D_{circle}/D	Stenosis Grade
0.5	0.5 ($D_{\text{circle}}= 11.5\text{mm}$)	Moderate
0.3	0.3 ($D_{\text{circle}}=6.9\text{mm}$)	Severe

Table 10 Summary of the values of D_{circle}/D taken from literature, the values used in the work and the classification of the severity grade.

Pattern 2 – Arc/Partial Arc Shape

Arc and partial arc were obtained in the *preliminary model*, as shown in Figure 88.



Figure 88 Arc shape pattern are shown. On the left spots-shape, on the right planar shape.

The thickness was set again 1 mm. The expansion in covered surface due to the progression from moderate to severe stenosis was realized using partial arc shape (surface area 34 mm^2) evolving in arc shape (55 mm^2).

It has to be mentioned, that planar shapes were used, as shown in Figure 88, to preliminary assess the stability of the adhesion between the calcific deposits and the cusps. They were also useful to investigate the accumulation of embedding silicon around the calcific pattern, that could lead to non-reliable values of thickness.

The same pattern was also reproduced in the *parametrized CAD design* in order to improve the fitting of the calcific deposit on the valve-mold, and to easily change the parameter to shift from moderate to severe stenosis. The steps to obtain the pattern are illustrated and explained below:

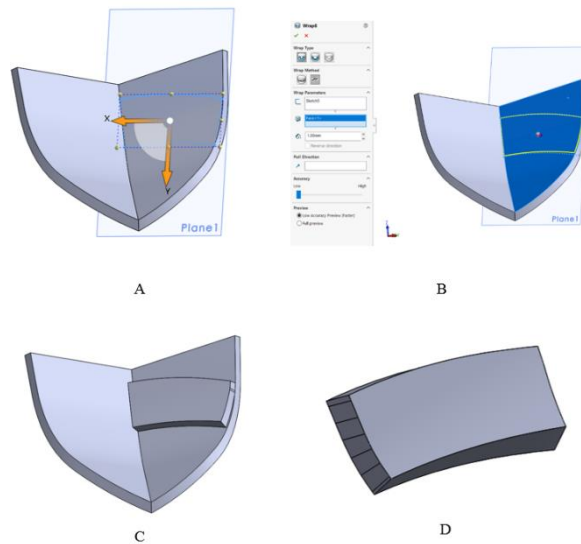


Figure 89 Representation of the CAD process of realization of the calcific pattern 1.

Two cusps were isolated from the CAD valve model file. A plane parallel to the cusp on the right was generated and there half of the sketch of the arc pattern was drawn (Figure 89, A). It was necessary to draw the pattern onto a plane external to the cusp, since its surface is curvilinear. To extrude the designed sketch, the function “Wrap” is selected (Figure 89, B) and the desired shape is obtained (Figure 89, C). In order to extrapolate from the design only the calcification pattern (Figure 89, D), the same methodology explained for the Radial pattern is exploited. Mirroring the pattern allows to have a complete arc pattern above the entire cusp. Technical drawings are recorded in Appendix B.

As highlighted from the analysis made by literature, thickness values were set at 1 mm for moderate stenosis and 1.5 mm for severe stenosis. To quantify the area of the surface that have to be covered by the calcific pattern, following before mentioned Halevi study, the “measure” tool provided by SolidWorks was used. The total tricuspid cusp surface was 267 mm², hence the area shielded by the pattern was 85 mm² for moderate stenosis, and 120 mm² for severe stenosis. It has to be noticed that the percentage of the total leaflet area that was covered by calcification has a constant growth rate of 1 mm/year [97], so the calcified area increases quadratically before saturating when the whole leaflet is covered.

Arc Shape pattern was designed not only for the reproduction of calcifications in tricuspid aortic valve models, but also in the bicuspid aortic valve models. The same procedure, mentioned before, for the obtainment of the design can be applied for this case. The only difference is the location of

the calcification pattern, that was the coaptation line for tricuspid valve, and it was in the cusps attachment [53] for bicuspid valves, as shown in Chapter 1. It could be developed in further works.

3.8. Assessment of the Leaflets Thickness with Preliminary Pattern

The evaluation of the **thickness** of the silicone leaflets affected by preliminary calcification pattern, was carried on based on the following assumptions:

- The thickness of the calcification pattern was set by design 1 mm.
- The silicone samples of Tricuspid Valve (Section 3.7.) were collected in groups:
 - Physiological valves (TP): 5 samples
 - Radial pattern valves (TR): 4 samples
 - Arc/partial arc valves (TA): 4 samples
- For every sample, measurements through digital caliper were performed to obtain values of thickness of the leaflet including the calcification.

For every sample, only 1 cusp was measured, assuming all the cusps were equal, since same calcification patterns were embedded in every cusp. For every cusp, a free margin area and a belly area were distinct, as defined in literature [100].

For the analyzed cusp, measurements shown in Figure 90 were done, in order to obtain a mean value and standard deviation. The selected points intended to be measured were derived from literature [99] :

- In TP group: measure of free margin area, measure of belly area.
- In TR group: measure of belly area.
- In TA group: measure of free margin area.
- For each group (TP, TR, TA), the mean value of thickness and standard deviation among the samples within the group were obtained.



Figure 90 Representation of the selected measurement points in the cusp. From the left: TP, TR, TA.

The results, obtained through Excel, were compared with values highlighted from literature [99] and a previous work [4].

3.9. Assessment of the Cusp Surface Covered by Preliminary Pattern

As mentioned in Chapter 3.7., the evaluation of the grade of stenosis was carried out, not only with respect to the thickness of the calcific pattern, but also regarding the percentage of cusp surface covered by the calcification.

The surface of one cusp can be considered fixed, due to geometrical design. Thanks to SolidWorks tool, it was possible to assess that the area measured 311.8 mm^2 .

The calcification patterns were also designed constant, in order to obtain 33% of covered cusp in moderate stenosis, and 45% in severe stenosis, values highlighted from literature [6].

3.10. Manufacturing Protocols

3.10.1. Leaflets Manufacturing Protocol

In order to obtain the silicon models of the aortic valves, both physiological and pathological cases, a protocol is established, and its steps are reported below.

1. Prepare the silicon mixture (Sorta Clear 18), as described in *Chapter 3.2.3*.
2. Slowly pour 15 gr of silicone into the *Dipping Container*.
3. Connect *inner valve mold* to the *Shaft Support* through specific encaster.
4. Dip the assembly valve mold and support into the *Dipping Container*. Slowly lift the valve mold & support from the container, paying attention to remove with a spatula extra material dripping down (1st Dip Coating into silicone, Figure 91).
5. Two situations:
 - For physiological valve reproduction, go on point 6 (2nd Dip Coating, Figure 91).
 - For calcified valve model, apply with the help of tweezers the 3D printed calcification patterns (Chapter XYZ) on the silicon (Calcification Embedding, Figure 91).
6. Insert the *Shaft Support* into *Spinning Device* and fix it to the valve carrier with a M3 screw in the specific hole. Turn on Spinning Device. Set the power supply to values of voltage 8-9 V and at inclination angle of 40° (Model Curing, Figure 91).
7. Leave the valves spinning for the Cure Time of the silicone (24 hrs for SortaClear 18), removing extra material leaking down from the leaflets along the shaft with a spatula (Model Curing, Figure 91).
8. At the end of the cure time, repeat steps 4, 6, 7 (2nd Dip Coating, Model curing, Figure 91).

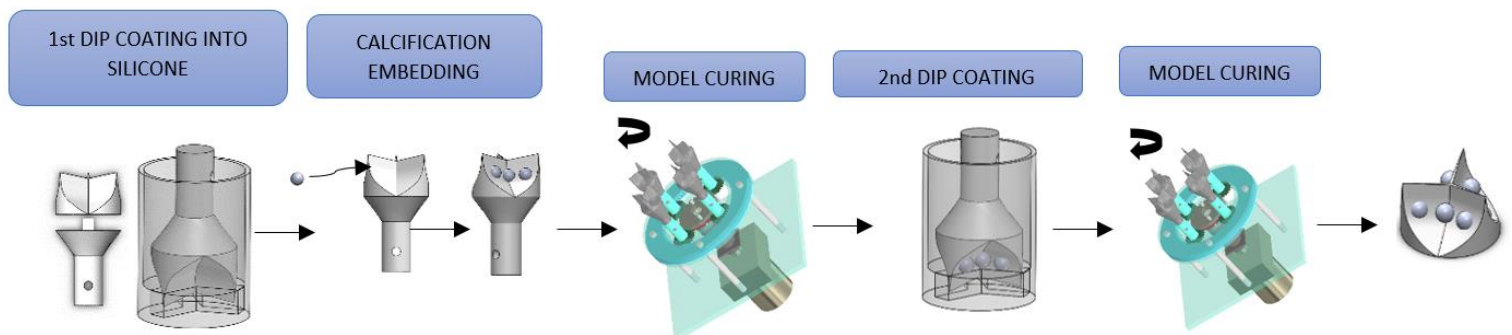


Figure 91 Representation of the leaflets manufacturing process, with .

3.10.2. Custom Inner Mold Manufacturing Protocol

SM Manufacturing Protocol

1. Prepare the silicone mixture (Sorta Clear 18), as described in *Chapter 3.2.3*.
2. Couple the outer and inner SCMs (Figure 92).
3. Inject the silicone mixture by syringe into the mold using the casting channels.
4. Wait for the polymerization of the material at a temperature between 20° and 30° for the curing time (24 hours, for Sorta Clear 18).
5. Decouple SCMs outer and inner components.

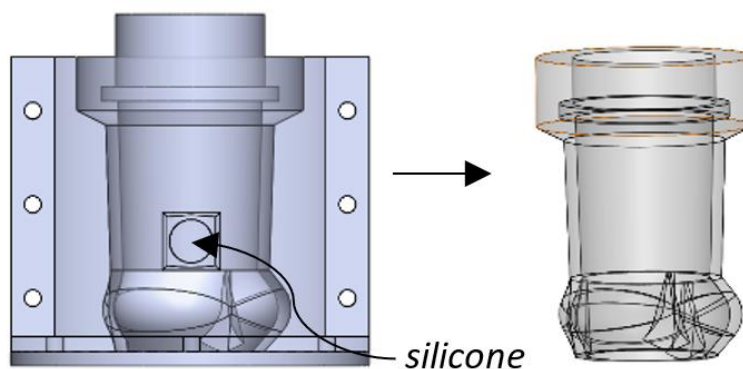


Figure 92 On the left frontal view: one side of the outer SCM and the inner SCM. On the right, the obtained SM – final configuration.

Custom Inner Mold Protocol

1. Prepare the epoxy resin mixture (E-30 Epoxy Resin), as described in *Chapter 3.2.2*.
2. Place fabricated silicone CAV on the CAV mold inside SCM (Figure 93).
3. Poor the epoxy resin mixture inside SM.
4. Wait for the solidification of the material at a temperature between 20° and 30° for at least 10 hours.
5. Remove the epoxy resin from SM. Custom Inner Mold has obtained calcification pattern and SV shape.

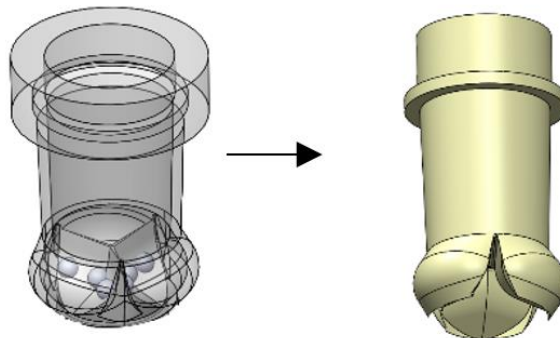


Figure 93 SM with the CAV inserted, on the left, and final Custom Inner Mold in epoxy.

3.10.3. AR Manufacturing Protocol

Preliminary AR

1. Prepare the silicone mixture (Sorta Clear 18), as described in Chapter 3.2.3.
2. Assemble AR preliminary molds, polymeric CAV and Custom Inner Mold.
3. Inject the silicone mixture by syringe into the mold using the casting channels.
4. Wait for the polymerization of the material at a temperature between 20° and 30° for at least 24 hours.
5. Decouple the outer and inner molds of the assembly.

Final AR

1. Prepare the silicone mixture (Sorta Clear 18), as described in *Chapter 3.2.3*.
2. Assemble AR final molds, AV mold covered by the polymeric CAV and Custom Inner Mold (Assembly, Figure 94).
3. Inject the silicone mixture by syringe into the mold using the injection ports. Inject firstly from the channel of the bottom mold. When the silicon material reaches the annulus level, add the upper mold and go on casting silicone from its holes at STJ level (Silicone casting, Figure 94) .
4. Wait for the polymerization of the material at temperature between 20° and 30° for at least 24 hours.
5. Decouple the outer and inner molds of the assembly to obtain the silicone model.

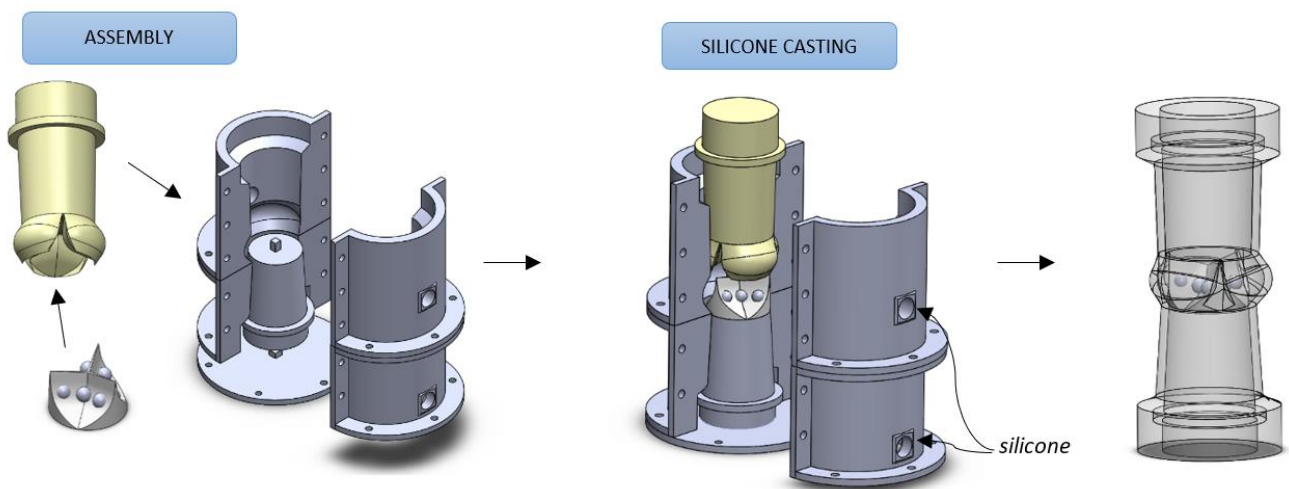


Figure 94 Representation of manufacturing process of Aortic Root- final configuration).

4. RESULTS

The objective of the thesis was the development of a manufacturing method for the realization of calcified aortic valve models. Their anatomical geometry was derived from information obtained from literature, in order to provide an average design that respects general pathophysiological characteristics. As explained in the previous chapter, the manufacturing process of aortic valves consisted in dip-spin-coating procedure supplemented by the embedding of calcified patterns. Successively, the silicone aortic roots were casted around the aortic valves, in order to obtain a complete **phantom model**, that could be used as support for clinicians' training in transcatheter therapies. In this Chapter the realized prototypes of aortic valve, aortic root and custom inner mold are shown and analyzed in order to evaluate the success of the proposed manufacturing process.

4.1. Verification of the Manufacturing Technique of the Aortic Valve

Dip-spin coating technique was verified as valid method for the obtainment of thin physiological and calcified aortic valves, by the obtainment of 12 samples of tricuspid aortic valve (4 physiological, 4 radial calcification, 4 arc/partial arc calcification).

An example of physiological Aortic Valve Model is shown in Figure 95.



Figure 95 Physiological Aortic Valve Model obtained through dip-spin coating of Sorta Clear 18. Frontal, top views. On the right the free edge is cut through a cutter.

	Natural Aortic Valve [99]	Schiena Model [4]	Phantom Model
Free Margin Thickness [mm]	0.87 ± 0.27, 20-59 years 1.42 ± 0.51, ≥ 60 years	1	0.79 ± 0.03
Belly Thickness [mm]	0.41 ± 0.09	1	0.69 ± 0.02

Table 11 Comparison between thickness values: mean value and standard deviation of natural physiological aortic valve from literature, objective value of a previous work from literature and mean value and standard deviation of manufactured phantom models. The values for the natural aortic valve are combination of the thickness of the three cusps.

Comparing these data, it is possible to highlight that the leaflet thickness of the valve models produced by a dip-spin coating technique are within the range of physiologic natural valves and this technique could provide thinner valve leaflets, with respect to the casting technique used by Schiena.

Another benefit brought by the manufacturing technique introduced in the present work of thesis, is the capability to embed calcific deposits into the leaflets, without excessively increasing the thickness value of the valve cusps. This was not possible through the casting technique used in previous works. 8 calcified aortic valve models were obtained with the following calcific deposit patterns: radial and arc/partial arc patterns (Chapter 3.7.), as shown in

Table 12. The preliminary ad-hoc 3D printed patterns gave results that can be considered for the reproduction of moderate and severe grade of stenosis, since they fulfill the requirements of increasing thickness and covered surface of the cusp, assessed in Chapter 3.7. The realized calcified phantoms satisfied the parameters highlighted from literature:

- Values of thickness of the calcified cusp of the phantoms fit the range 1-4.8 mm [6].
- Percentage of one cusp surface covered by calcific deposits shifts from 33% (moderate case) to 45% (severe case) [6].

Preliminary and parametrized pattern configurations are shown in Table 12.


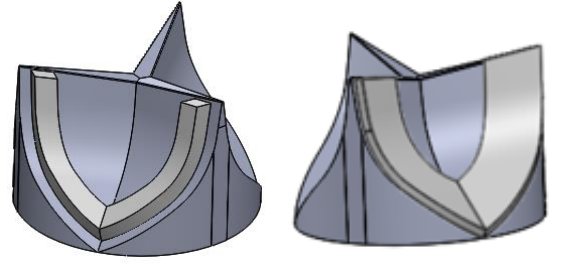

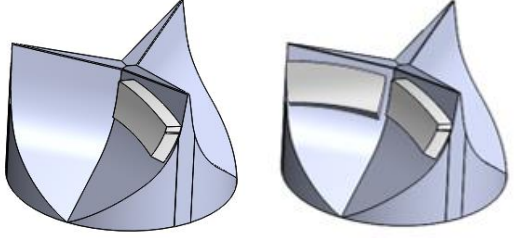
	Preliminary Pattern Configuration	Parametrized Pattern Configuration
Radial Pattern	 <p>Moderate Severe</p>	 <p>Moderate Severe</p>
Thickness [mm]	<p>2.34 ± 0.29</p>	<p>Hypothetical 2.58 mm (0.79 mm 1st dip-coating + 1 mm calc + 0.79 mm 2nd dip-coating)</p>
Partial Arc / Arc Pattern	 <p>Moderate Severe</p>	 <p>Moderate Severe</p>
Thickness [mm]	<p>2.76 ± 0.10</p>	<p>Hypothetical 2.58 mm (0.79 mm 1st dip-coating + 1 mm calc + 0.79 mm 2nd dip-coating)</p>

Table 12 Thickness mean values and standard deviation of the Calcified Aortic Valves.

For the two patterns of the preliminary configuration, the value of thickness is obtained as mean value and standard deviation, since it is the mean of the values of thickness measured from the 4 samples of each pattern. The classification in moderate and severe stenosis, with respect to the covered surface, fulfilled literature requirements by geometrical design. For the final

configuration, only hypothetical values can be presented. Effective measurements should be assessed in further works.

4.2. Aortic Root

To validate the efficiency of the developed aortic root manufacturing protocol, two prototypes of AR were obtained and analysed: preliminary and final aortic root configurations.

The obtained ARs included Calcified Aortic Valve (prototypes described in Chapter 4.1.), Aortic Root (from annulus to STJ, comprising VS), Inflow Tract, Ascending Aorta tract (AA) and extension portions of the aortic root wall to connect the model to hydraulic set ups. Both ARs replicated the physiological height of aortic root highlighted from literature (20 mm, Table 1). The main features of the obtained AR models are summed up in Table 13.

	Preliminary AR	Final AR
Annulus and STJ Diameters	23 mm (min value from liter.)	26 mm (average value from liter.)
VS Maximum Diameter AR	30 mm	35 mm
inflow+AA	20 mm	70 mm
Total Height of the Model	60 mm	110 mm
Wall Thickness	5 mm	2.5 mm
Commissure Geometry	Rectangular	Triangular

Table 13 Summary of the ARs dimensions.

The change in commissure geometry of the AR, shifting from rectangular to triangular shape of the commissures, proved to have improved effects on the sealing between silicone aortic valve and aortic root. Rectangular shape of the commissures, respect to rectangular one, was responsible of a smaller attachment area for the silicon leaflets, hence less stability of the valve, and more probability of valve breakage in future fluidynamic tests. Also, inflow and AA were longer, in order to allow implantation of the TAVI device of various sizes and designs within the model. Bubbles very visible in the preliminary AR, are not present anymore in the final AR, hence proving a best casting performance within the final AR Molds (as mentioned in Chapter 3.3.3., final molds were decomposed into 4 pieces, and the injection holes were positioned at the bottom of every piece). They are shown in Figure 96 and Figure 97.

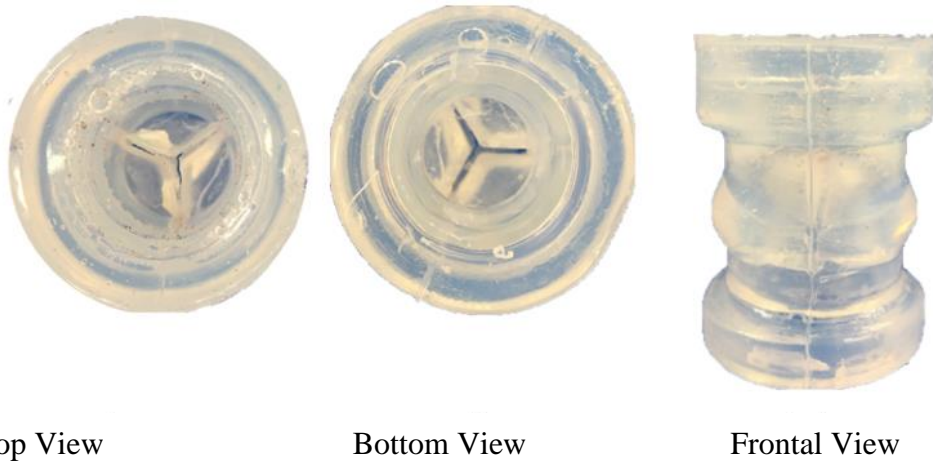


Figure 96 Prototype of preliminary AR model. It includes AV with partial arc calcification pattern.



Figure 97 Prototype of final AR model. It includes AV with radial calcification pattern.

As indicated in Chapter 3.5., an intermediate phase was introduced to obtain the silicone aortic root model. The Custom Inner Mold provided the solution for the obtainment of the inner shape of the AA tract of the AR, and above all it allowed to protect the silicone leaflets during the casting, making an airtight custom covering of the valve, even in the most irregular spots, due to the embedded calcifications. The use of epoxy resin was found to be optimal for this purpose because it proved:

- The ability to perfectly mould the calcific patterns, fitting the smallest cracks, when at liquid state.
- The easy detachment from silicone, once at the solid state.
- The conservation of the solid shape, in order to be used as inner mold during the casting technique.

Produced Custom Inner Molds, both for preliminary and final aortic root, are shown in Figure 98.

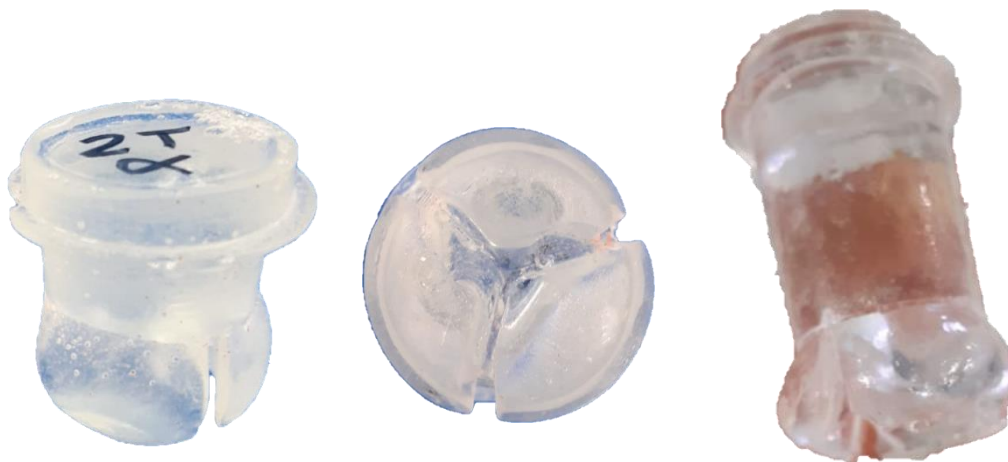


Figure 98 Custom Inner Molds. On the left for preliminary AR in frontal view and top view to show the cavities, molds of the calcific patterns. On the right custom inner mold for the final AR.

5. CONCLUSION, LIMITATIONS AND FURTHER DEVELOPMENTS

This study mainly focused on the development of the manufacturing techniques for models of stenotic aortic valves, whose flexible structures, such as leaflets and aortic root, were made of Sorta Clear 18 silicone, and the calcification patterns of 3D printed PLA.

The rise of the new technologies for cardiovascular therapies, especially complex and critical approaches such as percutaneous prosthetic implants and transcatheter treatments, bring forth the requirement of training interventional clinicians. The need of simulator-based training programs has also been encouraged by authorities as FDA in April 2004 in order to speed up the learning process of the complex approaches. In this scenario ranks this work of thesis, with the goal of realize phantom models that can be used in training programs.

Through the analysis of literature, the developed manufacturing protocol employed the combination of three main technologies in a multistep process.

First of all, the dip-coating technique allowed the obtainment of silicone valve leaflets. The ad-hoc developed Spinning Device allowed the contemporary realization of 4 valves models, speeding up production times and allowing uniform thicknesses of the silicone models.

Furthermore, the epoxy resin casting on the silicone valve allowed to obtain inner molds custom for any type of calcification pattern.

The pourable property of silicone allowed to achieve the realization of anatomical shapes characterized by complex geometries, through casting process.

The presented protocols show the possibility to reach the prescribed goal, using cost-effective and easily accessible materials and manufacturing technologies. Therefore, the analysis of the obtained prototypes proved and validate the techniques used in the manufacturing of CAV and AR.

The embedding technique allowed to entrap within the silicone leaflets the calcific deposits, in particular radial and arc shape patterns, highlighted from literature. However, the embedding efficiency has yet to be verified by testing the models to the pulsatile flow conditions. A method to reproduce moderate and severe grades of stenosis was presented, designing a preliminary and a parametrized pattern and changing its surface area and thickness, hence reducing the effective orifice area of the polymeric valve.

Limitations and future developments

Since this work was focused on the development of a manufacturing protocol for models aimed to clinicians' training, the introduction of the coronary arteries into the aortic root design could provide a more complete anatomical structure and more realistic behaviour under fluid dynamic testing conditions.

Even though the efficiency of the presented manufacturing process was validated by the produced phantoms, the intermediate phase that allowed to impress any calcification pattern in a custom inner mold, slowed down and complicated the production process. The use of standardized calcification patterns could make possible to have a standard 3D printed inner mold and simplify the process.

The choice of the materials, both PLA and Sorta Clear 18, was made taking into consideration previous studies from literature (Chapter 3) but their mechanical properties differ from those of the natural tissue. The focus of the work was the development of the manufacturing technology, nonetheless, there is a need to assess the mechanical properties and compliance behaviour of the chosen materials to effectively simulate aortic tissue and calcification.

Hemodynamic assessment is needed to quantify the hemodynamic performance of the developed models in stationary and pulsatile flow.

Furthermore, the models are designed for training purposes, hence it would be necessary to use materials which are compatible with imaging techniques used during interventional cardiology training, such as echocardiography or X rays/fluoroscopy. Sorta Clear 18 showed the best echogenic properties among tested silicone materials in the preliminary assessment [3] while its compatibility with X rays was not yet demonstrated. The compatibility with medical imaging of the materials for calcification reproduction was not tested in this work. However, from the value of PLA attenuation coefficient, highlighted from the analysis of literature [101], the compatibility with fluoroscopy imaging is evinced. Furthermore, metallic cover for PLA or 3D printing of specific PLA, that are filled up to 70% by weight with high density ceramics (LATIGRAY, LATI s.p.a, Gornate Olona (VA), Italy), could be an alternative to provide improved visibility under X-rays. Clinician test should also be carried in order to evaluate the grade of fidelity in the reproduction of dimension and geometries, the grade of visibility through echography technique of the phantom, the catheter and the artificial aortic valve.

In addition, the developed manufacturing protocol could also be broadened to the realization of models aimed to pre-procedural planning, starting from the segmentation of patient clinical

images, instead of from general geometries. For the moment, the presented methodology provides models that are a valid support for hand-on clinicians training and the spread of interventional techniques, that are increasingly important in a social context where life expectancy is growing.

ABBREVIATIONS

AA: Ascending Aorta Tract

A(V)S: Aortic (Valve) Stenosis

AP: Aortic Pressure

AR: Aortic Root

AV: Aortic Valve

AVA: Aortic Valve Annulus

BAV: Bicuspid Aortic Valve

CAD: Computer Aided Design

CAV: Calcified Aortic Valves

CDC: Conventional Dip-Coating

CIM: Custom Inner Mold

CT: Computed Tomography

DM: Direct Measurements

ECG: Echocardiographic

EOA: Effective Orifice Area

FDA: Food and Drug Administration

LC: Left-Coronary

LF: Left Ventricle

LVP: Left Ventricle Pressure

LHS: Left Heart Simulator

MDCT: Multidetector Row Computed Tomography

MSCT: Multislice Computed Tomography

NC: Non-Coronary

PAV Physiological Aortic Valve

PAR: Paravalvular Aortic Regurgitation

PET: Polyethylene Terephthalate

PET: Positive Electrons Tomography

PG: Planet Gear

PGS: Planetary Gear System

PLA: Poly-Lactic-Acid
PS: Power Supply
PVR: Paravalvular Regurgitation
RC: Right-Coronary
RG: Ring Gear
SAVR: Surgical Aortic Valve Replacement
SCM: Silicone Casting Mold
SD: Spinning Device
SG: Sun Gear
SM: Silicone Mold
SS: Shaft Support
STJ: Sinotubular Junction
STL: Stereoligraphic file
SV: Sinuses of Valsalva
TA: Tricuspid Arc
TAVI: Transcatheter Aortic Valve Implantation
TAVR: Transcatheter Aortic Valve Replacement
TMVR: Transcatheter Mitral Valve Replacement
TP: Tricuspid Physiological
TR: Tricuspid Radial
TEE: Trans-esophageal Echo
TTE: Transthoracic Echocardiogram
VAJ: Ventriculo-Aortic Junction
VC: Valve Carrier
VS: Valsalva Sinuses
VHD: Valvular Heart Disease
VMTK: Vascular Modeling Toolkit
VIC: Valve Interstitial Cell
WSS: Wall Shear Stress

APPENDIX A

In this section are collected the datasheet of the used materials: silicone rubber, mold-surface coating and imprinting resin.

SORTA-Clear™ Series

Addition Cure Silicone Rubber Compounds



www.smooth-on.com

PRODUCT OVERVIEW

SORTA-Clear™ Series rubbers are premium water white translucent silicone rubbers (platinum catalyst) which cure at room temperature with negligible shrinkage. Available in Shore **12A, 18A, 37A and 40A hardness**, these rubbers feature high tensile and tear strength. SORTA-Clear™ 12 and SORTA-Clear™ 37 offer the convenience of a 1A:1B by volume mix ratio. The 18A and 40A products require a gram scale for measuring parts A + B.

SORTA-Clear™ silicones are ideal for making prototype, jewelry or other molds of any configuration where model visibility is important (i.e. extracting a model from the mold via cutting). Materials such as urethane, epoxy or polyester resins can then be cast into SORTA-Clear™ silicone without application of a release agent. Other materials such as wax and low melt metal alloys can also be cast into SORTA-Clear™. SORTA-Clear™ can be pigmented with **SILC Pig™ silicone pigments**.

SORTA-Clear™ 18, SORTA-Clear™ 37 and SORTA-Clear™ 40 are **FOOD SAFE** and can be used for culinary applications including casting chocolate and other confections. (See separate technical bulletin for usage instructions available at www.smooth-on.com). **SORTA-Clear™ 12 is not food safe**, and should not be used for food related applications. **SORTA-Clear™ 18** is skin safe and certified by an independent laboratory.

TECHNICAL OVERVIEW

	Mixed Viscosity (ASTM D-2393)	Specific Gravity (g/cc) (ASTM D-1475)	Specific Volume (cu. in./lb.) (ASTM D-1475)	Mix Ratio	Pot Life (ASTM D-2471)	Cure Time	Shore A Hardness (ASTM D-2240)	Tensile Strength (ASTM D-412)	100% Modulus (ASTM D-412)	Elongation at Break % (ASTM D-412)	Die B Tear Strength (ASTM D-624)
SORTA-Clear™ 12	6,000 cps	1.07	25.9	1A:1B by volume	40 min.	12 hrs	12A	320 psi	23 psi	590%	80 pli
SORTA-Clear™ 18	21,000 cps	1.08	25.6	100A:10B by weight	60 min.	24 hrs	18A	425 psi	35 psi	545%	80 pli
SORTA-Clear™ 37	35,000 cps	1.08	25.6	1A:1B by volume	25 min.	4 hrs	37A	600 psi	90 psi	400%	105 pli
SORTA-Clear™ 40	35,000 cps	1.08	25.6	100A:10B by weight	60 min.	16 hrs	40A	800 psi	90 psi	400%	120 pli

*All values measured after 7 days at 73°F/23°C

Shrinkage* (in./in.) (ASTM D-2566) < .001

Color: Water Clear Translucent

PROCESSING RECOMMENDATIONS

PREPARATION... Safety – Use in a properly ventilated area ("room size" ventilation). Wear safety glasses, long sleeves and rubber gloves to minimize contamination risk. Wear vinyl gloves only. Latex gloves will inhibit the cure of the rubber.

Store and use material at room temperature (73°F/23°C). Warmer temperatures will drastically reduce working time and cure time. Storing material at warmer temperatures will also reduce the usable shelf life of unused material. These products have a limited shelf life and should be used as soon as possible.

Cure Inhibition – Addition-cure silicone rubber may be inhibited by certain contaminants in or on the pattern to be molded resulting in tackiness at the pattern interface or a total lack of cure throughout the mold. Latex, tin-cure silicone, sulfur clays, certain wood surfaces, newly cast polyester, epoxy or urethane rubber may cause inhibition. If compatibility between the rubber and the surface is a concern, a small-scale test is recommended. Apply a small amount of rubber onto a non-critical area of the pattern. Inhibition has occurred if the rubber is gummy or uncured after the recommended cure time has passed.

Because no two applications are quite the same, a small test application to determine suitability for your project is recommended if performance of this material is in question.

To prevent inhibition, one or more coatings of a clear acrylic lacquer applied to the model surface is usually effective. Allow any sealer to thoroughly dry before applying rubber. Note: Even with a sealer, platinum silicones will not work with modeling clays containing heavy amounts of sulfur. Do a small scale test for compatibility before using on your project.

Safety First!

The Material Safety Data Sheet (MSDS) for this or any Smooth-On product should be read prior to use and is available upon request from Smooth-On. All Smooth-On products are safe to use if directions are read and followed carefully.

Keep Out of Reach of Children

Be careful. Use only with adequate ventilation. Contact with skin and eyes may cause irritation. Flush eyes with water for 15 minutes and seek immediate medical attention. Remove from skin with waterless hand cleaner followed by soap and water.

Important: The information contained in this bulletin is considered accurate. However, no warranty is expressed or implied regarding the accuracy of the data, the results to be obtained from the use thereof, or that any such use will not infringe upon a patent. User shall determine the suitability of the product for the intended application and assume all risk and liability whatsoever in connection therewith.

Applying A Release Agent - Although not usually necessary, a release agent will make demolding easier when pouring into or over most surfaces. Ease Release™ 200 is a proven release agent for making molds with silicone rubber. Mann Ease Release™ products are available from Smooth-On or your Smooth-On distributor.

IMPORTANT: To ensure thorough coverage, lightly brush the release agent with a soft brush over all surfaces of the model. Follow with a light mist coating and let the release agent dry for 30 minutes.

If there is any question about the effectiveness of a sealer/release agent combination, a small-scale test should be made on an identical surface for trial.

MEASURING & MIXING...

Before you begin, pre-mix Part B thoroughly. After dispensing the required amounts of Parts A and B into mixing container, **mix thoroughly for 3 minutes making sure that you scrape the sides and bottom of the mixing container several times.** After mixing parts A and B, vacuum degassing is recommended to eliminate any entrapped air. Vacuum material for 2-3 minutes (29 inches of mercury), making sure that you leave enough room in container for product volume expansion.

POURING, CURING & MOLD PERFORMANCE...

Pouring - For best results, pour your mixture in a single spot at the lowest point of the containment field. Let the rubber seek its level up and over the model. **A uniform flow will help minimize entrapped air.** The liquid rubber should level off at least 1/2" (1.3 cm) over the highest point of the model surface.

Curing - Allow the material to cure fully at room temperature (73°F/23°C) before demolding. SORTA-Clear™ 12 cures in 12 hours, SORTA-Clear™ 18 cures in 24 hours, SORTA-Clear™ 37 cures in 4 hours, and SORTA-Clear™ 40 cures in 16 hours. Do not cure rubber where temperature is less than 65°F/18°C.

Time to demold can be reduced with mild heat. **IMPORTANT: Rubber will darken considerably when exposed to heat.** Note: Allow mold to cool to room temperature before handling.

Smooth-On's Plat Cat™ platinum silicone accelerator can also be used to accelerate Sorta-Clear rubber. See the Plat Cat™ technical bulletin at www.smooth-on.com.

Post Curing - Post curing the mold will aid in quickly attaining maximum physical and performance properties. After curing at room temperature, expose the rubber to 176° F / 80° C for 2 hours and 212° F / 100° C for one hour. Allow mold to cool to room temperature before using. **IMPORTANT:** Rubber will darken considerably when exposed to heat.

Using The Mold - New silicone rubber molds exhibit natural release characteristics. Depending on what is being cast into the mold, mold lubricity may be depleted over time and parts will begin to stick. No release agent is necessary when casting wax or gypsum. Applying a release agent such as Ease Release™ 200 (available from Smooth-On) prior to casting polyurethane, polyester and epoxy resins is recommended to maximize mold life. Visit Smooth-On's FAQ section at www.smooth-on.com for information on a powder coating technique that will yield a dry matte finish to cured castings.

Mold Performance & Storage - The physical life of the mold depends on how you use it (materials cast, frequency, etc.). Casting abrasive materials such as concrete can quickly erode mold detail, while casting non-abrasive materials (wax) will not affect mold detail. Before storing, the mold should be cleaned with a soap solution and wiped fully dry. Two part (or more) molds should be assembled. Molds should be stored on a level surface in a cool, dry environment.



Call Us Anytime With Questions About Your Application.

Toll-free: (800) 381-1733 Fax: (610) 252-6200

The new www.smooth-on.com is loaded with information about mold making, casting and more.

070919-JR

XTC-3D™

High Performance 3D Print Coating



PRODUCT OVERVIEW

XTC-3D™ is a protective coating for smoothing and finishing 3D printed parts. It does not melt plastic. Two liquids are mixed together and brushed onto any 3D print. Coating self-levels and wets out uniformly without leaving brush strokes. Working time is 10 minutes and cure time is about 4 hours (depending on mass and temperature). **XTC-3D™** cures to a hard, impact resistant coating that can be sanded, primed and painted. Adding colors and metal effects is easy.

Inexpensive to Use – 1 oz covers 100+ square inches (see coverage information below).

90% Time & Labor Savings: XTC-3D™ fills in 3D print striations and creates a smooth, high gloss finish. The need to post finish is almost eliminated.

Coat any 3D Print Surface - XTC-3D™ can be applied to both SLA and SLS prints. It works with PLA, ABS, Laywoo, Powder Printed Parts and other rigid media. It also can be used to coat EPS, EPDM and urethane foam as well as wood, plaster, fabric, cardboard and paper.

XTC-3D™ does not contain VOC's, phthalates or phosphates.

Material Properties	
Mix Ratio By Volume	2A : 1B
Mix Ratio By Weight	100A : 42B
Mixed Viscosity - CPS. (ASTM D2393)	350
Specific Gravity - Mixed; g./c.c. (ASTM D1475)	1.09
Spec. Volume - Mixed; cu. in./lb. (ASTM D792)	25.1
Pot Life In Mass - (ASTM D2471)*	10 minutes
Pot Life In Flat Tray (Reduced Mass)	15 Minutes
Thin Film Working Time	20 minutes
Thin Film Tacky Recoat Time	90 minutes
Thin Film Tack Free Time	2 hours
Cure Time In Mass (100g)	2 hours
Cure Time In Thin Layer	3.5 hours
Color In Thin Layer (Slightly Yellow In Thick Sections)	Clear
Shore D Hardness (ASTM D2240)**	80D
* Dependant on mass ** Value measured after 7 days at 73°F / 23°C	

PROCESSING RECOMMENDATIONS

Preparation – Materials should be stored and used in a room temperature environment (73°F/23°C). Elevated temperatures will reduce Pot Life. XTC-3D™ Part A resin and Part B Hardener must be properly measured and thoroughly mixed to achieve full, high-strength, solid-cure properties. **Because no two applications are quite the same, a small test application to determine suitability for your project is recommended if performance of this material is in question.**

Avoid eye and skin contact. Avoid breathing fumes - use in a well ventilated area. NIOSH approved respirator is recommended. Wear safety glasses, long sleeves and rubber gloves to minimize skin contact. This material has a high exotherm (generates heat). Do not mix components in glass or foam containers.

Coverage – A very small amount of XTC-3D™ is needed to coat an average size 3D print. 1 oz / 28.3 grams of mixed material will cover 101 in² (651 cm²) applied at 1/64" (.04 cm) thickness.

Pre-Mix Part B: Before using, shake container vigorously.

Measuring and Dispensing – You need to be accurate in measuring for XTC-3D™ to cure properly. Parts A and B can be measured by either volume or weight. Dispense proper proportions of parts A and B into clean plastic, metal or wax-free paper containers (do not use foam or glass cups).

Extending Working Time - If left in a mixing cup with a concentrated mass, pot life will be short and material may cure in your cup due to exotherm. **Important** - Reduce the mass of the mixture to increase working time. **Example:** layer two sheets of aluminum foil together and create a single-use flat tray with vertical sides to contain the liquid resin. After mixing parts A and B, pour mixture into the aluminum foil to reduce the mass. Your working time will be significantly increased.

Mixing – Be sure mixing utensils have a square edge and are clean. Combine and mix proper amounts of Parts A and B. Mix thoroughly for at least 1 minute. Aggressively scrape the sides and bottom of mixing container several times. Use the square edge of mixing stick to bring material off of the sides and bottom of container and blend.

Important - Mixed XTC-3D™ Resin is exothermic, meaning it generates heat. A large, concentrated mass of mixed material in a container can generate enough heat to melt a plastic cup, burn your skin or ignite combustible materials. If material begins to exotherm, move it outside to an open air environment.

Safety First!

The material safety data sheet (MSDS) for this or any Smooth-On product should be read before using and is available on request. All Smooth-On products are safe to use if directions are read and followed carefully.

XTC-3D™ Resin PART A:

WARNING: IRRITANT TO EYES, SKIN & MUCOUS MEMBRANES.

XTC-3D™ Resin is irritating to the eyes and skin. Avoid prolonged or repeated skin contact to prevent possible sensitization. Avoid breathing vapors and use only with adequate ventilation. Wear personal protective equipment.

First Aid: In case of eye contact, flush thoroughly with water for 15 minutes and get immediate medical attention. In case of skin contact, wipe clean with white vinegar and wash thoroughly with soap and water. If irritation persists, get medical attention. If swallowed, do not induce vomiting. Drink 1 - 2 glasses of water and get immediate medical attention. If vapors are inhaled or if breathing becomes difficult, remove person to fresh air. If symptoms persist, get medical attention.

Keep Out Of Reach Of Children.

XTC-3D™ PART B Hardener:

WARNING: IRRITANT TO EYES, SKIN & MUCOUS MEMBRANES.

Epoxy Hardeners are corrosive materials and can cause severe eye and skin burns. They are sensitizers that may cause dermatitis from skin contact or vapor inhalation. Use these products only with adequate ventilation. Remove contaminated clothing and wash from skin with soap and water.

First Aid: In case of eye contact, flush thoroughly with water for 15 minutes and get immediate medical attention.

Keep Out Of Reach Of Children.

IMPORTANT: The information contained in this bulletin is considered accurate. However, no warranty is expressed or implied regarding the accuracy of the data, the results to be obtained from the use thereof, or that any such use will not infringe upon a patent. User shall determine the suitability of the product for the intended application and assume all risk and liability whatsoever in connection therewith.

Adding Color - XTC-3D™ can be colored with UVO™ or IGNITE™ colorants. Pre-mix color with Part A before combining with Part B.

Adding Fillers - A variety of dry fillers can be added such as Cast Magic™ or bronze or other metal powders, Glow Worm™, Quarry Tone™ or Ure-Fil™ powders. The maximum filler load is an amount equal to Part A by volume. Pre-mix filler with Part A before combining with Part B.

Applying XTC-3D™ - Use a disposable chip brush or foam brush to apply XTC-3D™. To achieve the thinnest coating possible we recommend applying material with a foam brush. Brushing on one thin layer of mixed material is recommended for most prints to create a smooth, uniform coating: less than 1/64"(.039 cm). To avoid drips and runs, continue brushing and working the surface until the resin begins to set up. For particularly complicated prints with intricate detail you may want to coat one section at a time for better control. XTC-3D™ bonds to itself.

If Adding More Layers - allow first layer to partially cure until "tacky hard" before applying the next layer. For best results, each layer should be applied thinly: less than 1/64"(.039 cm).

Curing: One layer will cure tack free in about 2 hours at room temperature (73°F/23°C). Mild heat (150° F/60° C) will cure material within 15 minutes. **Be careful:** some 3D print media will melt at temperatures above 200°F. Fully cured material will be hard and unable to penetrate with a finger nail.

Post Finishing - Cured material can be machined or sanded (wear NIOSH approved respirator mask to prevent inhalation).

Painting - XTC-3D™ can be painted and/or primed and then painted with acrylic enamel paints. For best results, lightly sand surface prior to painting.

Thinning XTC-3D™ for Coating Starch / Powder Printed Parts: Viscosity can be lowered with acetone or denatured alcohol to penetrate porous parts.

Mix Ratio	Cure Time
Thin: Mix 200 Parts A + 100 Parts B + 25 Parts Solvent.	12 Hours
Thinner: Mix 200 Parts A + 100 Parts B + 50 Parts Solvent.	24 Hours

The more solvent added, the longer XTC-3D™ will take to cure. Cured material will be more flexible.

Smoothing Surface - granular surface texture can be smoothed by applying a second coat of XTC-3D™ (for glossy finish) or lightly sanding for matte finish.

Applying a Release Agent - For applications where adhesion is not desired, a spray release Ease Release 200 available from Smooth-On may be used.

Removing Uncured Material: Scrape as much material as possible from the surface using a scraper. Clean the residue with E-POX-EE KLEENER™ available from Smooth-On, lacquer thinner, acetone or alcohol. Follow safety warnings pertaining to solvents and provide adequate ventilation.

Making Molds of Models Coated with XTC-3D™: Liquid mold making rubbers will adhere to cured XTC-3D™. Before mixing and applying Smooth-On silicone or urethane mold making rubbers, apply a thorough coating of Ease Release™ 200 or 205 release agent over cured XTC-3D™ and let dry.



Call Us Anytime With Questions About Your Application

Toll-free: (800) 381-1733 Fax: (610) 252-6200

The new www.smooth-on.com is loaded with information about mold making, casting and more.

050719-JR

E-30

FORMULATO EPOSSIDICO DA COLATA

Caratteristica principale di questo formulato è l'elevata trasparenza dei suoi componenti.

Viene impiegato nel settore artistico, nell'artigianato e nel modellismo, per realizzare colate trasparenti di spessore anche elevato, per l'inglobamento di oggetti, o ottenere l'effetto acqua. Viene inoltre utilizzato nell'industria della bigiotteria nell'imitazione degli smalti vetrosi.

Il prodotto colato in una superficie in piano si autolivella perfettamente; dopo l'indurimento la superficie risulta lucida e priva di aloni.

Prodotto a due componenti da miscelare prima dell'uso.

Componente A è una resina epossidica liquida esente da solventi, derivata da bisfenolo F.

Componente B è un indurente addotto a base di ammina cicloalifatica.

Caratteristiche dei componenti

	Comp. A resina	Comp. B indurente
Viscosità (mPa·s a 25°C)	1.800-2.000	350-450
Densità (gr/cm ³ a 25°C)	1,15	1,03
Colore Gardner	max 1	max 1
Rapporto miscela in peso	100	60

Cicli di indurimento

Pot-life della miscela a 25°C - massa 200 gr:	40 minuti
Indurimento apparente a 25°C - massa 200 gr, 3 mm:	8 ore
Indurimento completo a 25°C - massa 200 gr, 3 mm:	72 ore
Indurimento apparente a 25°C - massa 200 gr, 5 mm:	7 ore
Indurimento completo a 25°C - massa 200 gr, 5 mm:	72 ore

Il termine pot-life indica la vita utile della miscela per l'utilizzo in minuti, prima che inizi a riscaldare e quindi ad indurire. Il valore è riferito su una massa di 200 gr. Con masse maggiori i tempi di utilizzo si riducono.

L'indurimento apparente è uno stato di solido o semisolido che il prodotto raggiunge dopo che si è dissipato il calore sviluppatosi durante la reazione. Il pezzo è abbastanza duro da essere maneggiato, ma cede sotto la pressione dell'unghia



L'indurimento totale viene raggiunto quando tutte le molecole hanno reagito fra loro, creando macromolecole a lunga catena. A questo punto il pezzo ha raggiunto la sua stabilità, risulta indeformabile e acquisisce la sua resistenza meccanica definitiva.

La temperatura ambiente ha un'influenza notevole sia sulla viscosità dei 2 componenti, che sui tempi di indurimento della miscela. Con l'abbassare della temperatura la resina si addensa sensibilmente.

Questo non comporta però variazioni apprezzabili sul risultato finale.

La temperatura influisce anche sui tempi di indurimento. A tal proposito bisogna tener conto anche del calore che sviluppa la reazione: maggiore è la massa, più calore si sviluppa durante la reazione e minore è la dissipazione del calore prodotto.

Vi è una notevole differenza nei tempi di indurimento in relazione allo spessore dello strato colato. A parità di temperatura ambiente, uno strato di 3 mm può impiegare 8-10 ore prima di entrare nella fase di indurimento (causa la maggior dissipazione del calore) Mentre se lo spessore è di 8-10 mm inizia ad indurire dopo appena 3 ore.

I tempi sopra citati si riducono se la temperatura ambiente è più elevata, e si allungano con le basse temperature.

L'umidità dell'aria o la contaminazione con acqua possono dare opacità superficiale (fenomeno della "Carbonatazione"): quindi è necessario evitare tali condizioni durante il lavoro.

Se alcuni pezzi presentano tale fenomeno, è possibile eliminare l'opacità semplicemente lucidandoli con pasta abrasiva.

Suggerimenti per ottenere risultati ottimali

1. Conservare il prodotto in un luogo riscaldato durante la stagione invernale, in modo che la resina si mantenga fluida e scorrevole, mai a temperature inferiori a 5°C. Infatti, al di sotto di questa soglia, il componente A potrebbe presentarsi liquido e opaco, in fase gel e/o solido lattiginoso.

In tal caso, per riportare la resina allo stato normale, basta riscaldare a temperature di almeno 60°C.

2. Dosare i componenti sempre in peso, possibilmente con una bilancia a lettura digitale con sensibilità 1 o 2 gr rispettando le dosi indicate. Non variare mai il rapporto.

3. Mescolare accuratamente con una spatola a lama allungata, cercando di rimuovere il prodotto attorno alle pareti e sul fondo del contenitore, in modo da ottenere una miscela omogenea in tutta la massa. Attendere qualche minuto per la deaerazione prima di colare.

4. Lavorare in ambienti con temperature non inferiori a 18°C.

5. Dopo la colata verificare se non vi sono rimaste inglobate bolle d'aria, specialmente in corrispondenza di angoli o sottosquadro. Eventualmente agevolarne la fuoriuscita agendo con uno stecchino.



Fare indurire in un luogo riparato dalla polvere, possibilmente a temperatura più elevata: 30-40°C

In questo modo la resina si stende completamente e la superficie risulta perfettamente lucida e regolare.

6. Igiene sul lavoro: Indossare guanti protettivi durante la manipolazione dei componenti. Evitare il contatto con gli occhi e mucose. A fine lavoro lavare le mani prima con acqua e sapone, poi eventualmente con alcol etilico.

Non imbrattare il piano di lavoro, pulire con carta monouso. Ripulire gli attrezzi con alcool o DILUENTE EPOX PROCHIMA.

Confezionamento

320 e 800 gr, 1,6, 8, 24 Kg

Stoccaggio

Componente A: 5-35°C. Teme il gelo.

Componente B: 5-35°C.

Avvertenze

Non usare a temperature inferiori a 12-13°C.

Non usare oltre il tempo di lavorazione, trascorso il quale, in caso di aumento della viscosità, non bisogna assolutamente aggiungere diluente credendo di aumentare la vita utile del prodotto.

Consigli per l'uso in sicurezza

Indossare guanti e occhiali protettivi sia durante la miscela che nell'applicazione.

Lavare rulli e attrezzi con diluente epossidico o diluente nitro o alcol etilico denaturato appena terminato il lavoro.

Non gettare i residui ed il solvente di lavaggio nelle fognature.

Smaltire presso recuperatore autorizzato sia il solvente di lavaggio che gli imballaggi vuoti contaminati dai prodotti.



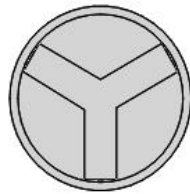
PROCHIMA S.r.l.
Via G. Agnelli, 6
61030 Calcinelli di Saltara (PU)
tel 0721.897635 - fax 0721.899655

APPENDIX B

In this section are recorded all the technical drawings of each CAD component: the Dipping Container, the molds employed for the prototyping of the aortic valve, the calcification patterns applied to the valve in order to simulate the stenotic pathology and the Shaft Support.

Dipping Container

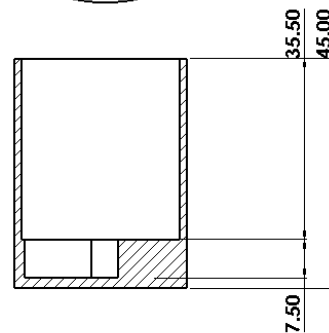
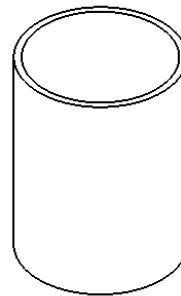
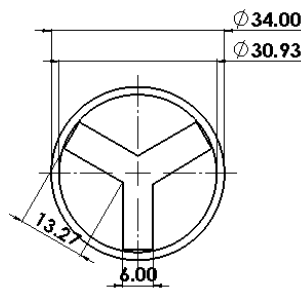
It was used in the dip coating process.



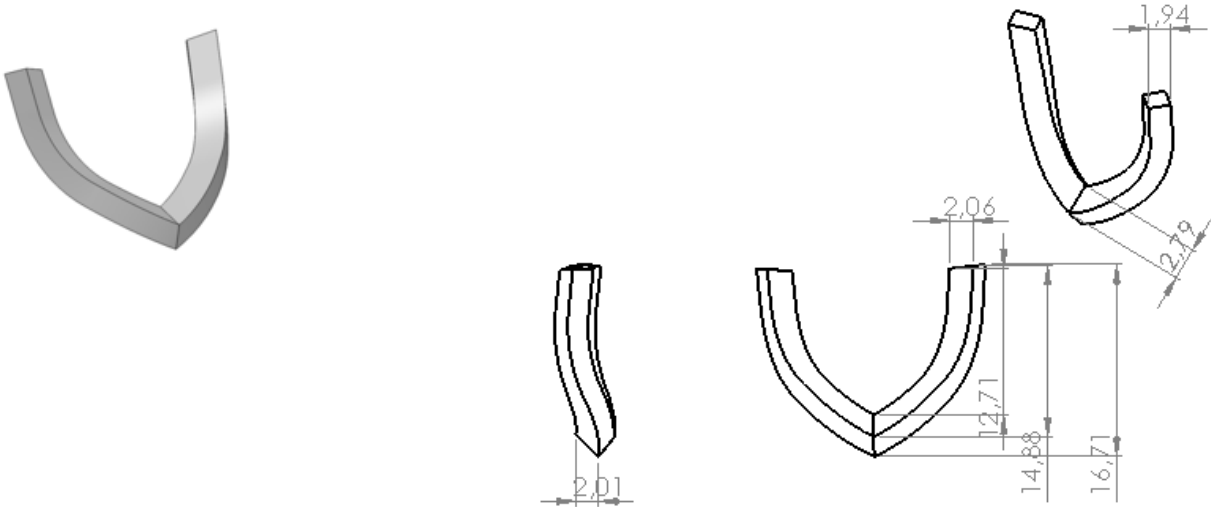
Top View



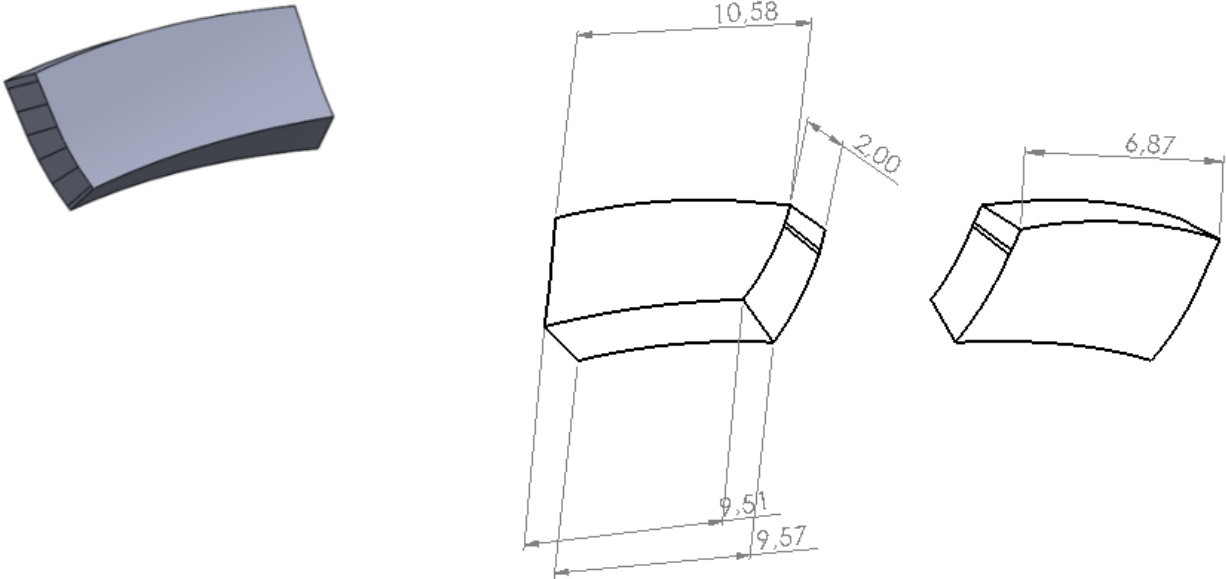
Frontal View



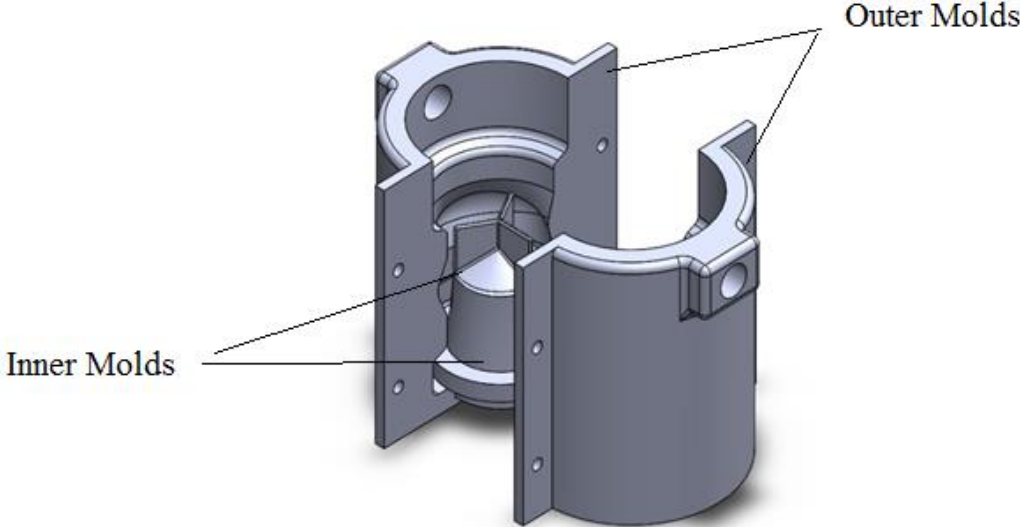
Radial Pattern



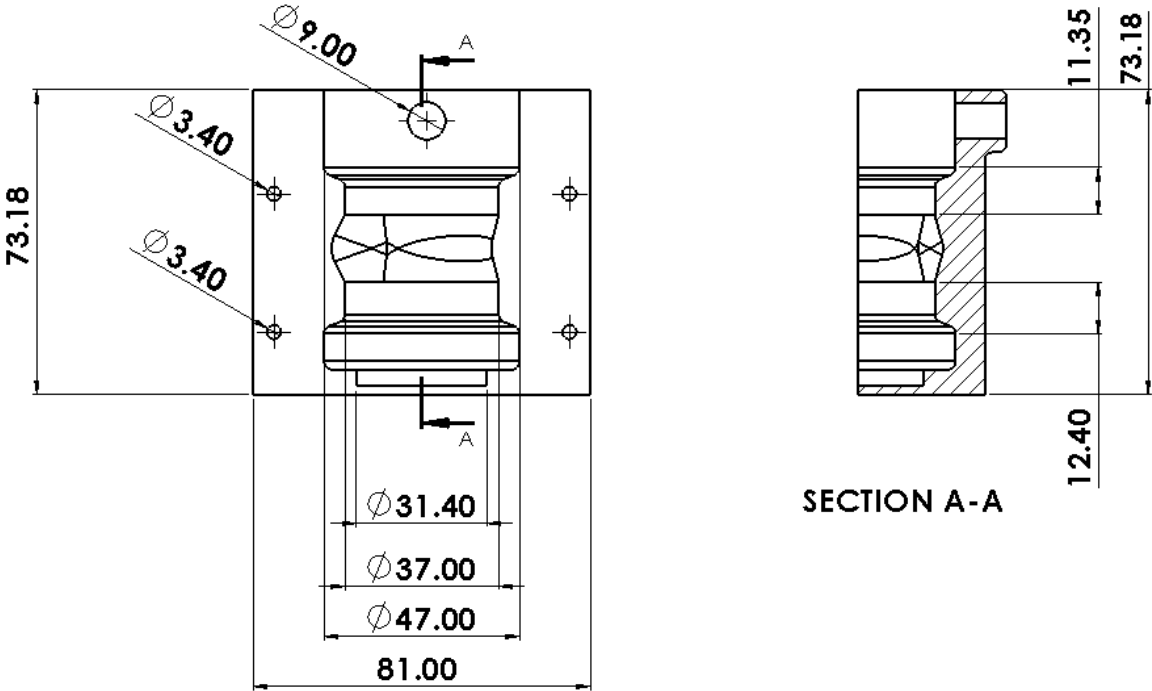
Arc Shape Pattern – moderate stenosis case



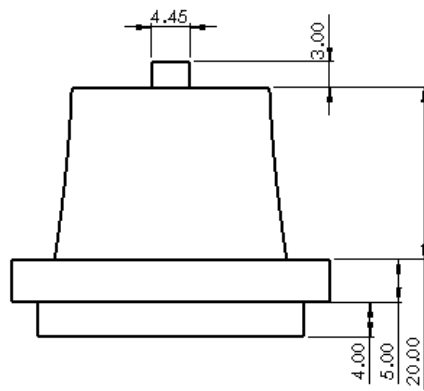
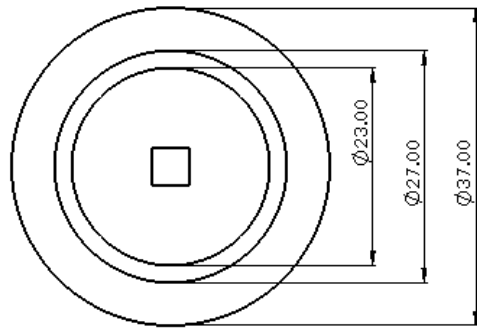
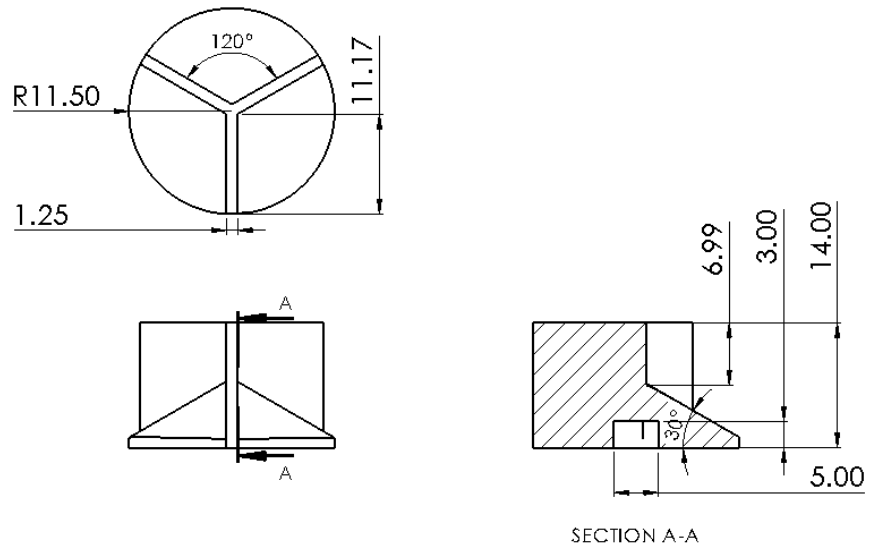
Preliminary Aortic Root



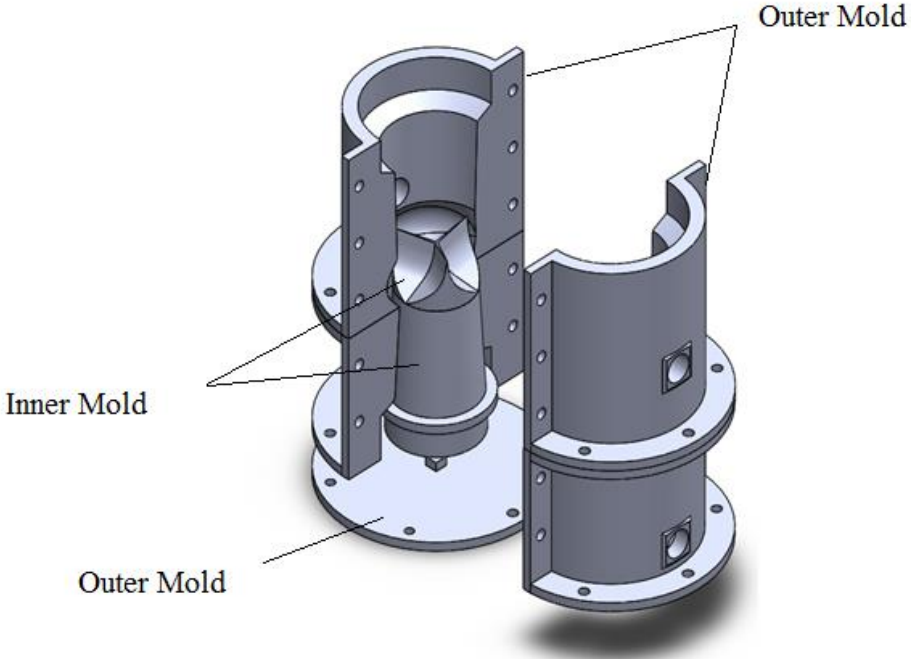
Outer Molds



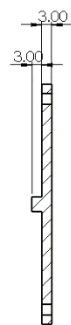
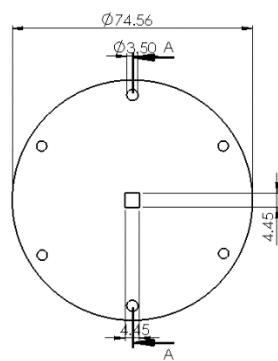
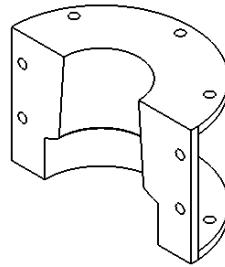
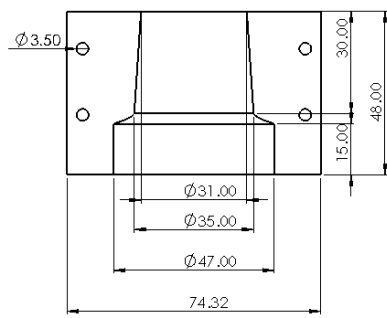
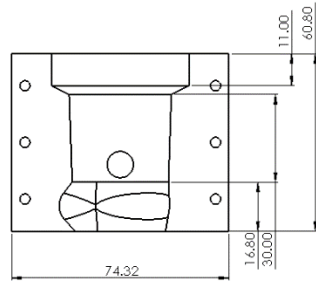
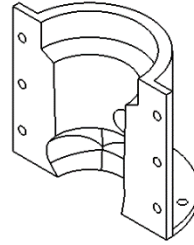
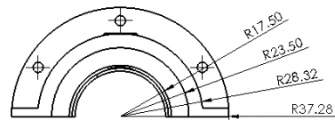
Inner Molds



Final Aortic Root

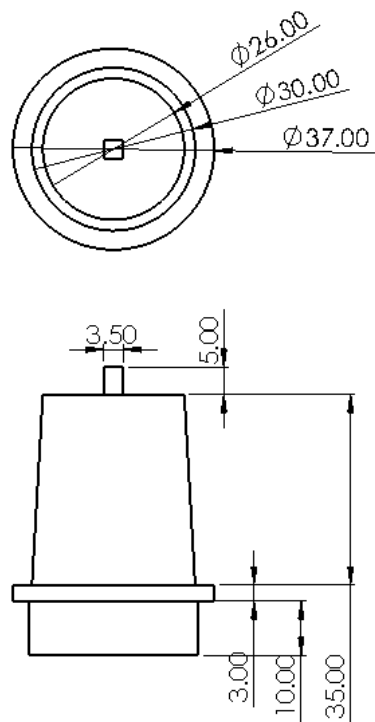
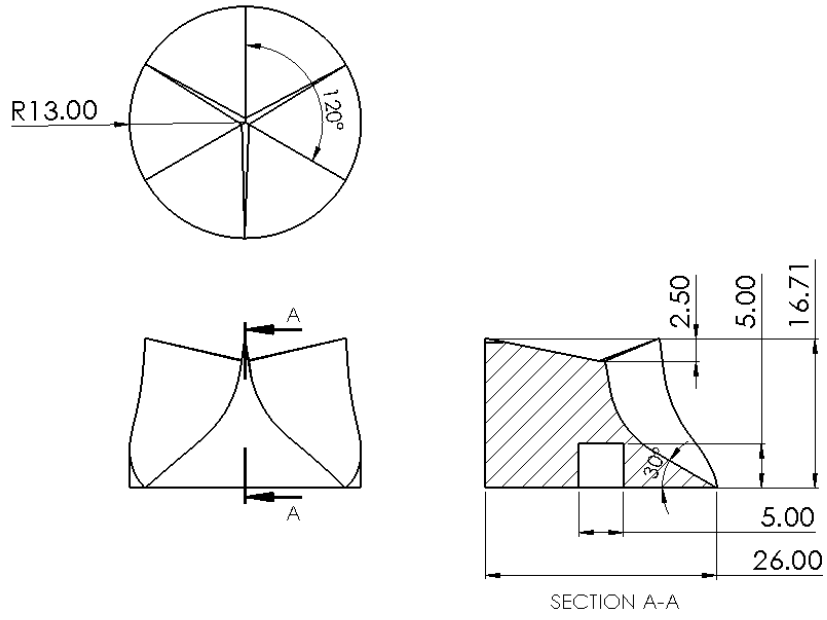


Outer Molds

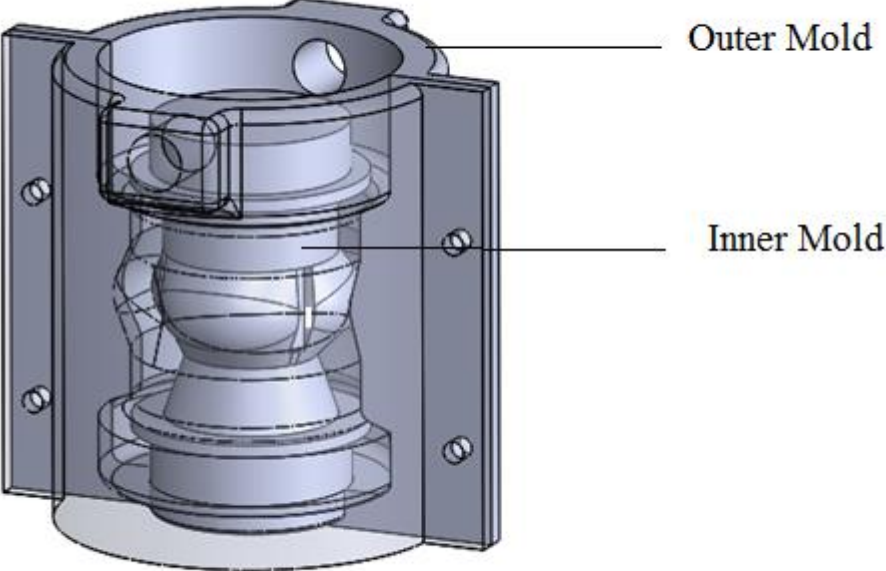


SECTION A-A

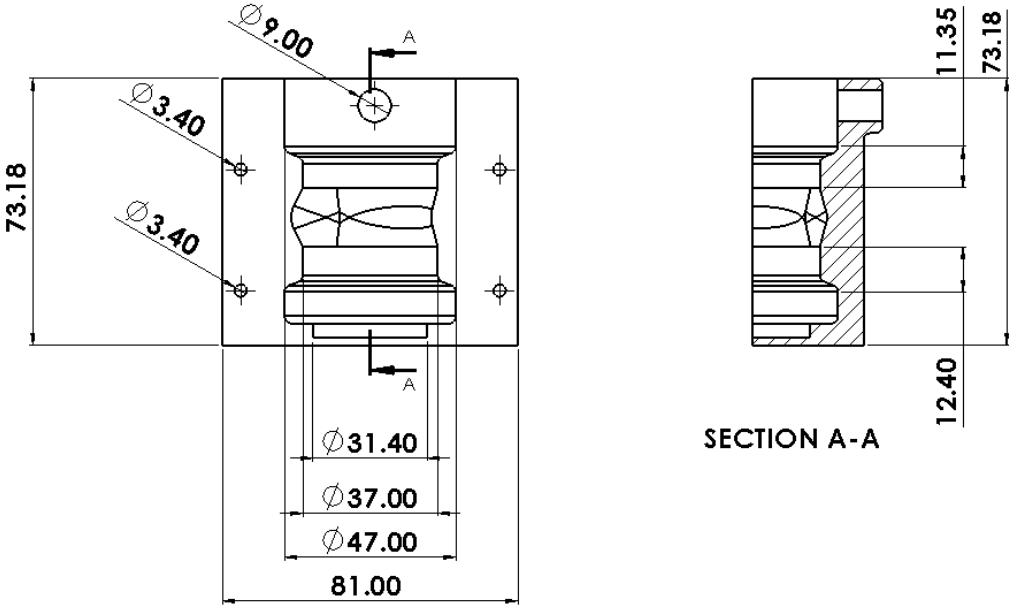
Inner Molds



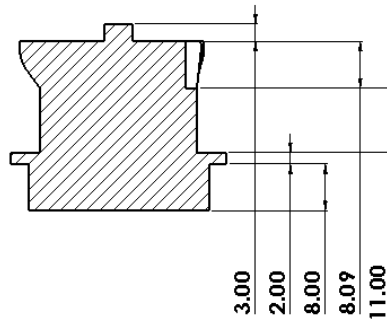
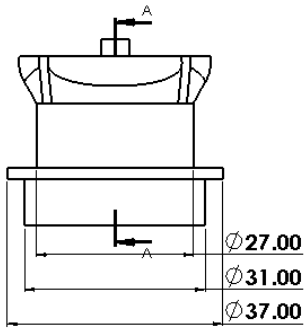
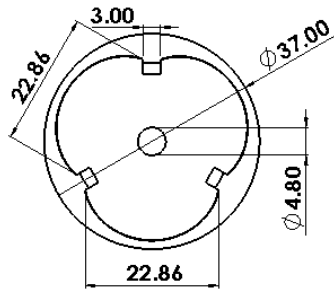
Preliminary Silicon Casting Mold



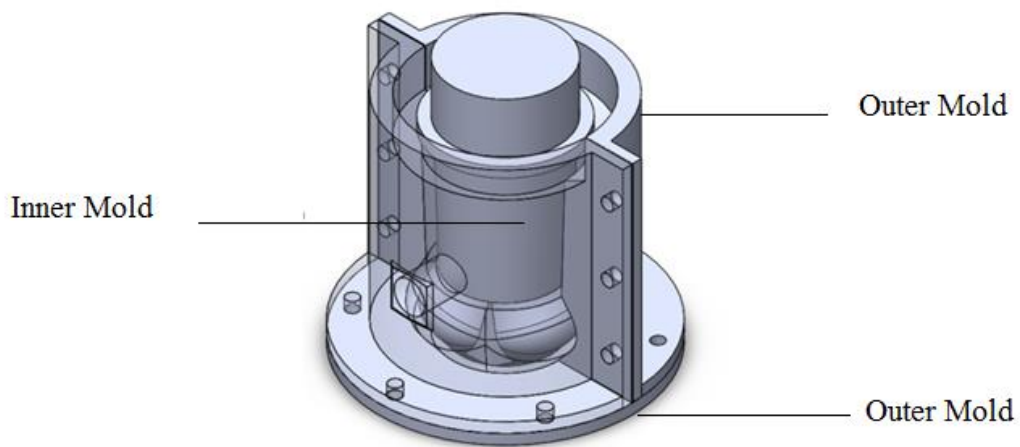
Outer Mold



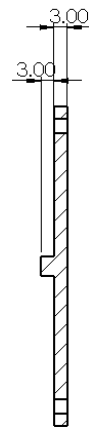
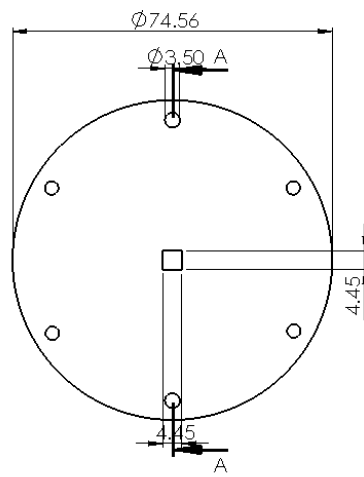
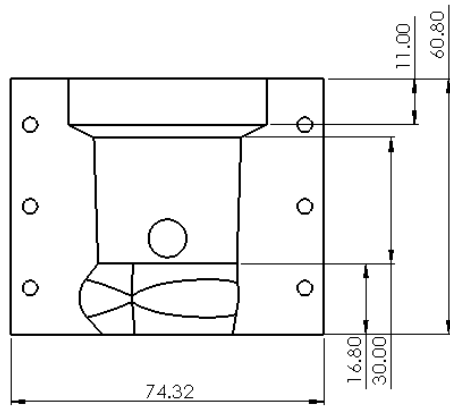
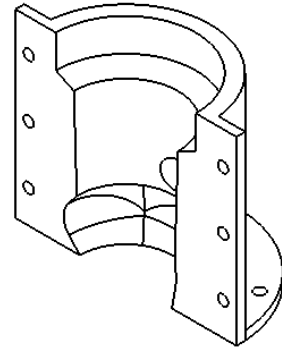
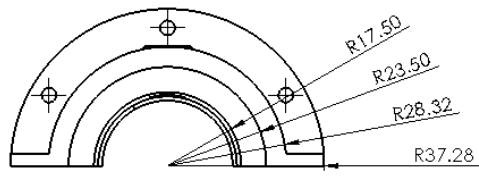
Inner Mold



Final Silicon Casting Mold

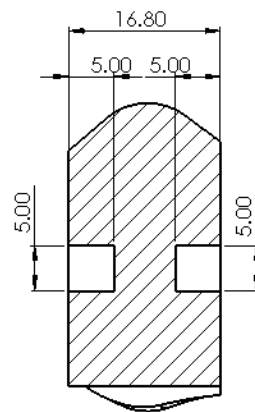
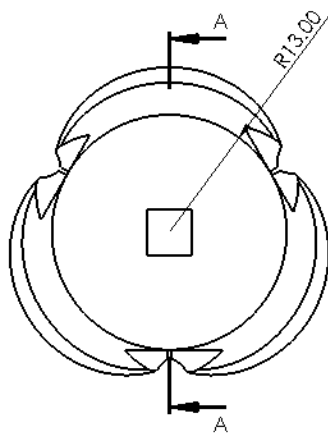
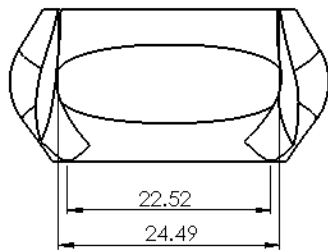
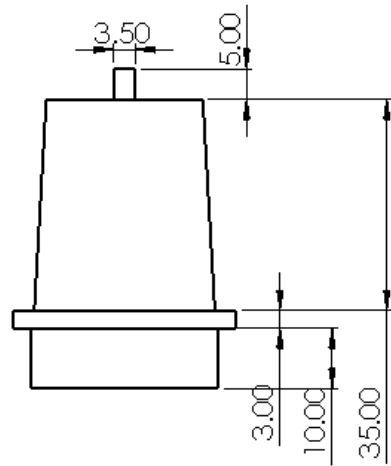
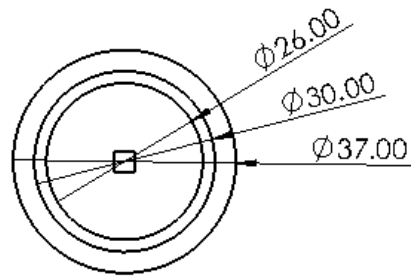


Outer Mold



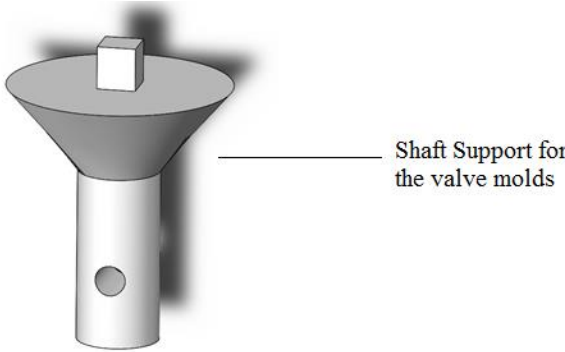
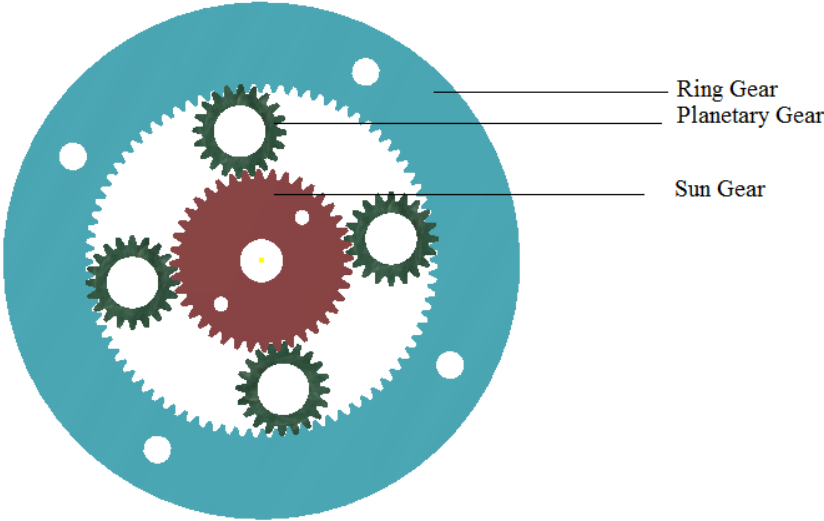
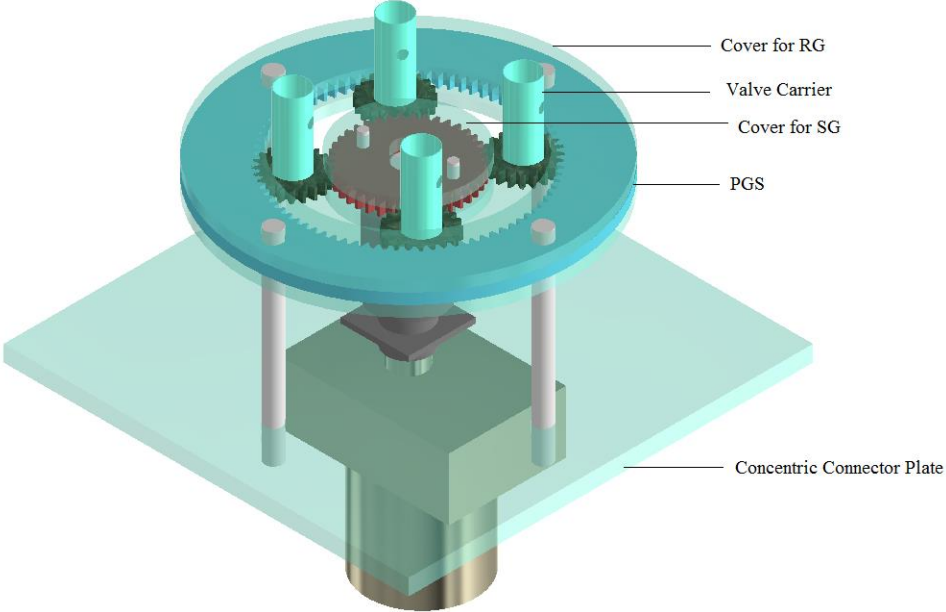
SECTION A-A

Inner Mold

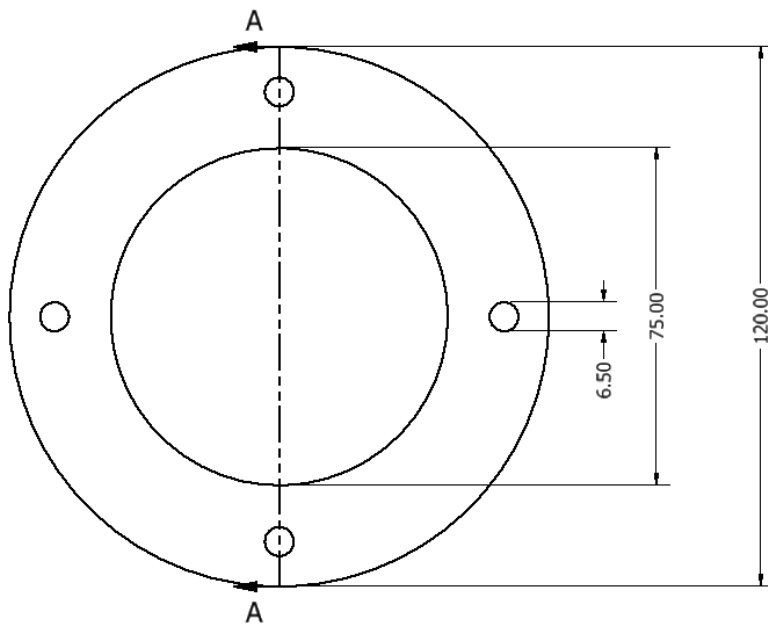


SECTION A-A

Spinning Device

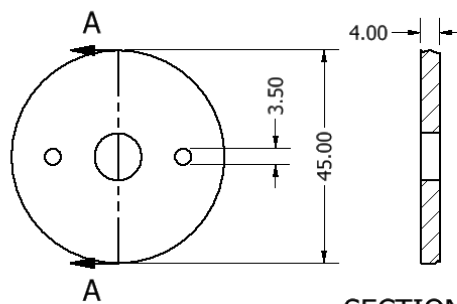


COVER for RG



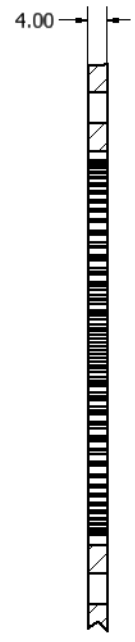
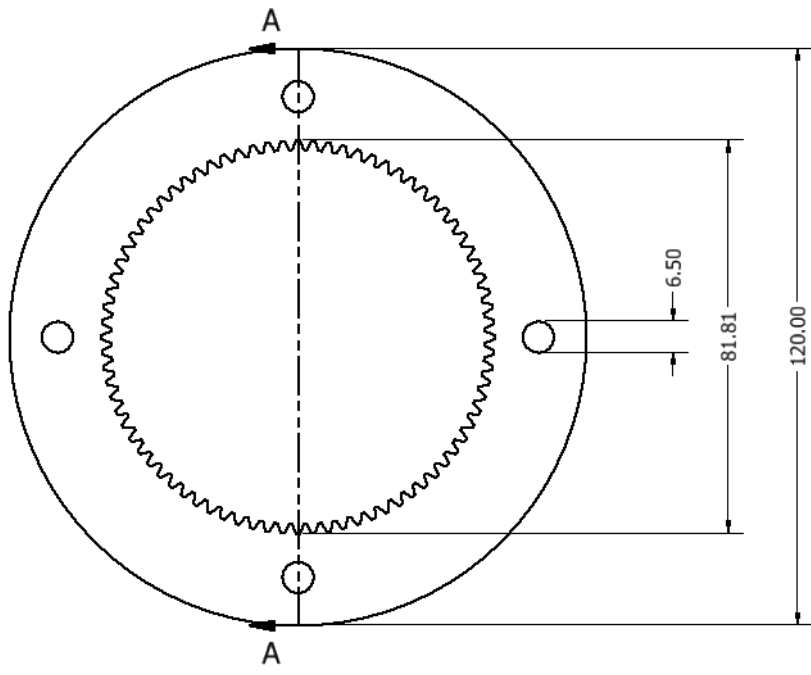
SECTION A-A
SCALE 1 : 1

COVER for SG



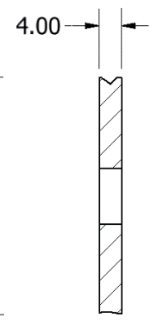
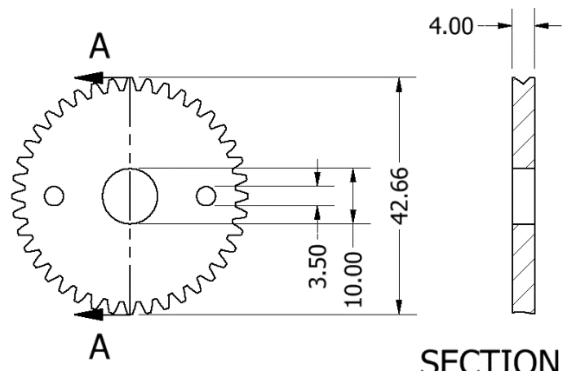
SECTION A-A
SCALE 1 : 1

Ring Gear



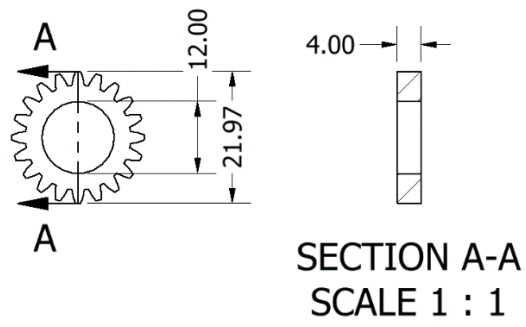
SECTION A-A
SCALE 1 : 1

Sun Gear

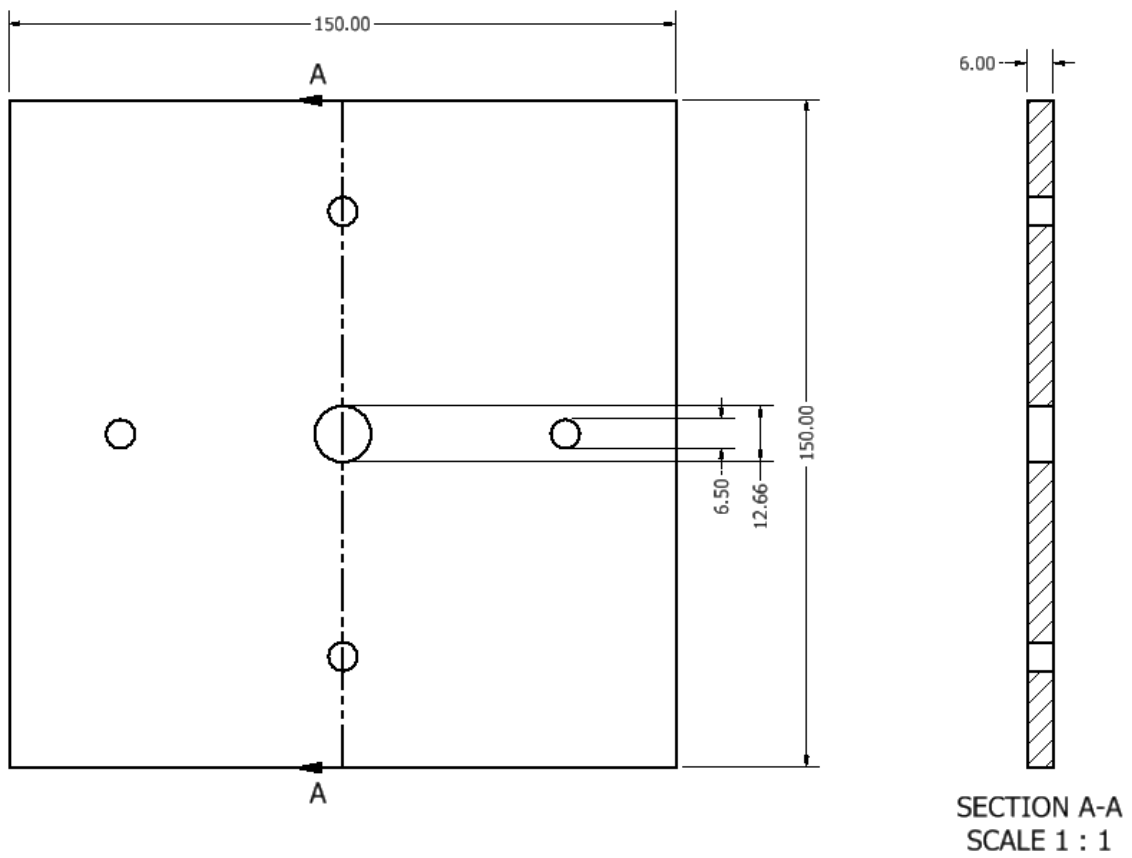


SECTION A-A
SCALE 1 : 1

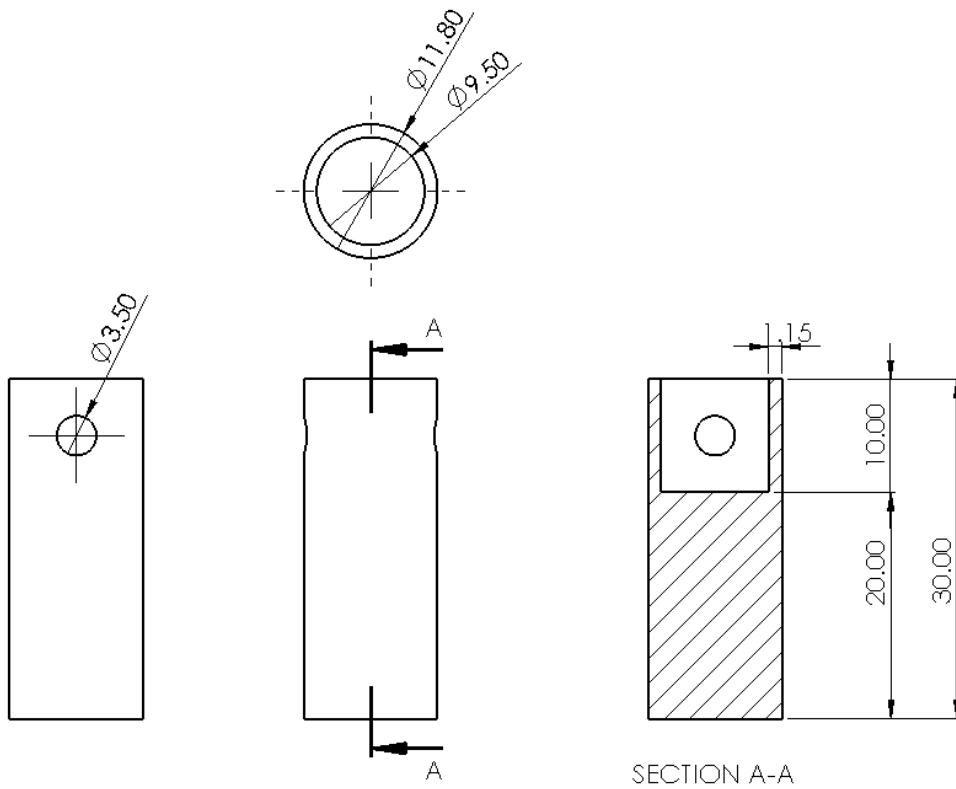
Planetary Gear



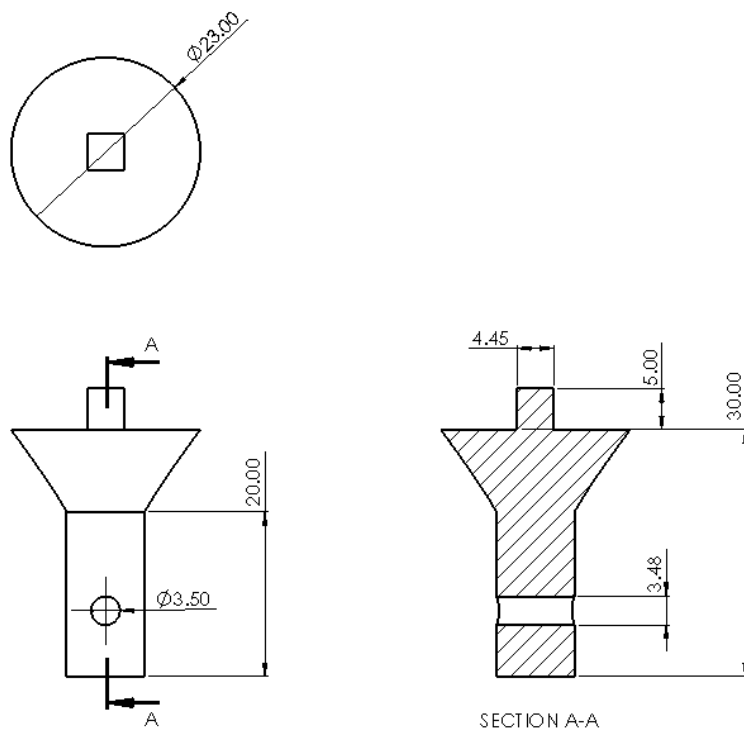
Concentric Connector Plate



Valve Carrier



Shaft Support fo Valve Molds



BIBLIOGRAPHY

- [1] R. L. J. Osnabrugge *et al.*, "Aortic stenosis in the elderly: Disease prevalence and number of candidates for transcatheter aortic valve replacement: A meta-analysis and modeling study," *J. Am. Coll. Cardiol.*, vol. 62, no. 11, pp. 1002–1012, 2013, doi: 10.1016/j.jacc.2013.05.015.
- [2] R. Gurvitch *et al.*, "Transcatheter aortic valve implantation: Lessons from the learning curve of the first 270 high-risk patients," *Catheter. Cardiovasc. Interv.*, vol. 78, no. 7, pp. 977–984, 2011, doi: 10.1002/ccd.22961.
- [3] F. Perico, "Sviluppo di un metodo per la realizzazione di modelli vascolari paziente-specifici per il training in operazioni transcatheter," Politecnico di Milano, 2019.
- [4] D. Schiena, "Progettazione, Realizzazione E Caratterizzazione Di Modello Polimerici Funzionali Di Valvole Cardiache Per Il Training Cardiochirurgico," Politecnico di Milano, 2018.
- [5] M. J. Thubrikar, J. Aouad, and S. P. Nolan, "Patterns of calcific deposits in operatively excised stenotic or purely regurgitant aortic valves and their relation to mechanical stress," *Am. J. Cardiol.*, vol. 58, no. 3, pp. 304–308, 1986, doi: 10.1016/0002-9149(86)90067-6.
- [6] R. Halevi, A. Hamdan, G. Marom, M. Mega, E. Raanani, and R. Haj-Ali, "Progressive aortic valve calcification: Three-dimensional visualization and biomechanical analysis," *J. Biomech.*, vol. 48, no. 3, pp. 489–497, 2015, doi: 10.1016/j.jbiomech.2014.12.004.
- [7] T. Thom *et al.*, *Heart disease and stroke statistics - 2006 Update: A report from the American Heart Association Statistics Committee and Stroke Statistics Subcommittee*, vol. 113, no. 6. 2006.
- [8] B. Lung *et al.*, "A prospective survey of patients with valvular heart disease in Europe: The Euro Heart Survey on valvular heart disease," *Eur. Heart J.*, vol. 24, no. 13, pp. 1231–1243, 2003, doi: 10.1016/S0195-668X(03)00201-X.
- [9] A. Yazdanyar and A. B. Newman, "The Burden of Cardiovascular Disease in the Elderly: Morbidity, Mortality, and Costs," *Clin. Geriatr. Med.*, vol. 25, no. 4, pp. 563–577, Nov. 2009, doi: 10.1016/J.CGER.2009.07.007.
- [10] Y. J. Woo and E. A. Nacke, "Robotic minimally invasive mitral valve reconstruction yields less blood product transfusion and shorter length of stay," *Surgery*, vol. 140, no. 2, pp. 263–267, 2006, doi: 10.1016/j.surg.2006.05.003.
- [11] A. Carpentier *et al.*, "First computer assisted open heart operation," *Comptes Rendus l'Academie des Sci. - Ser. III*, vol. 321, no. 5, pp. 437–442, 1998, doi: 10.1016/S0764-4469(98)80309-0.
- [12] E. L. HANNAN, H. KILBURN, J. F. O'DONNELL, G. LUKACICK, and E. P. SHIELDS, "Adult Open Heart Surgery in New York State," *Surv. Anesthesiol.*, vol. 35, no. 3, p. 163, 1991, doi: 10.1097/00132586-199106000-00036.
- [13] M. Lindroos, M. Kupari, J. Heikkilä, and R. Tilvis, "Prevalence of aortic valve abnormalities in the elderly: An echocardiographic study of a random population sample," *J. Am. Coll. Cardiol.*, vol. 21, no. 5, pp. 1220–1225, 1993, doi: 10.1016/0735-1097(93)90249-Z.
- [14] A. Harky *et al.*, "The Future of Open Heart Surgery in the Era of Robotic and Minimal Surgical Interventions," *Heart Lung Circ.*, vol. 29, no. 1, pp. 49–61, 2020, doi: 10.1016/j.hlc.2019.05.170.
- [15] A. Cribier, "Development of transcatheter aortic valve implantation (TAVI): A 20-year odyssey," *Arch. Cardiovasc. Dis.*, vol. 105, no. 3, pp. 146–152, 2012, doi: 10.1016/j.acvd.2012.01.005.
- [16] C. V. Bourantas *et al.*, "The evolution of device technology in transcatheter aortic valve

implantation," *EuroIntervention*, vol. 14, no. 18, pp. e1826–e1833, 2019, doi: 10.4244/eij-d-18-01048.

- [17] P. . Peter C. Fong, M.D., David S. Boss, M.Sc., Timothy A. Yap, M.D., Andrew Tutt, M.D., Ph.D., Peijun Wu, Ph.D., Marja Mergui-Roelvink, M.D., Peter Mortimer, Ph.D., Helen Swaisland, B.Sc., Alan Lau, Ph.D., Mark J. O'Connor, Ph.D., Alan Ashworth, Ph.D., James, "New England Journal Medicine," *N. Engl. J. Med.*, vol. 361, no. 2, pp. 123–134, 2009, doi: 10.1056/NEJMoa0900212.
- [18] F. Sacco, "Sviluppo di un modello in vitro di valvola aortica stenotica," Politecnico di Milano, 2015.
- [19] J. Bismuth *et al.*, "Incorporating simulation in vascular surgery education," *J. Vasc. Surg.*, vol. 52, no. 4, pp. 1072–1080, 2010, doi: 10.1016/j.jvs.2010.05.093.
- [20] R. M. Satava, A. Gaspari, and N. Lorenzo, *Emerging Technologies in Surgery*. 2007.
- [21] U. Govindarajulu, S. Bedi, A. Kluger, and F. Resnic, "Survival analysis of hierarchical learning curves in assessment of cardiac device and procedural safety," *Stat. Med.*, vol. 37, no. 28, pp. 4185–4199, 2018, doi: 10.1002/sim.7906.
- [22] K. E. Roberts, R. L. Bell, and A. J. Duffy, "Evolution of surgical skills training," *World J. Gastroenterol.*, vol. 12, no. 20, pp. 3219–3224, 2006, doi: 10.3748/wjg.v12.i20.3219.
- [23] P. A. G. Morais, "Development of a patient-specific phantom model," 2015.
- [24] J. Jose, G. Manik, and M. Abdel-Wahab, "Setting up a transcatheter aortic valve implantation program: Indian perspective," *Indian Heart J.*, vol. 68, no. 5, pp. 732–736, 2016, doi: 10.1016/j.ihj.2015.12.006.
- [25] K. Hayashida *et al.*, "True percutaneous approach for transfemoral aortic valve implantation using the prostar XL device: Impact of learning curve on vascular complications," *JACC Cardiovasc. Interv.*, vol. 5, no. 2, pp. 207–214, 2012, doi: 10.1016/j.jcin.2011.09.020.
- [26] K. Trehan, C. D. Kemp, and S. C. Yang, "Simulation in cardiothoracic surgical training: Where do we stand?," *J. Thorac. Cardiovasc. Surg.*, vol. 147, no. 1, pp. 18-24.e2, 2014, doi: 10.1016/j.jtcvs.2013.09.007.
- [27] B. Ripley *et al.*, "3D printing based on cardiac CT assists anatomic visualization prior to transcatheter aortic valve replacement," *J. Cardiovasc. Comput. Tomogr.*, vol. 10, no. 1, pp. 28–36, 2016, doi: 10.1016/j.jcct.2015.12.004.
- [28] R. L. Izzo *et al.*, "3D printed cardiac phantom for procedural planning of a transcatheter native mitral valve replacement," *Med. Imaging 2016 PACS Imaging Informatics Next Gener. Innov.*, vol. 9789, p. 978908, 2016, doi: 10.1117/12.2216952.
- [29] M. R. Labrosse, C. J. Beller, F. Robicsek, and M. J. Thubrikar, "Geometric modeling of functional trileaflet aortic valves: Development and clinical applications," *J. Biomech.*, vol. 39, no. 14, pp. 2665–2672, 2006, doi: 10.1016/j.jbiomech.2005.08.012.
- [30] L. Sherwood, "Cardiac physiology," in *Fundamentals of Human Physiology*, 4th ed., Anonymous Belmont, Ed. Calif: Brooks/Cole: Cengage Learning, 2012, p. 229.
- [31] A. J. Weinhaus and K. P. Roberts, "Anatomy of the human heart," *Handb. Card. Anatomy, Physiol. Devices Second Ed.*, pp. 59–85, 2005, doi: 10.1007/978-1-60327-372-5_5.
- [32] H. Fukuta and W. C. Little, "The Cardiac Cycle and the Physiologic Basis of Left Ventricular Contraction, Ejection, Relaxation, and Filling," *Heart Failure Clinics*, vol. 4, no. 1. pp. 1–11, Jan-2008, doi: 10.1016/j.hfc.2007.10.004.
- [33] P. L. and M. T. D. Berdajs, "The Anatomy of the aortic root," in *Cardiovasc. Surg.*, 2002, pp. 320–327.

- [34] R. H. Anderson, "The surgical anatomy of the aortic root," *Multimed. Man. Cardio-Thoracic Surg.*, vol. 2007, no. 0102, pp. 2527–0, 2007, doi: 10.1510/mmcts.2006.002527.
- [35] M. Loukas, E. Bilinsky, S. Bilinsky, C. Blaak, R. S. Tubbs, and R. H. Anderson, "The anatomy of the aortic root," *Clin. Anat.*, vol. 27, no. 5, pp. 748–756, 2014, doi: 10.1002/ca.22295.
- [36] H. E. S. Standring BKB. Berkovitz, "Chapter Heart and Great Vessels," in *Gray's Anatomy: The Anatomical Basis of Clinical Practice*, 39th ed., C. Livingstone, Ed. London, UK, 2005, pp. 1003–1006.
- [37] P. A. Patel *et al.*, "The functional aortic annulus in the 3D era: Focus on transcatheter aortic valve replacement for the perioperative echocardiographer," *J. Cardiothorac. Vasc. Anesth.*, vol. 29, no. 1, pp. 240–245, 2015, doi: 10.1053/j.jvca.2014.05.027.
- [38] R. B. Hokken, M. M. Bartelings, A. J. Bogers, and A. C. Gittenberger-de Groot, "Morphology of the pulmonary and aortic roots with regard to the pulmonary autograft procedure," *J. Thorac. Cardiovasc. Surg.*, vol. 113, no. 3, pp. 453–461, Mar. 1997, doi: S0022-5223(97)70357-X [pii].
- [39] J. P. Sutton, S. Y. Ho, and R. H. Anderson, "The forgotten interleaflet triangles: A review of the surgical anatomy of the aortic valve," *Ann. Thorac. Surg.*, vol. 59, no. 2, pp. 419–427, 1995, doi: 10.1016/0003-4975(94)00893-C.
- [40] A. Arjmand Shabestari *et al.*, "Comparison of aortic root dimension changes during cardiac cycle between the patients with and without aortic valve calcification using ECG-gated 64-slice and dual-source 256-slice computed tomography scanners: results of a multicenter study," *Int. J. Cardiovasc. Imaging*, vol. 29, no. 6, pp. 1391–1400, 2013, doi: 10.1007/s10554-013-0217-7.
- [41] D. Maselli, A. Montalto, G. Santise, G. Minardi, C. Manzara, and F. Musumeci, "A normogram to anticipate dimension of neo-sinuses of valsalva in valve-sparing aortic operations," *Eur. J. Cardiothoracic Surg.*, vol. 27, no. 5, pp. 831–835, 2005, doi: 10.1016/j.ejcts.2005.01.063.
- [42] L. F. Tops *et al.*, "Noninvasive Evaluation of the Aortic Root With Multislice Computed Tomography. Implications for Transcatheter Aortic Valve Replacement," *JACC Cardiovasc. Imaging*, vol. 1, no. 3, pp. 321–330, 2008, doi: 10.1016/j.jcmg.2007.12.006.
- [43] L. M. De Heer, R. P. J. Budde, W. P. T. M. Mali, A. M. De Vos, L. A. Van Herwerden, and J. Kluin, "Aortic root dimension changes during systole and diastole: Evaluation with ECG-gated multidetector row computed tomography," *Int. J. Cardiovasc. Imaging*, vol. 27, no. 8, pp. 1195–1204, 2011, doi: 10.1007/s10554-011-9838-x.
- [44] F. Auricchio, M. Conti, S. Demertzis, and S. Morganti, "Finite element analysis of aortic root dilation: A new procedure to reproduce pathology based on experimental data," *Comput. Methods Biomech. Biomed. Engin.*, vol. 14, no. 10, pp. 875–882, 2011, doi: 10.1080/10255842.2010.499867.
- [45] V. T. Nkomo, J. M. Gardin, T. N. Skelton, J. S. Gottdiener, C. G. Scott, and M. Enriquez-Sarano, "Burden of valvular heart diseases: a population-based study," *Lancet*, vol. 368, no. 9540, pp. 1005–1011, 2006, doi: 10.1016/S0140-6736(06)69208-8.
- [46] F. Auricchio, M. Conti, S. Morganti, and A. Reali, "Simulation of transcatheter aortic valve implantation: a patient-specific finite element approach," *Comput. Methods Biomech. Biomed. Engin.*, vol. 17, no. 12, pp. 1347–1357, 2014, doi: 10.1080/10255842.2012.746676.
- [47] D. M. Brinkley and E. V. Gelfand, "Valvular heart disease: Classic teaching and emerging paradigms," *Am. J. Med.*, vol. 126, no. 12, pp. 1035–1042, 2013, doi: 10.1016/j.amjmed.2013.05.022.
- [48] D. Garcia *et al.*, "Estimation of aortic valve effective orifice area by Doppler echocardiography: Effects of valve inflow shape and flow rate," *J. Am. Soc. Echocardiogr.*, vol. 17, no. 7, pp. 756–765, 2004, doi: 10.1016/j.echo.2004.03.030.
- [49] D. Garcia, J. G. Dumesnil, L. G. Durand, L. Kadem, and P. Pibarot, "Discrepancies between catheter

and doppler estimates of valve effective orifice area can be predicted from the pressure recovery phenomenon: Practical implications with regard to quantification of aortic stenosis severity," *J. Am. Coll. Cardiol.*, vol. 41, no. 3, pp. 435–442, 2003, doi: 10.1016/S0735-1097(02)02764-X.

- [50] K. H. Zheng, E. Tzolos, and M. R. Dweck, "Pathophysiology of Aortic Stenosis and Future Perspectives for Medical Therapy," *Cardiol. Clin.*, vol. 38, no. 1, pp. 1–12, 2020, doi: 10.1016/j.ccl.2019.09.010.
- [51] W. Wang, S. Vootukuri, A. Meyer, J. Ahamed, and B. S. Collier, "Association between shear stress and platelet-derived transforming growth factor- β 1 release and activation in animal models of aortic valve stenosis," *Arterioscler. Thromb. Vasc. Biol.*, vol. 34, no. 9, pp. 1924–1932, 2014, doi: 10.1161/ATVBAHA.114.303852.
- [52] "Cardiovascular Physiology Concepts - Richard Klabunde - Google Libri." [Online]. Available: https://books.google.it/books?hl=it&lr=&id=27ExgvGnOagC&oi=fnd&pg=PP2&dq=Cardiovascular+Physiology+Concepts+Second+Edition&ots=_ieA3jh-it&sig=APgXmj1Lb_lxGE3kDKnN_5m2O48&redir_esc=y#v=onepage&q=Cardiovascular+Physiology+Concepts+Second+Edition&f=false. [Accessed: 16-Mar-2020].
- [53] K. Orihashi, "Aortic Valve Replacement for Calcified Aortic Valves," *Calcif. Aortic Valve Dis.*, 2013, doi: 10.5772/53418.
- [54] B. M. Schaefer *et al.*, "The bicuspid aortic valve: An integrated phenotypic classification of leaflet morphology and aortic root shape," *Heart*, vol. 94, no. 12, pp. 1634–1638, 2008, doi: 10.1136/hrt.2007.132092.
- [55] S. Nistri, C. Basso, and G. Thiene, "La valvola aortica bicuspidae," *G. Ital. Cardiol.*, vol. 13, no. 1, pp. 25–37, 2012.
- [56] P. W. M. Fedak, S. Verma, T. E. David, R. L. Leask, R. D. Weisel, and J. Butany, "Clinical and pathophysiological implications of a bicuspid aortic valve," *Circulation*, vol. 106, no. 8, pp. 900–904, 2002, doi: 10.1161/01.CIR.0000027905.26586.E8.
- [57] W. M. C. Koenraadt *et al.*, "The extent of the raphe in bicuspid aortic valves is associated with aortic regurgitation and aortic root dilatation," *Netherlands Hear. J.*, vol. 24, no. 2, pp. 127–133, 2016, doi: 10.1007/s12471-015-0784-4.
- [58] A. Martinsson *et al.*, "Familial Aggregation of Aortic Valvular Stenosis: A Nationwide Study of Sibling Risk," *Circ. Cardiovasc. Genet.*, vol. 10, no. 6, 2017, doi: 10.1161/CIRCGENETICS.117.001742.
- [59] E. L. W. Tay, K. K. Poh, J. W. L. Yip, and W. K. F. Kong, "Transcatheter aortic valve implantation: From revolution to evolution," *Singapore Med. J.*, vol. 57, no. 7, pp. 406–407, 2016, doi: 10.11622/smedj.2016122.
- [60] C. Bleakley and M. J. Monaghan, "The Pivotal Role of Imaging in TAVR Procedures," *Curr. Cardiol. Rep.*, vol. 20, no. 2, 2018, doi: 10.1007/s11886-018-0949-z.
- [61] R. L. J. Osnabrugge *et al.*, "Aortic stenosis in the elderly: Disease prevalence and number of candidates for transcatheter aortic valve replacement: A meta-analysis and modeling study," *J. Am. Coll. Cardiol.*, vol. 62, no. 11, pp. 1002–1012, 2013, doi: 10.1016/j.jacc.2013.05.015.
- [62] S. M. Green *et al.*, "The current state of medical simulation in interventional cardiology: A clinical document from the Society for Cardiovascular Angiography and Intervention's (SCAI) Simulation Committee," *Catheter. Cardiovasc. Interv.*, vol. 83, no. 1, pp. 37–46, 2014, doi: 10.1002/ccd.25048.
- [63] L. Buellesfeld *et al.*, "2-Year Follow-Up of Patients Undergoing Transcatheter Aortic Valve Implantation Using a Self-Expanding Valve Prosthesis," *J. Am. Coll. Cardiol.*, vol. 57, no. 16, pp. 1650–1657, 2011, doi: 10.1016/j.jacc.2010.11.044.
- [64] "CoreValve Aortic Valve ISW." [Online]. Available: <https://www.medtronic.com/it-it/operatori->

sanitari/products/cardiovascular/heart-valves-transcatheter/transcatheter-aortic-valve-replacement-platform/indications-safety-warnings.html. [Accessed: 16-Mar-2020].

- [65] T. Pilgrim *et al.*, “Early versus newer generation devices for transcatheter aortic valve implantation in routine clinical practice: A propensity score matched analysis,” *Open Hear.*, vol. 5, no. 1, pp. 1–8, 2018, doi: 10.1136/openhrt-2017-000695.
- [66] G. Schymik *et al.*, “Evolution of transcatheter aortic valve implantation over 7 years: Results of a prospective single-centre registry of 2000 patients in a large municipal hospital (TAVIK Registry),” *BMJ Open*, vol. 8, no. 10, pp. 1–10, 2018, doi: 10.1136/bmjopen-2018-022574.
- [67] T. Kaneko and M. J. Davidson, “Use of the hybrid operating room in cardiovascular medicine,” *Circulation*, vol. 130, no. 11, pp. 910–917, 2014, doi: 10.1161/CIRCULATIONAHA.114.006510 [doi].
- [68] W. Zhou, P. H. Lin, R. L. Bush, and A. B. Lumsden, “Endovascular training of vascular surgeons: have we made progress?,” *Semin. Vasc. Surg.*, vol. 19, no. 2, pp. 122–126, 2006, doi: S0895-7967(06)00022-6 [pii].
- [69] A. Kheradvar, R. Zareian, S. Kawauchi, R. L. Goodwin, and S. Rugonyi, “Animal Models for Heart Valve Research and Development,” *Drug Discov. today. Disease Model.*, vol. 24, pp. 55–62, 2017, doi: 10.1016/j.ddmod.2018.04.001 [doi].
- [70] C. A. Anderson, W. C. Wood, L. DiBernardo, M. Erdmann, and A. P. Kypson, “An acute animal model of aortic stenosis: initial attempts at leaflet modification,” *J. Heart Valve Dis.*, vol. 21, no. 2, pp. 172–174, Mar. 2012.
- [71] D. Maragiannis, M. S. Jackson, S. R. Igo, S. M. Chang, W. A. Zoghbi, and S. H. Little, “Functional 3D Printed Patient-Specific Modeling of Severe Aortic Stenosis,” *J. Am. Coll. Cardiol.*, vol. 64, no. 10, pp. 1066–1068, 2014, doi: 10.1016/j.jacc.2014.05.058.
- [72] M. Weber *et al.*, “Multiple-Step Injection Molding for Fibrin-Based Tissue-Engineered Heart Valves,” *Tissue Eng. - Part C Methods*, vol. 21, no. 8, pp. 832–840, 2015, doi: 10.1089/ten.tec.2014.0396.
- [73] S. N. Kurenov, C. Ionita, D. Sammons, and T. L. Demmy, “Three-dimensional printing to facilitate anatomic study, device development, simulation, and planning in thoracic surgery,” *J. Thorac. Cardiovasc. Surg.*, vol. 149, no. 4, pp. 973-979.e1, 2015, doi: 10.1016/j.jtcvs.2014.12.059.
- [74] H. Maleki, S. Shahriari, M. Labrosse, P. Pibarot, and L. Kadem, “An in vitro model of aortic stenosis for the assessment of transcatheter aortic valve implantation,” *J. Biomech. Eng.*, vol. 136, no. 5, pp. 1–5, 2014, doi: 10.1115/1.4026576.
- [75] O. M. Rotman *et al.*, “HHS Public Access,” vol. 9, no. 3, pp. 339–350, 2019, doi: 10.1007/s13239-018-0356-z.Realistic.
- [76] B. Ripley *et al.*, “3D printing based on cardiac CT assists anatomic visualization prior to transcatheter aortic valve replacement,” *J. Cardiovasc. Comput. Tomogr.*, vol. 10, no. 1, pp. 28–36, 2016, doi: 10.1016/j.jcct.2015.12.004 [doi].
- [77] D. Schmauss *et al.*, “Three-dimensional printing of models for preoperative planning and simulation of transcatheter valve replacement,” *Ann. Thorac. Surg.*, vol. 93, no. 2, pp. e31-3, Feb. 2012, doi: 10.1016/j.athoracsur.2011.09.031 [doi].
- [78] M. R. Labrosse, K. Lobo, and C. J. Beller, “Structural analysis of the natural aortic valve in dynamics: From unpressurized to physiologically loaded,” *J. Biomech.*, vol. 43, no. 10, pp. 1916–1922, 2010, doi: 10.1016/j.jbiomech.2010.03.020.
- [79] H. Maleki, S. Shahriari, L. G. Durand, M. R. Labrosse, and L. Kadem, “A metric for the stiffness of calcified aortic valves using a combined computational and experimental approach,” *Med. Biol. Eng. Comput.*, vol. 52, no. 1, pp. 1–8, 2014, doi: 10.1007/s11517-013-1113-y.

- [80] R. L. Izzo *et al.*, “3D Printed Cardiac Phantom for Procedural Planning of a Transcatheter Native Mitral Valve Replacement,” *Proc. SPIE--the Int. Soc. Opt. Eng.*, vol. 9789, p. 10.1117/12.2216952. Epub 2016 Apr 5, Feb. 2016, doi: 978908 [pii].
- [81] X. Tang and X. Yan, “Dip-coating for fibrous materials: mechanism, methods and applications,” *Journal of Sol-Gel Science and Technology*, vol. 81, no. 2. Springer New York LLC, pp. 378–404, 01-Feb-2017, doi: 10.1007/s10971-016-4197-7.
- [82] I. A. Neacșu, A. I. Nicoară, O. R. Vasile, and B. Ș. Vasile, “Inorganic micro- and nanostructured implants for tissue engineering,” in *Nanobiomaterials in Hard Tissue Engineering: Applications of Nanobiomaterials*, Elsevier Inc., 2016, pp. 271–295.
- [83] J. Puetz and M. A. Aegerter, “Dip Coating Technique,” in *Sol-Gel Technologies for Glass Producers and Users*, Springer US, 2004, pp. 37–48.
- [84] “HISTOLOGY AND CYTOLOGY.”
- [85] A. A. Konta, M. García-Piña, and D. R. Serrano, “Personalised 3D printed medicines: Which techniques and polymers are more successful?,” *Bioengineering*, vol. 4, no. 4, 2017, doi: 10.3390/bioengineering4040079.
- [86] “Ultimaker 3: stampe 3D complesse rese semplici.” [Online]. Available: <https://ultimaker.com/it/3d-printers/ultimaker-3>. [Accessed: 23-Apr-2020].
- [87] G. A. Oosthuizen, D. Hagedorn-Hansen, and T. Gerhold, “Evaluation of Rapid Product Development Technologies for Production of Prosthesis in Developing Communities,” *SAIIE25 Proc.*, no. July, pp. 590.1-590.14, 2013.
- [88] “Polyjet technology materials specifications,” p. 2015, 2015.
- [89] D. Maragiannis *et al.*, “Replicating Patient-Specific Severe Aortic Valve Stenosis with Functional 3D Modeling,” *Circ. Cardiovasc. Imaging*, vol. 8, no. 10, pp. 1–8, 2015, doi: 10.1161/CIRCIMAGING.115.003626.
- [90] V. Images, “Case TAVR080 : Aortic Valve step-by-step guide 3D printing the aortic valve Case Airways - Learning objectives,” 2016.
- [91] Z. Qian *et al.*, “Quantitative Prediction of Paravalvular Leak in Transcatheter Aortic Valve Replacement Based on Tissue-Mimicking 3D Printing,” *JACC Cardiovasc. Imaging*, vol. 10, no. 7, pp. 719–731, Jul. 2017, doi: 10.1016/j.jcmg.2017.04.005.
- [92] V. Tuncay and P. M. A. van Ooijen, “3D printing for heart valve disease: a systematic review,” *Eur. Radiol. Exp.*, vol. 3, no. 1, 2019, doi: 10.1186/s41747-018-0083-0.
- [93] O. M. Rotman *et al.*, “Novel Polymeric Valve for Transcatheter Aortic Valve Replacement Applications: In Vitro Hemodynamic Study,” *Ann. Biomed. Eng.*, vol. 47, no. 1, pp. 113–125, 2019, doi: 10.1007/s10439-018-02119-7.
- [94] S.-J. Yoo *et al.*, “3D printing in medicine of congenital heart diseases,” *3D Print. Med.*, vol. 2, no. 1, 2016, doi: 10.1186/s41205-016-0004-x.
- [95] S. Engelhardt, S. Sauerzapf, B. Preim, M. Karck, I. Wolf, and R. De Simone, “Flexible and comprehensive patient-specific mitral valve silicone models with chordae tendineae made from 3D-printable molds,” *Int. J. Comput. Assist. Radiol. Surg.*, vol. 14, no. 7, pp. 1177–1186, 2019, doi: 10.1007/s11548-019-01971-9.
- [96] F. Bogoni, M. Cardamome, and M. Conti, “Modello valvolare aortico in materiale polimerico per il training cardiocirurgico.” Politecnico di Milano, 2019.
- [97] E. J. Weinberg, F. J. Schoen, and M. R. K. Mofrad, “A computational model of aging and calcification

in the aortic heart valve," *PLoS One*, vol. 4, no. 6, pp. 1–10, 2009, doi: 10.1371/journal.pone.0005960.

- [98] R. Halevi *et al.*, "A New Growth Model for Aortic Valve Calcification," *J. Biomech. Eng.*, vol. 140, no. 10, pp. 1–8, 2018, doi: 10.1115/1.4040338.
- [99] Y. Sahasakul, W. D. Edwards, J. M. Naessens, and A. J. Tajik, "Age-related changes in aortic and mitral valve thickness: Implications for two-dimensional echocardiography based on an autopsy study of 200 normal human hearts," *Am. J. Cardiol.*, vol. 62, no. 7, pp. 424–430, 1988, doi: 10.1016/0002-9149(88)90971-X.
- [100] F. Sturla *et al.*, "Impact of different aortic valve calcification patterns on the outcome of transcatheter aortic valve implantation: A finite element study," *J. Biomech.*, vol. 49, no. 12, pp. 2520–2530, 2016, doi: 10.1016/j.jbiomech.2016.03.036.
- [101] G. R. Veneziani, E. L. Corrêa, M. P. A. Potiens, and L. L. Campos, "Attenuation coefficient determination of printed ABS and PLA samples in diagnostic radiology standard beams," *J. Phys. Conf. Ser.*, vol. 733, no. 1, 2016, doi: 10.1088/1742-6596/733/1/012088.

Index of Figures

Figure 1 Manufacturing process for the obtainment of the silicon model.....	9
Figure 2 The protocol involves dip-coating, calcification embedding and polymerization in ad-hoc designed Spinning Device.	10
Figure 3 The protocol allows to obtain a mold that replicates any type of calcification pattern embedded in the aortic valve.	10
Figure 4 The protocol allows to merge CAV and AR.	10
Figure 5 Preliminary CAD model of tricuspid aortic valve.	11
Figure 6 Tricuspid and bicuspid realistic CAD models.....	11
Figure 7 Calcification patterns: upper, preliminary 3D printing, lower parametrized 3D printing.....	12
Figure 8 Schematic representation of the measured areas of the cusp.	12
Figure 9 Assembly of outer and inner aortic root molds.	12
Figure 10 Physiological Aortic Valve Model obtained through dip-spin coating of Sorta Clear 18.....	13
Figure 11 Commissure shape is highlighted in CAD and silicone models, for both preliminary and final ARs.	14
Figure 12 Pulmonary and Systemic Circulation blood-flow ways in the heart [25].	29
Figure 13 The graph shows the various events which occur simultaneously during an entire cardiac cycle. Three rows are separated concerning changes observed in the electrocardiogram; aortic, left ventricular and left atrial pressures; left ventricular volume [25].	32
Figure 14 The aortic root has been cut from the fibrous tissue located in between the cusps of the aortic and mitral valve. The level of sinotubular junction has been identified by the red dashed line. The interleaflet triangles and ventriculo-arterial junction has been represented by the red dotted line [29].	33
Figure 15 Semilunar shape of aortic leaflets and their hinge points [27].	34
Figure 16 The top view of the transected aortic root from the STJ illustrates which two valvular sinuses are the origin of the coronary arteries and are entitled as the right and left coronary aortic sinuses. The third sinus is called as a non-coronary sinus since there does not exist a coronary artery. Also AV is observed with its closed cusps and named as the same principle with the sinuses [26].	35
Figure 17 Aortic Root and Imaginary Rings [31].	36
Figure 18 The image of the Aortic Annulus (A), Sinuses of Valsalva (B) and Sinotubular Junction (C) is obtained axial in-plane. In image A, black arrow and dashed lines showed maximum and minimum diameters of the annulus (Dmax and Dmin). In image B, the dashed perpendicular line has been ascended to the deepest level of sinuses of Valsalva. Lines are drawn from each commissure till the corresponding cusps. In the image (C), the dashed perpendicular line reached ascending aorta.[35]	37
Figure 19 Schematic representation of the main valvular diseases. www.heartfoundation.org	39
Figure 20 Comparison between the physiological and the stenotic aortic valve in the opened and closed configurations. In the healthy valve, the leaflets are thin and properly sealing. Below the stenotic calcified AV. The tissue is thicker, stiffer and closure is not perfect, resulting in regurgitation during the diastolic phase. www.heartfoundation.org	40
Figure 21 The pathogenesis of Aortic Stenosis (AS) [45].	42
Figure 22 The drawing schematizes the shear wall stresses acting in the region of the aortic valve [46]	43
Figure 23 Graphics showing the different values of pressure in the physiological case (on the left) and in the pathological case of AVS (on the right). LVP: left ventricular pressure. AP: Aorta pressure. LAP: Left atrium pressure [49].	44
Figure 24 Radial pattern [5].	45
Figure 25 First type of calcification: radial pattern. On the left frontal view radiograph of the aortic valve cusp from the study of Thubrikar. Heavy calcific deposits are visible, starting from the attachment line and diffusing through the belly radially. On the right, top view of multiple large spots of calcifications, at the base of the leaflets (moderately calcified aortic valve). [50].	45

Figure 26 Arc Pattern) [5].	45
Figure 27 Radiographs of stenotic aortic cusps from Thubrikar studies with clear patterns. On the left frontal view of severe stenosis due to arc shape and partial arc. On the right top view of the same pattern, at moderate grade.	46
Figure 28 Calcification pattern in bicuspid aortic valves. [53]	46
Figure 29 Schaefer classification of the BAV morphology, as seen from a parasternal short axis view on echocardiography and their prevalence [44]. RCA: right coronary artery, LCA: left coronary artery, RC: right coronary cusp, LC: left coronary cusp, NC: non coronary cusp.....	48
Figure 30 SAPIEN valves, Edwards Lifesciences, Irvine, CA [42].	50
Figure 31 CORE valves, Medtronic Fridley, MN [42].	50
Figure 32 Edwards SAPIEN 3 [16]	51
Figure 33 ACURATE TA™ prosthesis. [16]	51
Figure 34 CoreValve Evolut™ R System. [16]	52
Figure 35 Portico™ valve. [16]	52
Figure 36 CENTERA valve. [16]	53
Figure 37 Evolution of TAVI approved by CE mark or China Food and Drug Administration approval. They are represented with respect to the date of regulatory approval. [16]	53
Figure 38 Phases of realization of patient-specific models. CT DICOM data converted in CAD-STL file, exported to a 3D printer to create concrete 2 material fused construct. Final CT of the model to compare the orifice area with the anatomical one [71].	56
Figure 39 Patient specific 3D models. The models are shown from the views of the aorta long axis and aortic valve area, to evidence the calcium distribution [71].	56
Figure 40 Mold components: ventricular and vascular stamps, and external shells[72].	57
Figure 41 Molding procedure:	58
Figure 42 Patient Specific 3D printed aortic root models, including right coronary artery RCA, left main artery LM (A,B,C). The figure represents CT images of annulus (D) and its 3D resin realization (E). There are also figured the scan of sinuses of Valsalva (F) and its 3D resin model (G). Also the final 3D models in elastic materials to mimic the tissue properties of the aorta are pictured (H-I). [76]	59
Figure 43 Rigid physical model of the porcelain ascending aorta (A) and Flexible 3D printed model of ascending aorta (B) [76].	60
Figure 44 Top, down and side view of the physical model of ascending aorta and stenotic valve. [74]	62
Figure 45 Physical model installed in ViVitro pulse duplicator system. [74]	62
Figure 46 Both closed and opened configuration of stenotic aortic valve model on the left, and transcatheter aortic valve on the right, recorded by high-speed camera.	63
Figure 47 From the CT images of Thubrikar's study (A), calcification pattern is chosen (B) and then realized through 3D-printing technique (C-D). [18]	63
Figure 48 Calcifications accommodation on the porcine leaflets through specific support on the left. Design of the centering support on the right. [18]	64
Figure 49 Software process flow of 3D printed heart phantom models. [80]	65
Figure 50 Cardiac Phantom (A, B) and Calcified Mitral Valve(C, D). [80]	66
Figure 51 Free margin profiles. On the top the new designed curvilinear one, on the bottom Labrosse' linear one. [4]	67
Figure 52 In blue, silicon (GLS-20PRO) casted inside of the PLA-mold, in black. [4]	67
Figure 53 CAD assembly of the molds for aortic valve and aortic root support. [4]	68
Figure 54 Stationary test set up. [4]	68
Figure 55 Pulsatile tests set up. [4]	69
Figure 56 In the figure are shown:	70
Figure 57 The Essential Steps of Dip Coating. [83]	73
Figure 58 Dipping Container front view during the mold dipping and top view.	73

Figure 59 The essential steps of casting technique. Silicone is shown as example of polymeric solution that is poured into an assembly of outer and inner molds. Once the silicone is cured, it can be extracted, obtaining a silicone model.....	74
Figure 60 Outer and Inner molds, composed by many sub-molds.	75
Figure 61 Iter of the manufacturing process for the obtainment of the silicon model.....	76
Figure 62 Graphical user interface of SolidWorks.	77
Figure 63 Graphic user interface Netfabb Standard.	78
Figure 64 Graphic user interface of Cura.	79
Figure 65 Scheme of the process of Fused Deposition Modeling. [81]	81
Figure 66 Ultimaker3 3D Printer. [82] The main components are:.....	82
Figure 67 Molds undergoing Post-Processing phase: rubbing down process via sanding paper on the left and brushing XTC-3D coating on the right.....	85
Figure 68 On the left explanation of the CAD components of the SD: RG: ring gear, SG: sun gear, PGS: planetary gear system. On the right demonstration of the inclined SD, including valve molds.....	91
Figure 69 The Planetary Gear System Configuration and its components. The sun gear has input rotational speed (w) and the planetary gears have output rotational speed (w). However, the ring gear has a fixed position meaning that $w=0$. The figure is designed in Inventor Autodesk Software.....	92
Figure 70 Spur Gear Component Generator and Design Parameters presented in Inventor Software.....	92
Figure 71 Design parameters of spur gears.	93
Figure 72 Valve Carrier, Shaft of the Valve Mold, and their fixation assembly that allows the rotational transition to the valve mold.	94
Figure 73 On the left CAD assembly, on the right the real assembly of the Spinning Device.	94
Figure 74 Spinning Device inclined at 40° , on the left, uploaded of the aortic valve molds into the VCs on the right.....	95
Figure 75 Representation of the three protocols developed for the silicone model manufacturing.	96
Figure 76 CAD assembly of some of the designed molds.....	97
Figure 77 On the left, the free edge of the leaflet angle was demonstrated. On the right, aortic valve geometry parameters: D_b , the base diameter; D_c , the commissure diameter; X_s , the height of the cooptation of leaflets in the center; α , the angle of the leaflet in the closed configuration.	99
Figure 78 CAD model of Preliminary Design.....	99
Figure 79 Final CAD model of the more physiological valve mold.	100
Figure 80 The CAD model of BAV	101
Figure 81 Preliminary (on the top) and final (on the bottom) configurations of the Aortic Root. From the left the two views of the CAD drawing, on the right the technical drawing to focus the attention on the commissures' area: rectangular for preliminary design and triangular for the final one.....	102
Figure 82 Aortic Root Inner and Outer Molds. On the top, the preliminary molds, on the bottom the final molds.	103
Figure 83 Example of Custom Inner Mold.....	104
Figure 84 Silicone Molds. On the left, the preliminary one, on the right the final one.	105
Figure 85 Silicon-Casting Molds. On the left the preliminary one, on the right the final one.	105
Figure 86 Ad-hoc 3D printed PLA preliminary pattern.	107
Figure 87 Representation of the CAD process of realization of the calcific pattern 1	108
Figure 88 Arc shape pattern are shown. On the left spots-shape, on the right planar shape.	109
Figure 89 Representation of the CAD process of realization of the calcific pattern 1.	110
Figure 90 Representation of the selected measurement points in the cusp. From the left: TP, TR, TA.....	111
Figure 91 Representation of the leaflets manufacturing process, with	113
Figure 92 On the left frontal view: one side of the outer SCM and the inner SCM. On the right, the obtained SM – final configuration.	114
Figure 93 SM with the CAV inserted, on the left, and final Custom Inner Mold in epoxy.	114
Figure 94 Representation of manufacturing process of Aortic Root- final configuration).....	115

Figure 95 Physiological Aortic Valve Model obtained through dip-spin coating of Sorta Clear 18. Frontal, top views. On the right the free edge is cut through a cutter.	116
Figure 96 Prototype of preliminary AR model. It includes AV with partial arc calcification pattern.	120
Figure 97 Prototype of final AR model. It includes AV with radial calcification pattern.....	120
Figure 98 Custom Inner Molds. On the left for preliminary AR in frontal view and top view to show the cavities, molds of the calcific patterns. On the right custom inner mold for the final AR.	121

Index of Tables

Table 1 Comparison between mean values and standard deviation of thickness of natural physiological aortic valve, previous work from literature and manufactured phantom model.....	13
Table 2 Manufactured Calcified Aortic Valves.....	14
Table 3 Summary of the ARs dimensions.	14
Table 1 Healthy aortic root dimensions with the tricuspid valve. Direct Measurements (DM), Trans-esophageal Echo (TEE), Multislice Computed Tomography (MSCT), and Multidetector Row Computed Tomography (MDCT). AV: Aortic Valve, STJ: Sinotubular Junction, VS: Valsalva Sinuses. Avg: average value.	37
Table 2 Schematic resume of the values used to define the grade of stenosis. EOA: effective orifice area, ΔP : pressure drop, Vmax: maximum velocity at systolic peak.	41
Table 6 Main parameters to be set before printing.	80
Table 7 Summary of the properties of interest of PLA.	84
Table 8 VeroWhitePlus™ Mechanical Properties. They were compared with PLA properties.....	85
Table 9 Mechanical properties comparison between TangoPlus [92] and other promising available silicones. Silicones' values are taken from their data sheets, in Appendix A.	88
Table 10 Summary of the values of D_{circle}/D taken from literature, the values used in the work and the classification of the severity grade.	109
Table 11 Comparison between thickness values: mean value and standard deviation of natural physiological aortic valve from literature, objective value of a previous work from literature and mean value and standard deviation of manufactured phantom models. The values for the natural aortic valve are combination of the thickness of the three cusps.	117
Table 12 Thickness mean values and standard deviation of the Calcified Aortic Valves.	118
Table 13 Summary of the ARs dimensions.	119